D I P L O M A R B E I T

M A S T E R ' S   T H E S I S

Influence of Annual Rings on Displacement and Stress Fields in Wood at Loading Perpendicular to the Grain

ausgeführt zum Zwecke der Erlangung des akademischen Grades eines Diplom-Ingenieurs

unter der Anleitung von

Dipl.-Ing. Dr. techn. **Karin Hofstetter**
Universitätsassistentin
Institut für Mechanik der Werkstoffe und Strukturen
Fakultät für Bauingenieurwesen
Technische Universität Wien

und

Univ. Prof. Dipl.-Ing. Dr. techn. **Josef Eberhardsteiner**
Institut für Mechanik der Werkstoffe und Strukturen
Fakultät für Bauingenieurwesen
Technische Universität Wien

eingereicht an der Technischen Universität Wien
Fakultät für Bauingenieurwesen

von

Stefan Gloimüller

Matr.Nr.: 03 25 810
Schenkenbrunn 9
A - 3512 Mautern

Wien, im April 2008

Danksagung

Abstract

Wood is facing a boom in the construction sector and is increasingly used for civil engineering purposes. Only recently, building regulations have been changed to allow for using wooden load-bearing components in multi-storied houses. In the static design of such constructions the orthotrophy of the material, which results mainly from the grown annual ring structure in a wood stem is of great importance. In wood processing such as the carpentry and the joinery, people learned to deal with the effect of the annual rings from experience and tradition.

This thesis takes a scientific approach to the influence of the annual rings on the stress, strain, and displacement fields in wood at loading perpendicular to the grain. Therefor a program which shows the influence of the annual rings in a cross-section of a stem is developed. The basic components of this program are the finite element method (FEM) for numerical simulation and a micromechanical model in combination with the digitalization of the annual rings from a picture of the cross-section in order to analyze samples with different annual ring patterns. The micromechanical model is used to estimate the varying stiffness values in earlywood and latewood, while the digitalization of the annual rings yields the varying principal material directions at these points.

COMSOL is used as FE-program, since the generated files can be modified in MATLAB. The modifications with MATLAB imply the allocation of different stiffness values in an annual ring, which result from the different stiffnesses of earlywood and latewood, and varying orientations of the annual rings to the integration points of the finite elements. The varying density of the annual ring bands in wood is obtained from the digitalization of a gray scale picture of the cross-section because of the correlation of the coloration and the local density which in turn is related to the stiffness of the tissue. The corresponding stiffnesses are determined by means of a micromechanical model, which was developed at the Institute for Mechanics of Materials and Structures (IMWS) at Vienna University of Technology. This model calculates the stiffness values for each integration point of the finite elements by three homogenization steps from the weight fractions and stiffness values of the basic wood components, namely cellulose, hemicellulose, lignin, extractives, and water, and from the varying densities of latewood and earlywood. The chemical composition of the samples, which is an input for the micromechanical model, was determined in a chemical laboratory by dissolving the constituents of wood with diverse acids, which dissolve only defined components of the wood sample.

Furthermore, the varying local orientations of the radial and tangential material directions, which result from the circular shape of the annual rings, have to be considered in the FE-model. For this purpose, the local inclination angle of the annual rings is determined from the digitalized picture of the cross-section at each integration point and used to transform the local stiffness matrixes into a global reference frame. Application of the model to the simulation of academic examples with typical annual ring patterns delivered insight into the fundamental effects of the annual rings on stress, strain, and displacement fields in the cross-section.

The practical part of this work deals with the validation of the developed FE-program. The samples were provided by the University of Natural Resources and Applied Life Sciences in Vienna and tested by a tension testing machine at the Laboratory of the IMWS. To obtain accurate deformation values in the range of micrometers across the whole surface

of the samples, an optical full-field deformation analysis system called Electronic Speckle Pattern Interferometry (ESPI) was used. The resulting deformation plots show the pattern of the annual rings, underlining the pronounced influence of the succession of stiffer latewood bands and weaker earlywood bands on the mechanical behavior. To compare the measured displacements with corresponding results of the numerical model, a picture of the cross-section of the samples was made and analyzed by means of the FE-program. On the whole, the simulation results show a good agreement with the measurement results, what confirms the suitability of the developed program for analysis of the mechanical behavior of wood at loading perpendicular to the grain. The annual rings are particularly important in relation to dimensional changes at varying moisture content, both during the drying process and during the utilization period. In this respect, an extension of the model by hydromechanical features will yield a powerful simulation tool suitable for process and product optimization in timber engineering and the wood products industry.

Kurzfassung

Der Werkstoff Holz erfährt zur Zeit einen starken Aufschwung am Bausektor und immer weitere Verbreitung im Bauingenieurwesen. So wurden in den letzten Jahren die Bestimmungen und Verordnungen für das Bauwesen dahingehend adaptiert, dass es nun möglich ist mehrstöckige Gebäude aus tragenden Holzbauteilen zu fertigen. Bei der statischen Berechnung von Holzkonstruktionen ist die Orthotropie dieses Werkstoffes, welche aus der natürlich gewachsenen Struktur von Holz resultiert und seit Jahrhunderten bekannt ist von großer Bedeutung. Zimmerer und Tischler im holzverarbeitenden Gewerbe kennen diese Effekte der Jahresringe aus der praktischen Anwendersicht. Zahlreiche wissenschaftliche Arbeiten beschäftigten sich bereits mit diesem Thema des orthotropen Holzwerkstoffes. Diese Arbeit untersucht systematisch den Einfluss von Früh- und Spätholz auf die Deformations- und Spannungsfelder bei einer Belastung normal zur Holzfaser auf wissenschaftlicher Basis.

Dafür wurde ein Computerprogramm erstellt, das die materialspezifischen Eigenschaften von Holz in einem Querschnitt anhand einer numerischen Simulation zeigen soll. Die Hauptbestandteile dieses Programmes sind die Berechnungsmethode mit Finiten Elementen (FE), ein Mikromechanikmodell für die Ermittlung der variierenden Steifigkeiten von Früh- und Spätholz und die Digitalisierung von Jahresringen anhand eines Bildes für die korrekte Materialausrichtung.

Als Programm für die FE-Berechnungen wurde COMSOL gewählt, da der Quellcode in MATLAB beliebig editierbar ist. Die Modifikation mit MATLAB beinhaltet die Zuteilung der verschiedenen Steifigkeitswerte innerhalb eines Jahresringes, die aus den unterschiedlichen Dichten von Früh- und Spätholz resultieren, und der variierende Ausrichtung der Jahresringe zu den Integrationspunkten der finiten Elemente. Die lokal variierenden Dichten werden aus einem Bild des Holzquerschnittes anhand der verschiedenen Graustufen ermittelt, da ein kausaler Zusammenhang der Färbung der Jahrringbereiche mit der Form und Größe der Holzzellen und in weiterer Folge mit der makroskopischen Dichte und Steifigkeit gegeben ist. Die Bestimmung der lokalen Steifigkeiten erfolgt mittels eines Mikromechanikmodells, welches am Institut für Mechanik der Werkstoffe und Strukturen an der Technischen Universität Wien entwickelt wurde. Dabei werden in drei Homogenisierungsschritten die Steifigkeitsmatrizen für jeden Integrationspunkt aus den Gewichtsfraktionen und Steifigkeitswerten der Holzkomponenten, nämlich Zellulose, Hemizellulose, Lignin, Extraktstoffe und Wasser, sowie aus der variierenden Dichte von Frühholz und Spätholz berechnet. Weiters ist die sich ändernde lokale Ausrichtung der radialen und tangentialen Materialhauptrichtungen aufgrund der annähernden Kreisform der Jahresringe im FE-Modell zu berücksichtigen. Dazu werden die lokalen Neigungswinkel der Jahresringe an jedem Integrationspunkt aus dem digitalisierten Querschnittsbild ermittelt und für die Transformation der lokalen Steifigkeitsmatrizen in ein globales Bezugssystem verwendet. Durch Anwendung des Modells zur Simulation von akademischen Beispielen mit typischen Jahrringmustern wurden die grundlegenden Effekte der Jahresringe auf die Spannungs-, Verzerrungs- und Verschiebungsverläufe im Querschnitt untersucht.

Der praktische Teil dieser Arbeit beschäftigt sich mit der Validierung dieses FE-Programmes. Dazu wurden von der Universität für Bodenkultur in Wien Proben aus einem Starkholzprojekt zur Verfügung gestellt. Diese wurden nach kurzen Bearbeitungsschritten mit einer einaxialen Zugprüfmaschine quer zur Faser auf ihre Steifigkeit getestet. Um die Verschiebungen möglichst genau und flächenhaft zu erhalten, wurde ein optisches und

berührungsloses Deformationsmessverfahren (Elektronische Speckle Interferometrie, ESPI) eingesetzt. In den gemessenen Verschiebungsbildern spiegeln sich die Muster der Jahresringe aufgrund der Abfolge von steifem Spätholz und weicherem Frühholz wider, was einen deutlichen Einfluss derselben auf das Materialverhalten beweist. Um die Ergebnisbilder des ESPI-Messsystems mit den Resultaten des Computermodels zu vergleichen, wurden die Querschnitte der Holzproben fotografiert und mit dem FE-Programm analysiert. Die chemische Zusammensetzung der Proben, die in das Mikromechanikmodell eingeht, wurde in einem Chemielabor bestimmt. Dies erfolgt durch zum Teil hoch konzentrierte Säuren, die jeweils nur gewisse Komponenten lösen und die zu bestimmenden Inhaltsstoffe nicht berühren. Insgesamt ist eine gute Übereinstimmung der Simulationsergebnisse mit den Messwerten zu beobachten, was die Eignung des entwickelten Programms zur Analyse des mechanischen Verhaltens von Holz bei Beanspruchung quer zur Faser belegt. Die Jahresringe spielen insbesondere bei Dimensionsänderungen zufolge Feuchtigkeitsschwankungen eine Rolle, welche im Holztrocknungsprozess und während der Nutzungsdauer auftreten. In diesem Hinblick soll das entwickelte FE-Programm als Grundlage für eine Erweiterung um hydromechanische Aspekte zu einem leistungsfähigen Simulationstool dienen, welches für Produkt- und Prozessoptimierung im Holzbau und der Holzindustrie von Interesse ist.

Contents

Chapter 1

Basic Concept

1.1 Motivation

The lateral cut of a tree normal to the grain consists of several rings. These annual rings result from the arrangement of the *less dense, lighter earlywood* and the *denser, darker latewood* arranged in *approximately concentric circles.* In between earlywood and latewood, there is a zone of changing density generally denoted as *transitionwood.* The
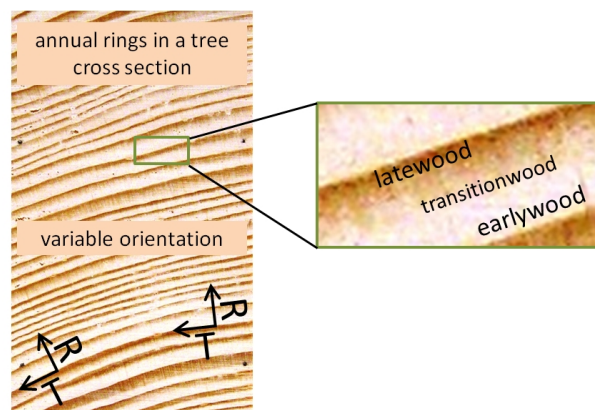
Figure 1.1: Annual rings

annual rings are visible to the naked eye as well as the transitionwood area (see Figure 1.1). The notations "early" and "late" indicate two out of four growth phases of wood over a year in European latitudes, which result in different densities and, in consequence, in varying stiffness values across a single annual ring. The principal material directions in the cross-sectional plane are oriented *orthogonally* and *tangentially* to the annual rings and are denoted as *radial direction* ($'R'$) and as *tangential direction* ($'T'$), respectively (confer Figure 1.1). Due to the round design of the annual rings, these *orientations vary locally.*

At a transverse loading, the annual rings have a considerable influence on the fields of stress, strain, and displacement. These effects are technically relevant, particularly with regard to moisture-induced stresses and inhomogeneous deformations during wood drying and during the service life of wooden constructions. The reasons for these stresses and the inhomogeneity of the deformations are the curved annual rings in the cross-section of a tree trunk.

In order to resolve and study these influences a *computer program* was developed, which operates on the basis of *finite elements* and a *micromechanical model*. This program allows to consider local density and, thus, local stiffness as well as the local orientation of the principal materials directions at each integration point of a finite element mesh.

The program starts off from a *digitalized photo of the cross-section* showing the annual ring pattern in different gray levels. By means of search algorithms, the course of the latewood bands is determined first in terms of coordinate points. Thereon, the local orientation of the radial direction can be determined by identification of the local normal direction to the latewood band. Moreover, the local gray level yields the local density, and the local stiffness by means of the micromechanical model.

In exemplary model applications and in the model validation, the focus is placed on loading perpendicular to the grain. Model evaluation for manually created pictures of characteristic annual ring patterns shall show the effects of annual rings at loading perpendicular to the grain. The validation is based on results of tension tests with full field displacement measurement using a *contact-free measurement system* (ESPI). These results are compared to the displacement distributions obtained with the computer program based on photos of the annual ring pattern of the samples.

1.2   Previous Work

The pronounced influence of annual rings on the mechanical behavior of wood has already motivated various research activities by both experimental and numerical means, which are exemplarily reviewed in the following.

Hoffmeyer et. al. [1] analyzed characteristic strength values under compression load perpendicular to the grain, where timber samples and glulam samples from Norway spruce were tested. Five different specimen types were investigated showing annual ring patterns with radial, tangential, or mixed orientation.

Nairn [2] performed finite element simulations in order to determine effective transverse elastic moduli of wood for different annual ring patterns in rectangular specimens. He found out that the curvature of the annual rings or off-axis loading reduce significantly the effective modulus. The heterogeneous model was compared to prior numerical methods using homogenized properties in the transverse plane. It is shown that the heterogeneous model is required to capture details in modulus calculations and to realistically model stress concentrations.

Lin et. al. [3] analyzed the effects of ring characteristics on the compressive strength and dynamic modulus of elasticity of seven softwood species by means of an ultrasonic wave technique. According to their statistical analysis, compressive strength was affected by various ring characteristics. Overall, compressive strength increased with decreasing ring width and increasing ring density. Ring density was related to compressive strength, but

was not the sole factor affecting the wood strength. The authors concluded that earlywood density and minimum density in a ring are equally important variables for evaluating the compressive strength of wood.

Shipsha and Berglund [4] investigated shear coupling effects on stress and strain distributions in wood subjected to transverse compression. These are relevant for the performance of glulam beams and solid wood structures. For the experiments, they used a whole-field digital speckle photography technique to measure the strains, which were compared to results of finite element calculations.

1.3 Structure

The thesis is organized in seven chapters. After the introductory chapter, in Chapter 2 the constituents of wood , their role in the formation of wood (Section 2.1), and their effects on the material behavior are described. Furthermore, the microstructure (Section 2.2) from the molecular scale up to the cross-section is described, combined with an outline of the formation of the annual rings in Section 2.3.

Chapter 3 describes the micromechanical model for wood elasticity. After the definition of the characteristic length scales of this model (Section 3.1), the three homogenization steps (Sections 3.3 and 3.5) and their theoretical fundamentals (Sections 3.2 and 3.4) are specified. The micromechanical model determines the stiffness values against the gray level and the assigned density, respectively.

Chapter 4 treats the digitalization progress of the computer program to calculate the local varying densities and orientations of the principal material directions. The first Section 4.1 in this chapter deals with the determination of the density from a gray scale picture. Section 4.2 is concerned with the restructuring of the stiffness matrix, which is calculated by the micromechanical model, for the changed coordinate system in the computer program. In Section 4.3 the compilation of the stiffness values for all finite elements are outlined. Furthermore, Section 4.4 describes the digitalization of the latewood bands from the cut and closed annual rings, and in succession the calculation of the local orientations of the principal material directions.

In Chapter 5 the developments of Chapters 2 and 4, and of Section 4.4 are combined and consolidate the FE-model. Sections 5.1 and 5.2 describe the arrangements in COMSOL in resulting in the superior file which controls the FE-calculation. The combination of the FE-model, the digitalization of the annual rings, and the micromechanical model is defined in Section 5.3. Section 5.4 gives a review of simulation results obtained for several characteristic annual ring patterns and the effect of these patterns on the stress, strain, and displacement fields of these calculated samples.

Chapter 6 defines the validation steps in order to compare the output of the developed computer program with test results of three wood samples. Sections 6.1 and 6.2 specify the used equipment for the tension tests of these three wood samples. Preliminary tests with non-uniform and uniform load application and validation tests as well as the displacement fields measured with the ESPI-system during the testing series are described in Sections 6.3 and 6.4.

Chapter 7 contains the conclusions of this project.

Appendix A reports on the determination of the wood constituents and their weight fractions in a chemical laboratory. The preparatory work is described in Section A.1, the determination of the weight fractions of the wood components in Section A.2 for extractives, in Section A.3 for lignin, and in Section A.4 for cellulose and hemicellulose.

Appendix B includes a compendium of the program code. Therein, ten sections include the superior file taking control of the entire simulation procedure, files for the digitalization of the annual rings, files for the micromechanical model and files for transforming and rearranging the stiffness values.

Chapter **2**

Microstructure and Formation of Wood

Wood exhibits a *strongly inhomogeneous structure*. The annual rings as successions of tissues with *alternatingly lower and higher density* are visible to the naked eye. But also at smaller length scales, wood shows a heterogeneous build-up of either cellular or composite type. Mechanical properties of the microstructural components and their geometric arrangement control the macroscopic mechanical behavior of wood. A mathematical formulation of these relations is provided by micromechanical models, such as the model used for stiffness estimation in the framework of this thesis. In order to better understand the *anatomical and biological background*, formation of wood are briefly reviewed in this chapter and the microstructure.

2.1 Formation of Wood

2.1.1 Cell Division

The *cambium*, which is located between the outermost annual ring and the bast, builds new wood material by cell division. This process is called *secondary growth of thickness*. Inside the cambium layer one cell division results in two new cells. One of them keeps the capability for further division, also called initial cell, while the other one becomes a *permanent cell*, which builds wood to the inside. It is possible that permanent cells divide one or two times again. After this, permanent cells take over functions like living tissue that carries organic nutrients, supporting tissue or tissue for storage. Ray cells supply the tree with *water and nutrients in radial direction*. While the *primary rays* extend from the core to the cambium, the *secondary rays* extend from the transport tissue to the cambium. A *bast ray* is the continuation of a primary ray or secondary ray inside the bast. The *cork cambium* produce the cork, a tough protective material. The *bast* transports water with soluted nutrients from the crown to the radix. The transport process from the radix to the

crown is done by the sapwood. The *bark* is the outermost layer of a tree and protects stem and branches against physical and mechanical influences. The arrangement of the tissues in the stem is illustrated in Figure 2.1.
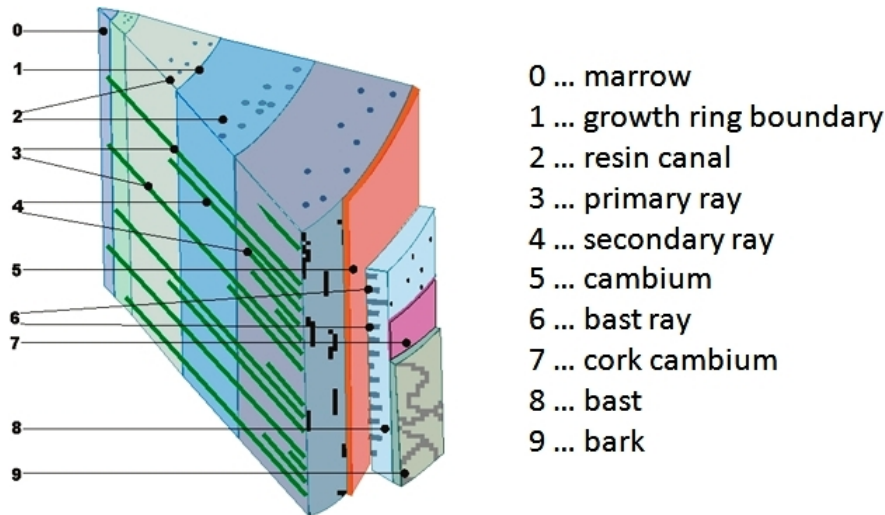
Figure 2.1: Structure of wood [5]

0 ... marrow
1 ... growth ring boundary
2 ... resin canal
3 ... primary ray
4 ... secondary ray
5 ... cambium
6 ... bast ray
7 ... cork cambium
8 ... bast
9 ... bark

2.2 Microstructure of Wood

2.2.1 Molecular Scale

The principal components of wood are *cellulose*, *hemicellulose*, *lignin*, *extractives*, and *water*. Moreover, *ash* may be incorporated in the wood tissue.

Cellulose Chains: Cellulose is the *main integral part* of wood and most abundant organic substance on earth. In softwood its weight fraction ranges between 42 % to 49 %. It is unsolvable in water and is only dissolved in intense acids at high temperature of about 125 ℃. The cellulose chains are composed of *β-D-glucose units* (Figure 2.2) and show the chemical formula $(C_6H_{10}O_5)_n$. The basic units build up parallel epipeds with dimension of
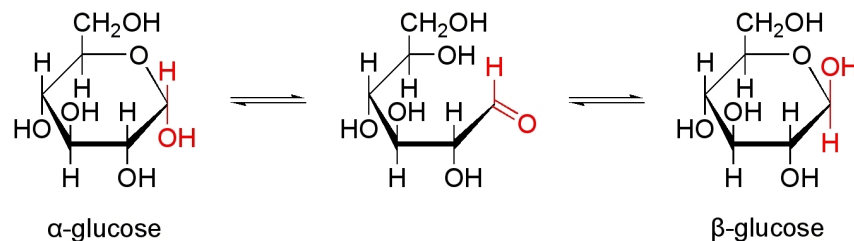
Figure 2.2: Glucose and its α- and β-configuration [6]

$0.84 \times 1.03 \times 0.79$ nm³. The cellulose chains are linked to each other and construct *cellulose fibrils* (Figure 2.3, Figure 2.4). These fibrils are visible under an electron microscope,
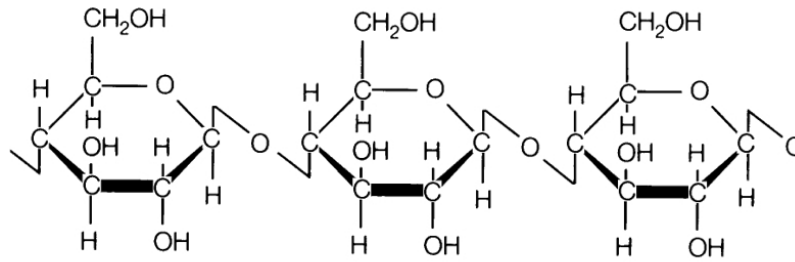
Figure 2.3: Multiple glucose molecules in β-configuration linked to a cellulose chain [7]
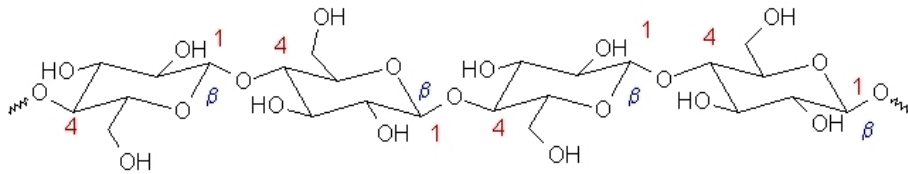
Figure 2.4: Connection of the glucose molecules by a β-1-4-junction to cellulose [8]

and combined to packs of macromolecules with a *wire-shaped structure*. Thereby, the fibrils are arranged in parallel in large parts and form crystalline structures. The surfaces of the fibrils are less ordered and show amorphous characteristics [6, 9]. The cellulose fibrils are in turn assembled into large *cellulosic fibers* with a diameter of 50 to 200 nm.

Matrix of Lignin and Hemicellulose: The spaces between the cellulose fibrils are filled with a matrix made up of lignin and hemicellulose. *Hemicellulose* builds the *bearing and frame structure* of the cell wall jointly with cellulose. It is composed of different sugar monomers (cf. Figure 2.5 showing exemplarily the molecular structure of galactoglucomannan). Similar to cellulose, it exhibits an elongated structure but includes also side chains. Compared to cellulose, hemicellulose are smaller macromolecules. In softwood, the weight fraction of hemicellulose amounts to 24 % to 30 % [5].
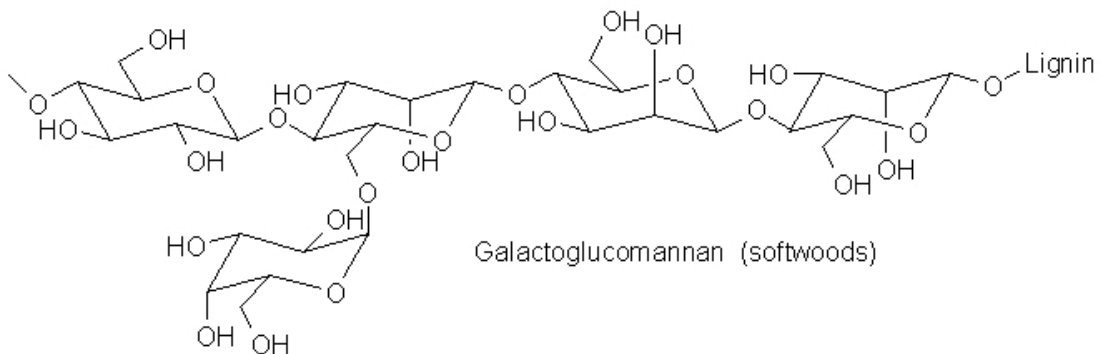
Figure 2.5: Molecular structure of galactoglucomannan - a hemicellulose typical of soft wood [8]
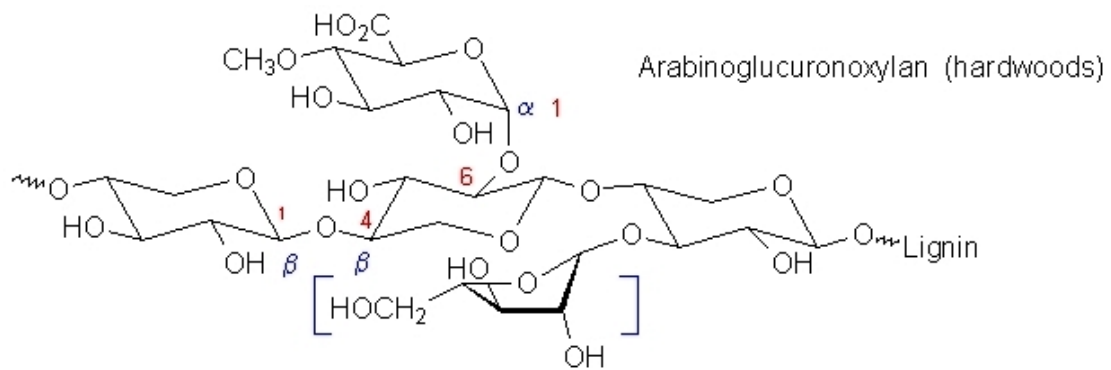
Figure 2.6: Molecular structure of arabinoglucuronoxylan - a hemicellulose typical of hard wood [8]

Lignin (Figure 2.7) fills up the gaps in the frame structure built up by cellulose and hemicellulose. Cells with intensive lignification have thick and stiff cell walls and die off.
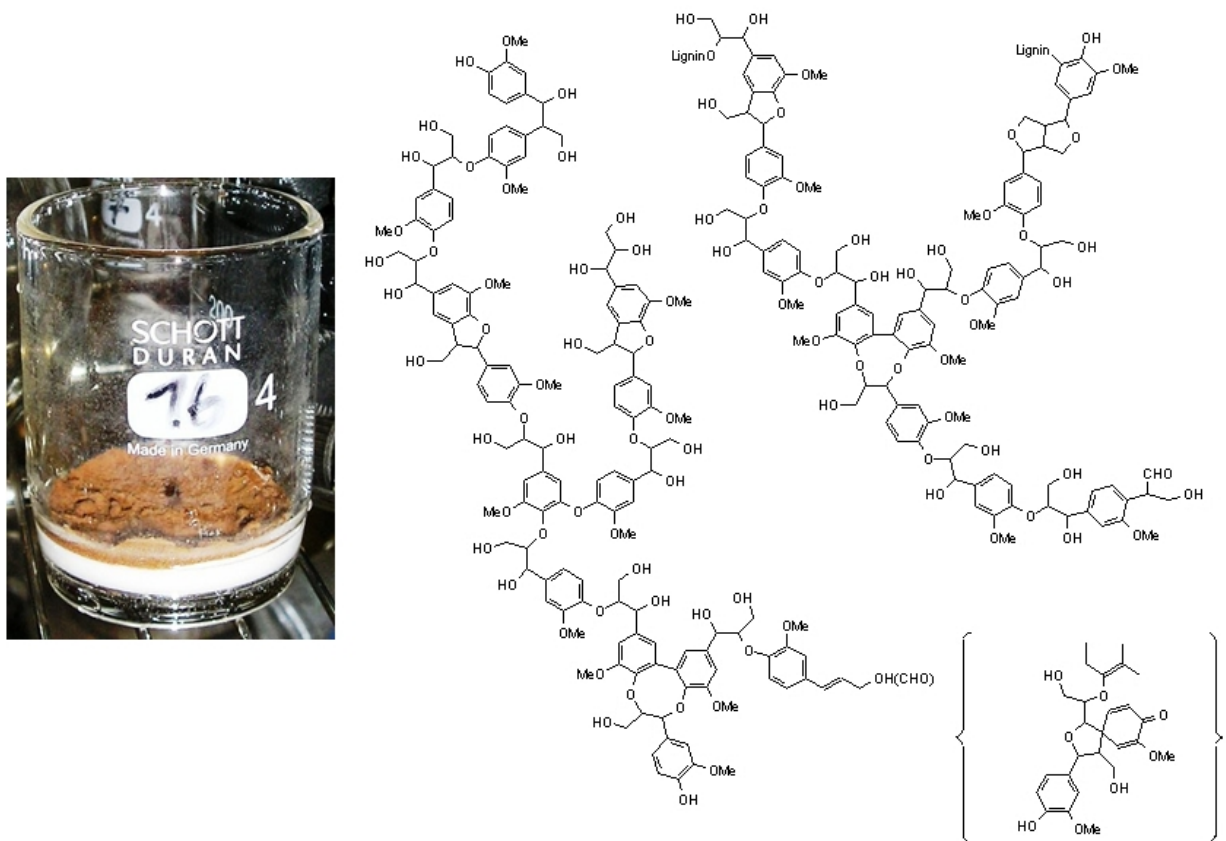
Figure 2.7: Lignin in extracted form (brown powder) and the molecular structure of lignin [8]

Ash is the inorganic part of wood and consists of oxides and carbonates of metals [5]. *Extractives* are chemical compounds which are unhinged from the plant tissue. For

example extractives can be resins or tannins. The weight fraction of extractives ranges between 2 % and 9 % [5].

At moist conditions, water molecules interpenetrate the matrix and are bound either *physically or chemically*. If there is more water than can be stored in the cell wall (about 30% in weight related to the mass of the dry cell wall), liquid water is placed in the lumens of the cell [10].

2.2.2   Cell Wall Layers

As described in Section 2.2.1, the six components cellulose, hemicellulose, lignin, extractives, ash, and water build up the material of the cell wall. As two main functions the *cell walls* provide *stability* to the cell and *impede swelling* in case of water intrusion. As shown in Figure 2.8, the cell wall is assembled of several layers, which differ in chemical composition and arrangement of the microstructural components. In particular, the orientation of the cellulosic fibrils changes from layer to layer [10]. From the inside to the outside, these layers are the *primary wall*, the *secondary wall*, and the *tertiary wall*. In the wood tissue, neighboring cells are connected by the so-called *middle lamella*. These walls, which are described in more detail in the following build up cell walls with thicknesses between 2 and 20μm. Their arrangement is shown in Figure 2.8.

Middle lamella: The middle lamella is formed during the *cell division*. It consists amongst others of pectin, is in principle free of cellulose and, as a main function, holds the cells together [11].

Primary wall: The primary cell wall is a thin, flexible and extensible layer which is formed during *cell growth* by mounting cellulose microfibrils on the middle lamella. These fibrils are connected by hydrogen bonds. On the whole, the amount of cellulose in the primary wall is very limited. The microfibrils are not structured but amorphous, so the cell wall remains *highly elastic* and does not impede cell growth. During the growth phase, the cell wall shrinks in thickness direction. The formed free space is filled up with new microfibrils [11].

The middle lamella and the primary wall are often combined in the so-called compound middle lamella. Nearly 60% of this compound middle lamella consists of lignin, while the content of cellulose is only 14% [12].

Secondary wall: This wall is built when the cell has completed its expansion growth phase and begins with the *thickness growth phase*. It consists basically of cellulose, hemicellulose, and lignin. The microfibrils are oriented helically at an inclination angle between 0° and 30° towards the cell axis and are arranged in multiple intersected layers (crosswisely arranged parallel textures). The cell dies if the secondary wall is lignified. The secondary wall has the *highest thickness of all layers* with a volume percentage of 73% in early wood and 82% in late wood [12] and accounts for 80 % to 90 % of the cell wall thickness. The ingredient lignin strengthens and waterproofs the secondary layer and hence the cell wall [10, 11]. About 60% of this layer consists of cellulose and only 27% of lignin.

Tertiary wall: This wall lies directly next to the cell membrane, consists mainly of pectin and contains only a small amount of cellulose [11].
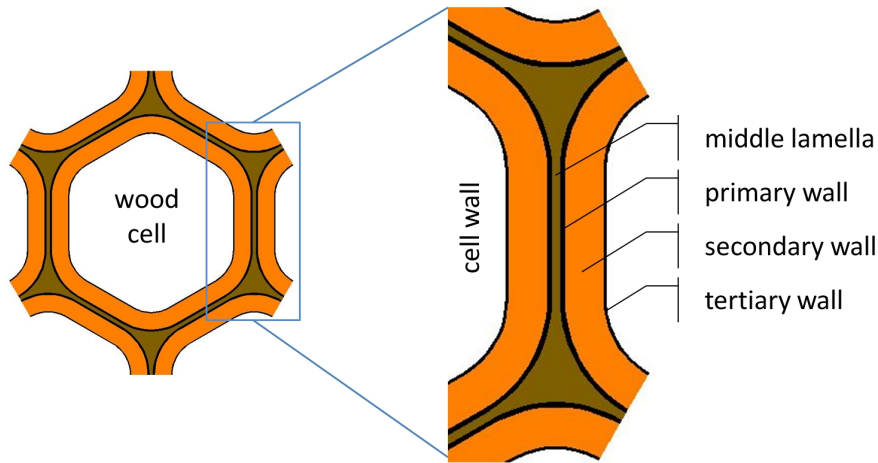
Figure 2.8: Cell wall layers

2.2.3   Wood Cells

Wood cells (Figure 2.9) are *hollow tubes* which are oriented along the stem direction (longitudinal direction). They have a diameter of $20 - 40$ μm in softwood, and of $20 - 500$ μm in hardwood, and a length of 2 to 10 mm. Cells in *earlywood* have *thin walls* and *big lumens* with polygonic or quadratic cross-sections, resulting in *low density* and generally *light coloration*. On the other hand, *latewood* cells show *thick walls* and *little lumens* with a rectangular cross-section. The density of latewood is higher than of earlywood, and the coloration is darker in most species and also in spruce [10].
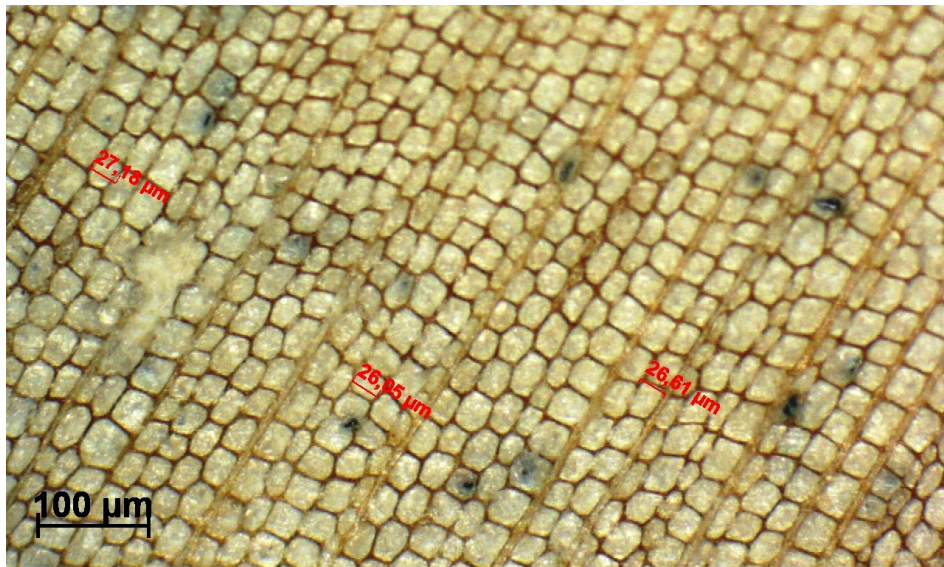
Figure 2.9: Wood cells in earlywood
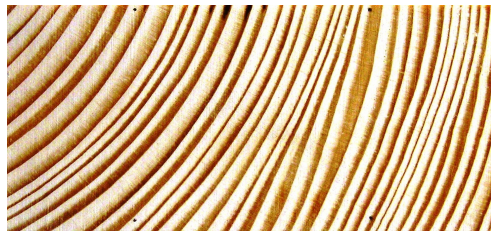
Figure 2.10: Annual rings

2.2.4 Cross-Section of a Stem

A stem consists of concentric rings of earlywood and latewood (Figure 2.10) at a characteristic scale of $2-4$ mm. Figure 2.11 shows the qualitative variation of density perpendicular to the annual rings. The dark band of an annual ring, namely latewood, shows the highest density in the cross-section. In opposition to the latewood, lighter earlywood exhibits low density. In anticipation of Section 2.3, Figure 2.11 shows the *abrupt reduction of the density from latewood to earlywood* in direction of the growth (radial direction towards the bark). Also Figure 2.12 shows this abrupt transition from latewood with small lumens and thick cell walls to earlywood with thin cell walls and wide lumens. This effect is because of the lower growth activity in the phases between deposition phase and growth phase (Section 2.3). The density of latewood can differ from annual ring to annual ring, such as the density of earlywood. However, the values of densities fluctuate only lowly around an average value.
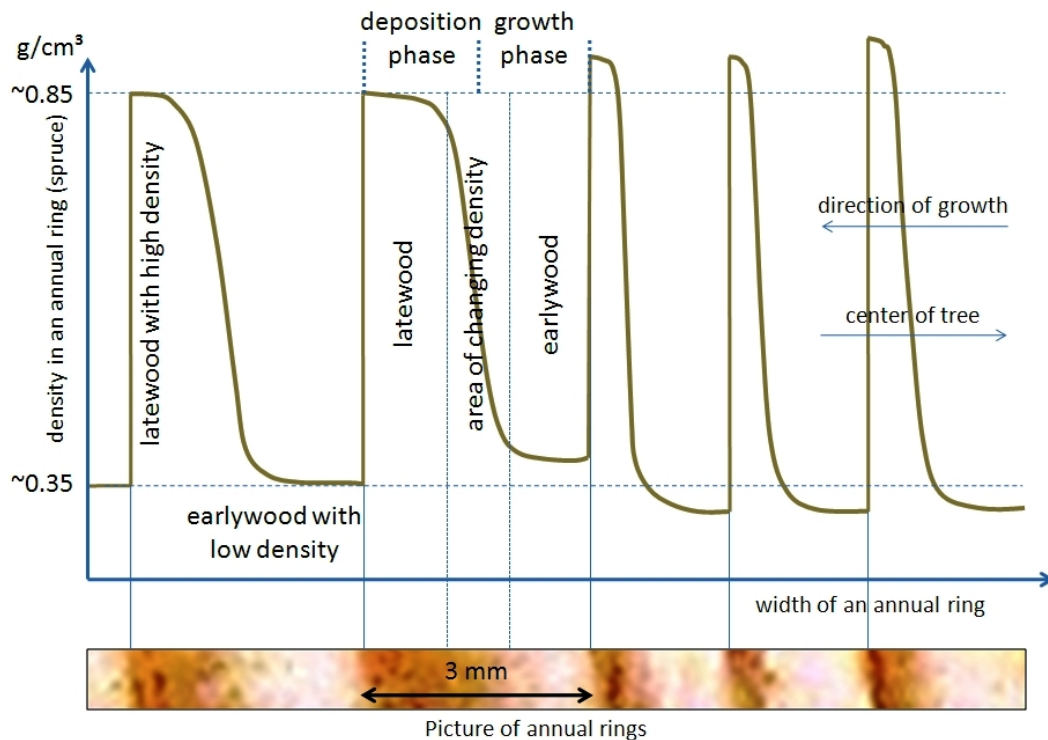
Figure 2.11: Variation of density in the radial direction
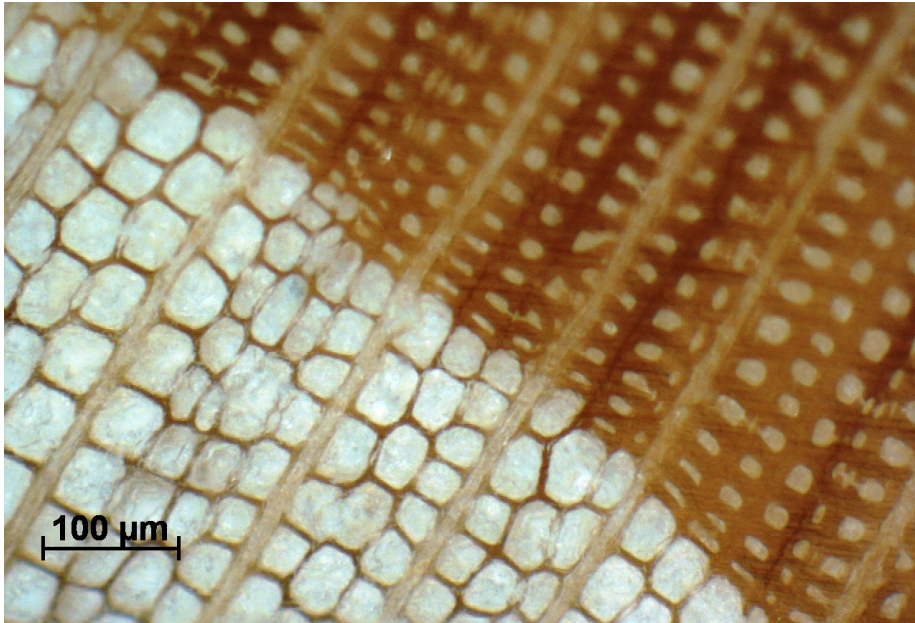
Figure 2.12: Abrupt transition from latewood (right side) to earlywood (left side)

2.3   Formation of Annual Rings

The growth activity of trees is not constant during a year. Variations are approximately coupled with the *seasons in our latitudes*, what results in *four periods of growth* within a year. Annual rings are generated in consequence of this climatic conditional phenomenon. The four growth periods read as:

Neutral phase from November to February: This phase is for *nutrient storage* and is also called dry season. There is no growth activity in this period.

Mobilization phase in March and April: In this phase, the nutrients stored during the neutral phase in winter are used. There is no growth activity in this period, but in a warm winter the following growth phase can start earlier, when the mobilization phase has not finished yet.

Growth phase from May to July: *Big lumens*, *thin cell walls* and *light colors* are the characteristics of cells which are built in the growth phase. The resulting tissue is also called earlywood. In contrast to latewood, earlywood has a wide texture appropriate to transport water and is *not mechanically stable.*

Deposition phase from August to October: Contrary to the cells generated in the growth phase, cells which were built in the deposition phase are *darker* with *smaller lumens* and *thicker cell walls.* They are refered to as latewood and *mechanically stabilizes* the wood tissue [13].

Chapter 3

Micromechanical Model for Wood Elasticity

All ingredients of wood affect the stiffness of the material in longitudinal, radial, and tangential direction. The computation of these stiffness values is done by means of a *micromechanical model* which starts at a nanometer level and scales up the stiffness values to a bigger length scales. This allows to determine *macroscopic stiffnesses of wood* from *mechanical and morphological properties* of its basic nanoscale constituents, namely cellulose, hemicellulose, lignin, extractives, and water, from the *arrangement of these constituents*, and from *changing densities* across the annual rings. The micromechanical model as well as its theoretical fundamentals are briefly reviewed in this chapter. To develop an understanding of wood micromechanics, the characteristic length scales of a wood tissue are shortly repeated at the beginning.

3.1 Length Scales of the Micromechanical Model

The characteristic length scales of microstructural features in wood include:

- spaces between cellulose fibers in wood cell wall filled by *polymer network* containing lignin molecules and hemicellulose molecules [8 to 20 nm],

- *cellulosic fiber* diameter [50 to 200 nm],

- thickness of *cell walls* [2 to 20 μm],

- *cell* diameter [20 to 40 μm], and

- thickness of *annual ring* [2 to 4 mm].

In order to link stiffness properties at various length scales, three homogenization steps are formulated. Thereby *continuum micromechanics* and the *unit cell method* are applied.

Continuum micromechanics is based on defining a so-called representative volume element (RVE) for the characterization of the heterogeneous microstructure of a material. One or more *homogeneous ingredients* with a characteristic dimension d_1 fill the *heterogeneous RVE* with the characteristic length l_1, which has to be small compared to the characteristic dimension L of the structure made up of the material. It is important that d_1 is at least an order of magnitude smaller than l_1 ($d_1 \ll l_1$). The phases can themselves exhibit a heterogeneous microstructure. Their stiffness may then be estimated by formulation of another homogenization step at smaller length scales. The characteristic length of the respective RVE, l_2, has to be smaller or equal to the characteristic dimension of the phase, d_1, and at least an order of magnitude larger than the typical dimensions of the micro-heterogeneities in this RVE, d_2. The whole *'separation of scale - condition'* reads as $d_2 \ll l_2 \leq d_1 \ll l_1 \ll L$. Homogenized materials with a typical length of l_1 could be the phases of a following homogenization step [Figure 3.1].
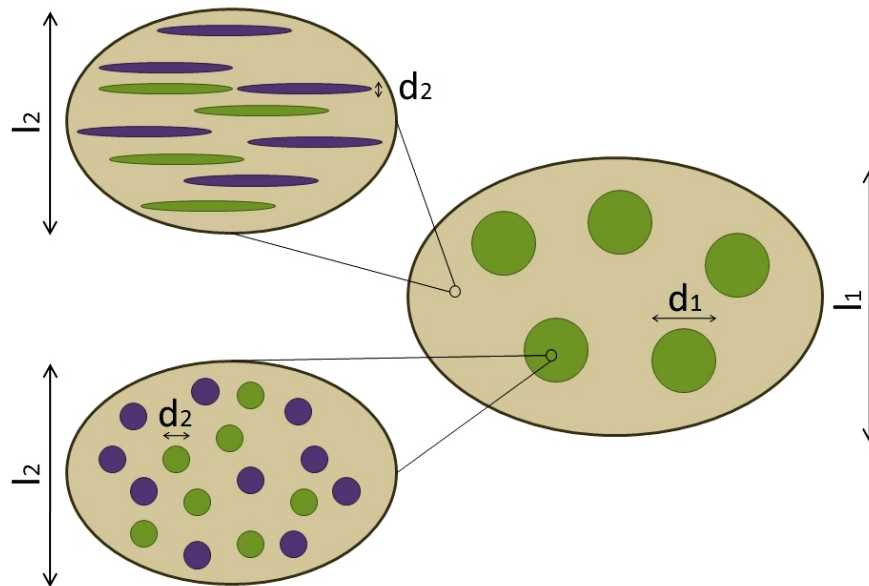
Figure 3.1: RVEs in multistep homogenization

In the unit cell method, the heterogeneous microstructure is represented by the basic periodically repeating unit (unit cell). The 'separation of scale-condition' is relieved here. While the dimensions of the structure and of the unit cell still have to be separated by at least one dimension, the micro heterogeneities inside the unit cell need not be small compared to the unit cell itself.

3.2 Fundamentals of Continuum Micromechanics

The explanations in this section for continuum micromechanics concern the *homogenization steps one and two* of the computer program. The fundamentals for the third homogenization step, which is performed by means of the unit cell method, are sketched in Section 3.4. In continuum micromechanics, the elastic behavior of the *homogenized material* is deter-

mined from the *material behavior* and the *arrangement of the single phases* in the RVE. In particular, the following characteristics of the single phases are considered:

- stiffness,

- dosage in the RVE,

- characteristic shape of the inclusions, and

- interactions with other phases.

Zaoui [14] formulated the relation between estimates for the stiffness tensor of a material, $\mathbb{C}^{est}$, and the stiffness matrixes and volume fractions of the phases in the following most general form:

$$\mathbb{C}^{est} = \sum_r f_r \mathbb{C}_r : \left[\mathbb{I} + \mathbb{P}_r^0 : \left(\mathbb{C}_r - \mathbb{C}^0 \right) \right]^{-1} : \left\{ \sum_s f_s \left[\mathbb{I} + \mathbb{P}_s^0 : \left(\mathbb{C}_s - \mathbb{C}^0 \right) \right]^{-1} \right\}^{-1}. \quad (3.1)$$

The *elastic stiffness* of each phase is defined by $\mathbb{C}_r$ or $\mathbb{C}_s$, respectively, and the *volume fraction* of each phase in the RVE is denoted by f_r and f_s. $\mathbb{I}$ stands for the fourth-order unity tensor. Both summations are executed over all phases. $\mathbb{P}_r$, which is a fourth-order tensor as well, accounts for the *characteristic shape of the inclusions of each phase r* in a matrix with a stiffness $\mathbb{C}^0$ [10]. Depending on the choice of $\mathbb{C}^0$ two different schemes are recovered

- the *Mori-Tanaka* scheme (MT in short), and

- the *self-consistent* scheme (SC in short).

The MT scheme is obtained if the stiffness matrix $\mathbb{C}^0$ is identical with the stiffness of one of the phases. It represents a *composite material* consisting of a *connected matrix* with *unconnected inclusions*. The SC scheme results if $\mathbb{C}^0 = \mathbb{C}^{est}$, what represents a dispersed arrangement of the phases typical for polycrystals, in which *all phases have mutual contact* [10].

Tissue-independent micromechanical phases: Amorphous cellulose, crystalline cellulose, lignin, hemicellulose, and water lumped together with extractives exhibit common properties in all wood tissues and, thus, serve as tissue-independent basic constituents in the micromechanical model. Because of their very small content, ashes are neglected in the model. These *five substances* are integrated in *three homogenization steps* (cf. Figure 3.2) in order to estimate the stiffness tensor of softwood. For hardwood, a fourth homogenization step is necessary. Since only spruce samples are considered in this thesis, the fourth homogenization step will not be detailed in the following (see [10] for a description).

STEP 1
self-consistent scheme
l = 8-20 nm

d = 1-5 nm

hemicellulose

lignin

extractives

water

STEP 2
Mori-Tanaka scheme
l = 0.5-1 µm

d = 6-10 µm

polymer network

crystalline cellulose

amorph. cellulose

d = 20-100 nm

STEP 3
unit cell method
l = 100-150 µm

l = 0.5-1 mm
SOFT WOOD
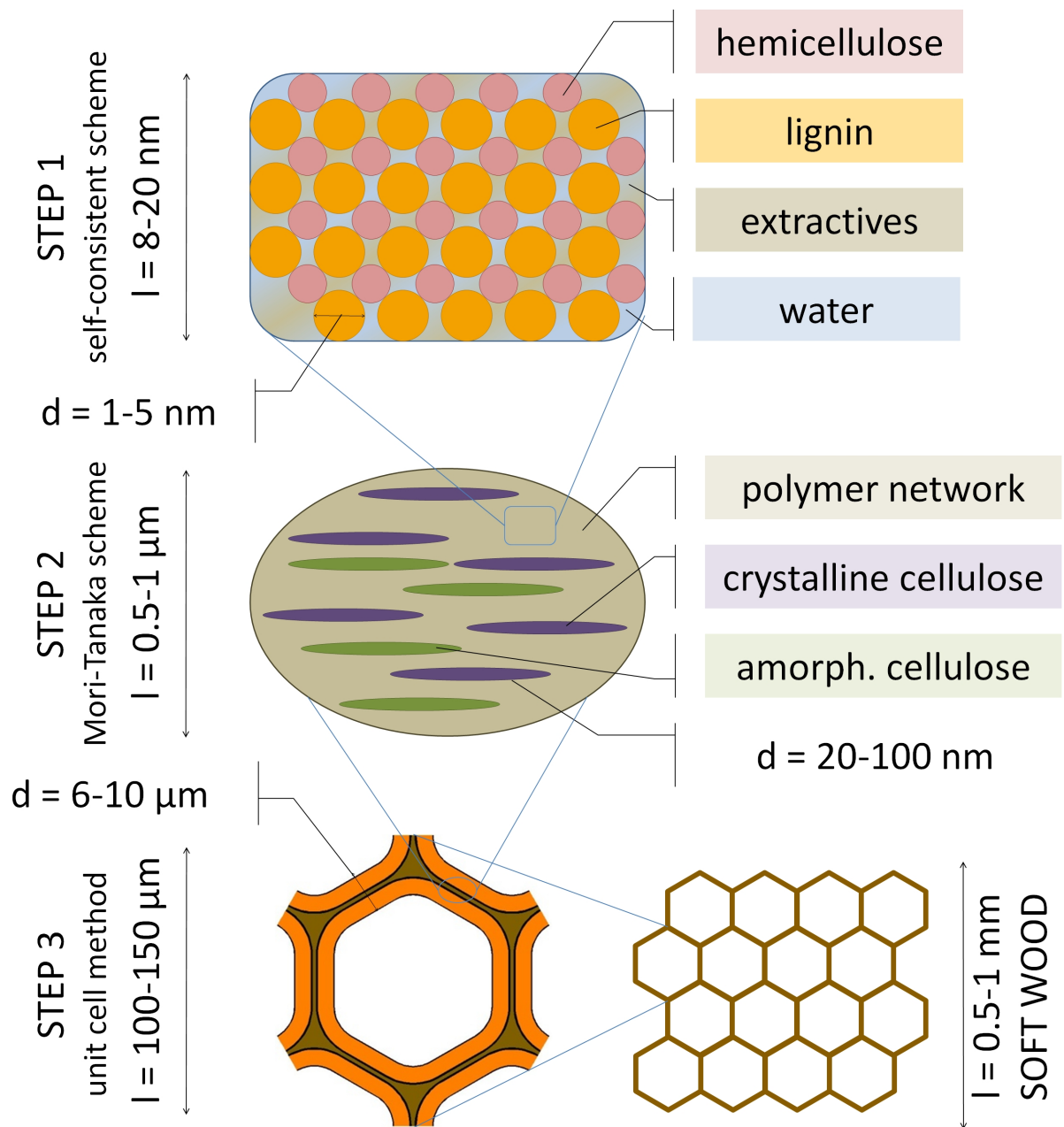
Figure 3.2: Homogenization steps for softwood

3.3 Micromechanics Model for Wood - Homogenization Steps One and Two

3.3.1 Self-Consistent Scheme: Polymer Network

The first step joins *hemicellulose, lignin, water* and *extractives* to a *polymer network* (Figure 3.2). This is done by means of the *self-consistent scheme*, with *spherically-shaped inclusions* and an *isotropic matrix*. The representative volume element (RVE) has a characteristic length of 8 to 20 nm and is filled with the first four ingredients with the volume fractions $\tilde{f}_{hemcel}$, $\tilde{f}_{lig}$, and $\tilde{f}_{H_2O+Ext}$, where

$$\tilde{f}_{hemcel} + \tilde{f}_{lig} + \tilde{f}_{H_2O+Ext} = 1 \,. \tag{3.2}$$

The self-consistent scheme is chosen because of the *dispersed arrangement* of the ingredients and the intimate mixing of polymers and water. So specifying Equation (3.1) for $r,s \in$ [*hemcel, lig, H_2O+Ext*], $\mathbb{C}^0 = \mathbb{C}_{polynet}^{SCI}$ and $\mathbb{P}_{hemcel}^0 = \mathbb{P}_{lig}^0 = \mathbb{P}_{H_2O+Ext}^0 = \mathbb{P}_{sph}^{polynet}$ results in the following equation

$$\mathbb{C}_{polynet}^{SCI} = \left\{ \sum_r \tilde{f}_r \mathbb{C}_r : \left[\mathbb{I} + \mathbb{P}_{sph}^{polynet} : \left(\mathbb{C}_r - \mathbb{C}_{polynet}^{SCI} \right) \right]^{-1} \right\}$$
$$: \left\{ \sum_s \tilde{f}_s \left[\mathbb{I} + \mathbb{P}_{sph}^{polynet} : \left(\mathbb{C}_s - \mathbb{C}_{polynet}^{SCI} \right) \right]^{-1} \right\}^{-1} \,. \tag{3.3}$$

$\mathbb{C}^r$ stands for the elasticity tensor of the isotropic phases and has the form

$$\mathbb{C}_r = 3k_r\mathbb{J} + 2\mu_r\mathbb{K} \,. \tag{3.4}$$

k_r is the *bulk modulus* and μ_r the *shear modulus* of phase r. $\mathbb{J}$ describes the *volumetric part* and $\mathbb{K}$ the *deviatoric part* of the fourth-order unity-tensor $\mathbb{I}$. They are defined as [10]

$$J_{ijkl} = 1/3 \ \delta_{ij}\delta_{kl} \,, \tag{3.5}$$
$$K_{ijkl} = I_{ijkl} - J_{ijkl} \,. \tag{3.6}$$

3.3.2 Mori Tanaka Scheme: Cell Wall Material

The second step joins *crystalline cellulose, amorphous cellulose*, and the *matrix from homogenization step one* to the *cell wall material* (Figure 3.2). This is done by means of the Mori-Tanaka scheme, with cylindrically-shaped inclusions and an isotropic matrix from Section 3.3.1. The individual cell wall layers are not considered in this homogenization step. Rather, an average value of the stiffness over the four cell wall layers is calculated. The RVE has a characteristic length of 0.5 to 1 μm, and the volume fractions of the ingredients are $f_{polynet}$ (first homogenization step), f_{crycel} and, f_{amocel} with

$$f_{polynet} + f_{crycel} + f_{amocel} = 1 \,. \tag{3.7}$$

The typical diameters of the cylindrical fiber-like inclusions of crystalline and amorphous cellulose are 20 to 100 nm. The Mori-Tanaka scheme is chosen because of the embedding

of the ingredients (fiber-like inclusions) in a matrix of polymer network. So specifying Equation (3.1) $r,s \in [polynet, crycel, amocel]$, $\mathbb{C}^0 = \mathbb{C}_{polynet} = \mathbb{C}_{polynet}^{SCI}$ from Equation (3.3) and $\mathbb{P}_{crycel}^0 = \mathbb{P}_{amocel}^0 = \mathbb{P}_{cyl}^{polynet}$, the following equation is obtained [10]:

$$
\begin{aligned}
\mathbb{C}_{cwm}^{MTI} \;=\; & \left\{ f_{polynet}\mathbb{C}_{polynet}^{SCI} + \sum_r f_r \mathbb{C}_r : \left[\mathbb{I} + \mathbb{P}_{cyl}^{polynet} : \left(\mathbb{C}_r - \mathbb{C}_{polynet}^{SCI} \right) \right]^{-1} \right\} \\
& : \left\{ f_{polynet}\mathbb{I} + \sum_s f_s : \left[\mathbb{I} + \mathbb{P}_{cyl}^{polynet} : \left(\mathbb{C}_s - \mathbb{C}_{polynet}^{SCI} \right) \right]^{-1} \right\}^{-1} .
\end{aligned}
\tag{3.8}
$$

3.4 Fundamentals of the Unit Cell Method

After these first two homogenization steps, the stiffness of softwood is calculated by the unit cell method, whose fundamentals are described in this section. The unit cell method is suitable for materials with a *periodic microstructure*, which can be represented by *uniform repeating basic elements*, so-called unit cells. The unit cell is subjected to *periodic, symmetry, or antisymmetry boundary conditions* for the displacements [15], such that the spatial averages of the corresponding strains are equal to the macroscopic strains related to the micro-heterogeneous material. The relation between the macrostrains and the macroscopic stresses yields the effective stiffness of the cellular material. For the ease of computation, unit macroscopic strain states are generally applied to the unit cell. This will be elaborated in relation to the third homogenization step in Section 3.5.1.

3.5 Micromechanics Model for Wood - Homogenization Step Three

3.5.1 Unit Cell Method: Softwood

The *third homogenization* step differs with respect to the method of calculation from the steps one and two. Inspection of the cross-section (plane in radial and tangential direction) of wood shows a *honeycomb-like structure of the cells*. A third homogenization step, by means of continuum micromechanics, with the material of the cell walls and cylindrical lumen pores as phases would not represent reactions in bending and shearing of the cell walls generally observed under transverse loading. This deficiency claims for a *homogenization procedure* that deals with *influences of bending and shear strains*. The unit cell method meets this requirement and is therefore used for the third homogenization step [16, 15]. This step completes the homogenization process (Figure 3.2) and provides estimates for the stiffness matrix $\mathbb{C}_{SW}^{UC}$. There, UC stands for 'unit cell method' and SW for 'softwood'.

Geometrical Input Parameters of Wood for the Unit Cell Method

The extraordinarily large extension of the wood cells in the longitudinal direction L, which is about 100 times the cross-sectional dimensions, allows *assumption of an infinite extension* of the unit cell in this direction. The honeycomb-like cross-section is defined by the relation

between its length l_R in radial direction R and the length l_T in tangential direction T, and by the inclination angle ϕ between the radial direction and the cell wall next to the radial axis as shown in Figure 3.3. The cross-sectional aspect ratio is defined as

$$\lambda = l_T/l_R \,. \tag{3.9}$$
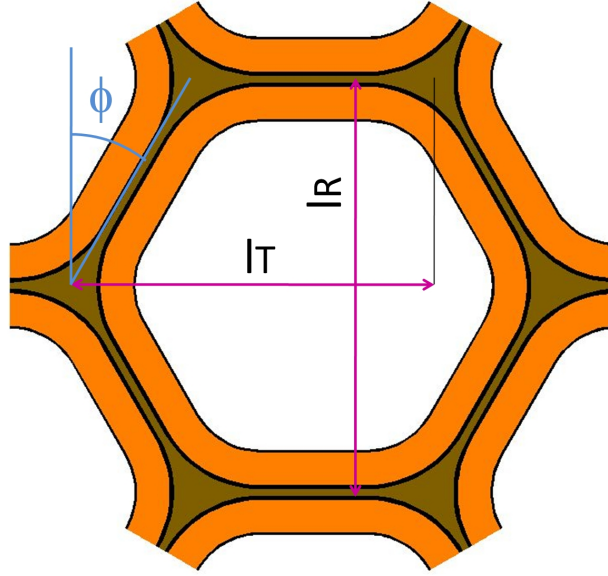
Figure 3.3: Definition of cross-sectional aspect ratio and of inclination angle

Procedure for Determination of Effective Stiffnesses

In order to identify the relations between applied macroscopic strains and resulting macroscopic stresses, *six independent displacement configurations* are imposed on the boundary of the unit cell, corresponding to unit values of macroscopic strain components [17], $E_{ij}, i, j = L, R, T$, namely

- symmetric longitudinal displacements $E_{LL}l_L = 1 \times l_L$ at the boundary produce unit axial strain in the L-direction,

- periodic radial displacements $E_{RR}l_R = 1 \times l_R$ at the boundary produce unit axial strain in the R-direction,

- symmetric tangential displacements $E_{TT}l_T = 1 \times l_T$ at the boundary produce unit axial strain in the T-direction,

- antisymmetric longitudinal displacements $2E_{TL}l_T = 2 \times l_T$ and $2E_{RL}l_R = 2 \times l_R$ at the boundary produce shear strains in the LT and LR-plane, and

- antisymmetric tangential displacements $2E_{RT}l_R = 2 \times l_R$ at the boundary produce unit shear strain in the RT-plane.

The components of the homogenized stiffness tensor $\mathbb{C}_{SW}^{UC}$ are equal to the spatial averages of the corresponding periodic microstresses. The respective equations for $\mathbb{C}_{SW}^{UC}$ depending on the stiffness of the cell wall material (from homogenization step two) and the geometric input parameters λ and ϕ are listed in the Appendix of [17].

Equation (3.10) shows an example for the first point in this itemization, at which a unit strain in the longitudinal direction L is applied. Association L with the first direction in a coordinate frame $1, 2, 3$ yields the following relations between macroscopic strains E_{ij} and macroscopic stresses σ_{ij} with $i, j = 1, 2, 3$:

$$
\begin{pmatrix} \sigma_{11} \\ \sigma_{22} \\ \sigma_{33} \\ \sigma_{12} \\ \sigma_{23} \\ \sigma_{31} \end{pmatrix} = \begin{bmatrix} \tilde{C}_{1111} & 0 & 0 & 0 & 0 & 0 \\ \tilde{C}_{2211} & 0 & 0 & 0 & 0 & 0 \\ \tilde{C}_{3311} & 0 & 0 & 0 & 0 & 0 \\ \tilde{C}_{1211} & 0 & 0 & 0 & 0 & 0 \\ \tilde{C}_{2311} & 0 & 0 & 0 & 0 & 0 \\ \tilde{C}_{3111} & 0 & 0 & 0 & 0 & 0 \end{bmatrix} \cdot \begin{pmatrix} \epsilon_{11} = 1 \\ \epsilon_{22} = 0 \\ \epsilon_{33} = 0 \\ \epsilon_{12} = 0 \\ \epsilon_{23} = 0 \\ \epsilon_{31} = 0 \end{pmatrix} . \tag{3.10}
$$

Thus, the component in the first column of the sought macroscopic stiffness tensor are equal to the resulting macrostresses. Analogously, the other five displacement configurations yields the remaining columns two to six of the macroscopic stiffness tensor.

An important factor at that third step is the *differing density* of the annual rings. While the input parameters for all other homogenization steps are constant in all points, the density changes across an annual ring and results in different relations between the cell dimensions and the thickness of the walls in third homogenization step by means of the unit cell method.

Chapter 4

Digitalization of Annual Rings and Determination of Local Stiffness Matrixes

The used continuum micromechanic model calculates the stiffness of wood, from the stiffness of the constituents, from their volume fractions, and from the varying densities of the annual rings, in three homogenization steps. The weight fractions of the constituents were determined at a chemical laboratory of the Institute of Wood Science and Technology at BOKU Vienna. These chemical analyses are described in Chapter A of the Appendix. The only *input parameter for the micromechanical model which varies across the annual rings*, is the density at a given point of the cross-section. This input value is *defined by the gray scales of a photo of the cross-section* like displayed in Figure 4.1. Besides the density, also the orientation of the principle material directions varies within a stem cross-section. This orientation also constitutes an important input value of the FEM-program for the investigation of the effect of the annual rings on deformation and stress fields in wood. Therefor the latewood bands are digitalized, and the local inclination angles of these bands are calculated from these digitalized coordinates of the bands.

4.1 Picture of the Cross-Section

The *color* of a point or an annual ring is related to the *size of the lumens* and the *thickness of the cell walls.* The thickness of the wall directly affects the stiffness of the cellular tissue, since the material of the walls is always approximately the same. So coloration or gray scale at a point, respectively, are an *indicator for the stiffness* of the wood tissue at this point of the cross-section. The latter correlation holds for spruce, but some other wood species produce pigments in the cell walls, so a checkup for this color effect would be necessary.
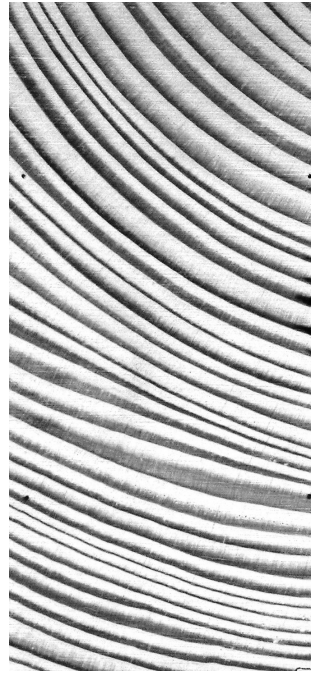
Figure 4.1: Example of a gray scale picture

4.1.1 Determination of Density from a Gray Scale Value

For a better handling the picture of the annual rings is transformed into a *gray scale picture*. At the importation into MATLAB every pixel of the photo is assigned a number between 0 (=black) and 255 (=white). This number reflects the gray scale of each pixel and is inserted into a matrix with the same number of components as there are pixels in the photo. After conversion of the gray scale values in corresponding densities, this provides the density information to the micromechanical model. Transformation of the photo in a gray scale picture is necessary to prevent the computation of three matrixes per picture (one for blue, one for red, and one for yellow).

In order to keep calculation times acceptable, only a limited member of user-defined density levels is considered, resulting in discrete approximation of the continuous density distribution. The stiffness matrixes corresponding to these density values are pre-calculated and are included in the input file of the computation.

4.2 Restructuring of the Stiffness Matrix

Homogenization steps one by three result in a stiffness matrix with the first axis aligned with the radial material direction, the second axis aligned with the tangential direction, and the third axis aligned with the longitudinal direction. In the finite element model, another assignment is chosen, so that the components of the matrix have to be rearranged. The following matrix (Equation (4.1)) shows the general occupation of the *stiffness matrix*

obtained from the *micromechanical model*:

$$\tilde{\mathbb{C}}_{SW}^{UC} = \begin{bmatrix} \tilde{C}_{1111} & \tilde{C}_{1122} & \tilde{C}_{1133} & \tilde{C}_{1112} & \tilde{C}_{1123} & \tilde{C}_{1131} \\ \tilde{C}_{2211} & \tilde{C}_{2222} & \tilde{C}_{2233} & \tilde{C}_{2212} & \tilde{C}_{2223} & \tilde{C}_{2231} \\ \tilde{C}_{3311} & \tilde{C}_{3322} & \tilde{C}_{3333} & \tilde{C}_{3312} & \tilde{C}_{3323} & \tilde{C}_{3331} \\ \tilde{C}_{1211} & \tilde{C}_{1222} & \tilde{C}_{1233} & \tilde{C}_{1212} & \tilde{C}_{1223} & \tilde{C}_{1231} \\ \tilde{C}_{2311} & \tilde{C}_{2322} & \tilde{C}_{2333} & \tilde{C}_{2312} & \tilde{C}_{2323} & \tilde{C}_{2331} \\ \tilde{C}_{3111} & \tilde{C}_{3122} & \tilde{C}_{3133} & \tilde{C}_{3112} & \tilde{C}_{3123} & \tilde{C}_{3131} \end{bmatrix}. \tag{4.1}$$

The matrix is symmetrical and the components in the top right quadrant and the bottom left quadrant (symmetry) as well as the off-diagonal components in the bottom right quadrant are equal to zero. So the *matrix* can be *simplified* to:

$$\tilde{\mathbb{C}}_{SW}^{UC} = \begin{bmatrix} \tilde{C}_{1111} & \tilde{C}_{1122} & \tilde{C}_{1133} & 0 & 0 & 0 \\ & \tilde{C}_{2222} & \tilde{C}_{2233} & 0 & 0 & 0 \\ & & \tilde{C}_{3333} & 0 & 0 & 0 \\ & & & \tilde{C}_{1212} & 0 & 0 \\ & symm. & & & \tilde{C}_{2323} & 0 \\ & & & & & \tilde{C}_{3131} \end{bmatrix}. \tag{4.2}$$

In the COMSOL FE-model (Chapter 5), the radial direction equals the y-direction (axis 2), the tangential direction equals the z-direction (axis 3) and, the longitudinal direction equals the x-direction (axis 1).

Thus, the matrix elements from the micromechanical model have to be rearranged by changing the indices in this mode:

- $\tilde{3} \to 1$,

- $\tilde{1} \to 2$,

- $\tilde{2} \to 3$.

This convention results in a *newly ordered matrix*:

$$\mathbb{C}_{SW}^{UC} = \begin{bmatrix} \tilde{C}_{3333} & \tilde{C}_{3311} & \tilde{C}_{3322} & 0 & 0 & 0 \\ & \tilde{C}_{1111} & \tilde{C}_{1122} & 0 & 0 & 0 \\ & & \tilde{C}_{2222} & 0 & 0 & 0 \\ & & & \tilde{C}_{2323} & 0 & 0 \\ & symm. & & & \tilde{C}_{3131} & 0 \\ & & & & & \tilde{C}_{1212} \end{bmatrix}, \tag{4.3}$$

which is *relabeled* in the following way:

$$\mathbb{C}_{SW}^{UC} = \begin{bmatrix} C_{1111} & C_{1122} & C_{1133} & 0 & 0 & 0 \\ & C_{2222} & C_{2233} & 0 & 0 & 0 \\ & & C_{3333} & 0 & 0 & 0 \\ & & & C_{1212} & 0 & 0 \\ & symm. & & & C_{2323} & 0 \\ & & & & & C_{3131} \end{bmatrix}. \tag{4.4}$$

4.3 Stiffness Values for all Finite Elements

Until now, the stiffness matrixes are *estimated for user-defined densities* which are *independent from the gray scale picture* and the matrix with densities that is generated from the cross-section picture, respectively. In the finite element simulations, the density has to be determined at each integration point of the elements. In order to link the finite element mesh to the gray scale picture, the coordinates of the integration points of the finite elements in the cross-section are needed. This information is obtained from a *first run of the finite element model* without consideration of stiffness variations in the cross-sectional plane. During this computation, the finite elements mesh is generated, and an intermediate step saves the sought *coordinates of the integration points*. For each direction one file with coordinate values is created (for example: *y_info_3d.dat* for all values of the y-direction). The next step is the generation of a matrix, named *integration point coordinates* (IPC in short), with two columns (first column for y-coordinates and second column for z-coordinates) that includes all coordinates of all integration points. That information is applied to the cross-section picture, and the gray scale values are fetched and converted to densities. With the same process as for the compilation of the coordinates, values of densities are consolidated in a vector named *density_vector*. This vector must have the same length as the number of lines in the IPC matrix.

Now the components of the density matrix are compared to the pre-defined densities, for which the micromechanical model has been evaluated. The stiffness matrixes obtained for the density coming closest to the respective entry in the density matrix are taken and compiled in a big matrix. The latter matrix, including the stiffnesses of all integration points, has six columns according to the six columns of the stiffness matrix, while the number of rows is six times the number of integration points. That way, the *first effect* of the annual rings, namely the *variation of stiffness* in a ring, is implemented into the computer program. The *second effect*, namely the *varying orientation* of the local principal material directions, remains to be considered. This requires a *change of the base system from local orientations* of radial and tangential direction to a global system, which is the same for the whole cross-section.

4.4 Changing Base System of the Stiffness Matrix

Annual rings have an *approximately circular shape*. Considering a cross-section, radial and tangential direction change from point to point, while the longitudinal direction remains more or less the same. So the *second effect* of the annual rings, next to the density-dependent stiffness variations, are the *locally different orientations of the principal material directions*. The local orientation of the radial and tangential direction is important because of the pronounced *anisotropy of wood*. Wood is approximately ten times stiffer in longitudinal direction than in radial direction, while the stiffness in tangential direction is approximately half of the radial stiffness.

The determination of the orientation of the radial and the tangential direction is based on the digitalization of the annual rings of the gray scale picture. After the registration of the points of all latewood rings, the local angles of the tangents to the annual ring points are estimated by the chord of an arc segment around an annual ring point, with the

annual ring point as midpoint of the arc segment. In the following, the determination of the annual rings by search algorithms, the determination of the local orientations of the principal material direction as well as the according transformation of the stiffness matrix are described in detail.

4.4.1 Digitalization of the Annual Rings

All following steps are coded in the file DIPL_cut_tree_rings.m!

Fundamentals

The procedure, in which all points of the *dark latewood bands* are identified, starts at the left top corner of the photo. A coordinate system with the y-direction pointing rightward, and the positive z-direction pointing upward is introduced. For a better detection all pixels which are darker than 130 are set to 10 and all pixels lighter than 180 to 245.

Digitalization Start

Each picture has borders on the *top*, *left*, *bottom*, and *right* side. In a first step, the first row or column of pixels, respectively, next to these borders is scanned in order to identify annual rings which start at the border. The coordinates of the starting points of all annual rings at all borders are collected in a matrix for each border (*mwcotr_t* = matrix with coordinates of tree ring _ top border). In this matrix, the first two columns are reserved for the z- and y-coordinate of the first annual ring, the third and fourth columns for the z- and y-coordinate of the second annual ring, and so on. The rows of the matrix refer to successive points of the annual rings. Only the first matrix row is defined in the first step showing the start of each annual ring.

Annual Ring Starts

Only dark *latewood bands* of each annual ring are detected (Figure 4.2), but the program code is in principle upgradeable for the light bands as well. For the ease of notation, the term annual ring will be used for its latewood part only in the following. In the first pixel-row of a picture, all pixels lighter than an assigned value are switched to ones, and all other to zeros. All *series of ones* characterize the *start of an annual ring*, and the starting point is defined at the middle of the series of ones. The coordinates of these starting points are registered in the matrix *mwcotr_t*, which is described in the previous section. Another factor that is stored is the number of annual rings starting at each border (*notr_t* = number of tree rings _ top border), which is necessary to define the number of loops in the following steps.

Progressive Digitalization

For the following program step, the starting point is placed on the beginning of an annual ring, defined by the coordinates of the previous section. From that point a *search algorithm* (Figure 4.2) advances along the annual ring to the next row (or column for left and right

border) of pixels. The band in which the pixels are scanned contains 40 pixels to the left and 40 pixels to the right in this row. For example when the search algorithm comes from the first line to the second line of pixels, it starts scanning pixel by pixel to the right. After it has found two subsequent pixels that have not the adjusted darkness, the search algorithm ends for the right side. The same procedure is performed to the left side as shown in Figure 4.2. The point, which indicates the *location of the latewood band of an annual ring* in the second row of pixels, is then defined by the *middle of right and left end* of the scanned section. The program detects this point and writes its coordinates in the second row of the matrix with the coordinates of annual ring points (*mwcotr_t*). This algorithm runs from the top border to the end of the annual ring. If the annual ring reaches any other border or turns into the reverse direction, the search algorithm stops.

Figure 4.2: Search algorithms

The same procedure is also applied to the left, bottom, and right border. *In short, vertical annual rings are analyzed by horizontal search algorithms in vertical progress (Table 4.1). Horizontal annual rings are analyzed by vertical search algorithms in horizontal progress.*

The individual search algorithms for top, left, bottom, and right border can be switched on independently of the other search and computation algorithms. After digitalization of all annual rings that start at one border, the matrix with coordinates of annual rings is saved in a mat-file (*mwcotr_t.mat* = outsourced matrix with coordinates of tree rings _ top

Name	Annual rings	Coordinates	Searching start	Search algorithm (sa)
top	*notr_t*	*mwcotr_t*	top border	horizontal sa - vertical down
left	*notr_l*	*mwcotr_l*	left border	vertical sa - horizontal rightwards
bottom	*notr_b*	*mwcotr_b*	bottom border	horizontal sa - vertical up
right	*notr_r*	*mwcotr_r*	right border	vertical sa - horizontal leftward

Table 4.1: Table of search algorithms and corresponding scanning

border).

In this way all annual rings that end at a border are going to be scanned. The output of this digitalization procedure for sample 28 as considered in Chapter 6 is shown in Figure 4.3.

a) gray picture with annual rings

b) digitalization of the annual rings

c) local orientation of radial direction
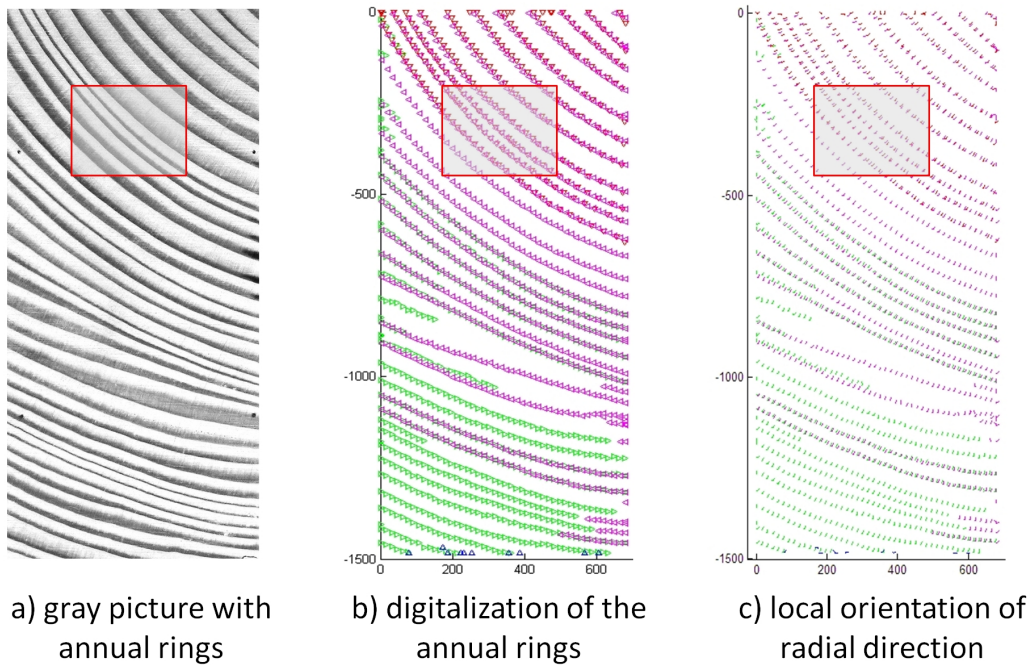
For a better description only the fifteenth points are shown in Pictures b), c), e), and f).

d) earlywood and latewood at an annual ring

e) triangles show the algorithm progress

f) arrows show the local orientation of radial direction
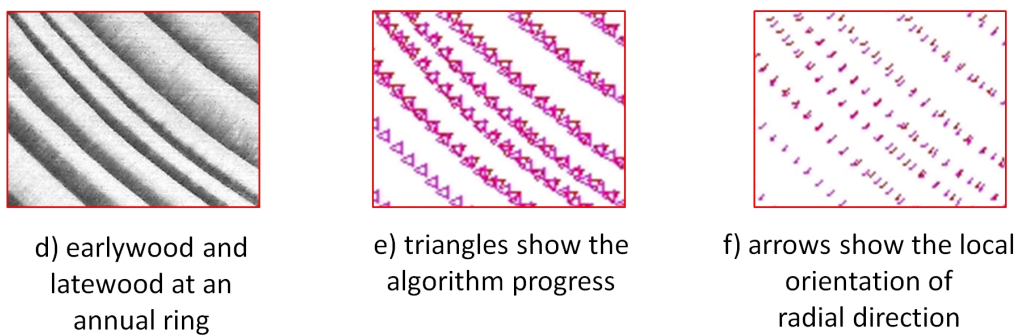
Figure 4.3: Digitalization of the annual rings

Second Run of Progressive Digitalization

A big problem of this algorithm are annual rings which start at one border and end at the same border. The digitalization algorithm detects two starting points for this annual ring, but this can easily be handled by the algorithm.

Problems arise from the changing direction of such rings perpendicular to the starting direction of the annual ring and to the algorithm progress direction, respectively. For example, a search algorithm starts at the top border and scans a nearly horizontal annual ring with a vertical progress. Big inaccuracies will be generated by the search algorithm in this case. The same problem exists, if the annual ring changes the progression rectangular to the search algorithm.

The inaccuracies can be prevented by a *second searching run*. For example, after completing the digitalization of an annual ring, which was checked with a horizontal search algorithm in vertical progress, a second run with a vertical search algorithm in horizontal progress is added. The same strategy is pursued for annual rings which are inspected with a vertical search algorithm in horizontal progress at the first run.

Second runs of searching are possible for all borders and can be individually switched on and off. Also for the second runs, matrixes with coordinates of annual rings are generated (*mwcotr_t2* = matrix with coordinates of tree rings _ top border second run) and stored in the internal mat-format of MATLAB (*mwcotr_t2.mat*).

4.4.2 Determination of the Local Inclination of the Annual Rings

The digitalization of annual rings out of a picture is required for determination of the *local orientation* of the *principal material directions* in the integration points of the finite elements. So the next step is to evaluate these orientations, in terms of inclination angles β for the tangential direction and α for the radial direction (Figure 4.4), from the coordinates of the annual rings.

All following steps coded in the file DIPL_alpha_cut_tree_rings.m!

At first, the code loads all needed matrixes with coordinates of annual rings and determines the number of annual rings (for example *notr_l*). For determination of the local inclination angle of the annual ring at a given annual ring point, an arc segment is constructed with the considered point in the middle. For a point with coordinates y and z (shown in Figure 4.4 as red point), the coordinates of the end points of the arc segments are five and six positions ahead and behind the considered point (shown in Figure 4.4 as orange and yellow points). Pairs of these points define the *chords of two arc segments*, and the *angles of these chords* in relation to the alignment of the picture define the *inclination angles* β_1 and β_2 of tangents to the annual ring at the given point. Two arc segments are considered to improve the accuracy of the algorithm. Finally the mean value of the two segments $\beta_m = \frac{1}{2} \cdot (\beta_1 + \beta2)$ is used as inclination angle of the tangential direction. This angle plus 90° (angle α) specifies the orientation of the radial direction. This angle is used for the transformation of the stiffness matrix at each integration point in the FE-simulation.

The angles α for all annual rings points are stored in a matrix (*mwaotrp_t* = matrix with angles of tree ring points _ top border). In combination with the matrix for the coordinates

Figure 4.4: Calculation of the local orientation of the radial and tangential directions

of the annual rings, the angles are clearly assignable. The matrix is also outsourced into a mat-file (*mwaotrp_t.mat*).

For checking purposes, it is possible to print the angles as arrows in a picture (Figure 4.3). This option can be switched off in order to considerably save computation time and memory reservation.

4.4.3   Digitalization of the Closed Annual Rings

Until now, the described program only detects annual rings that end at a border.

The following steps, dealing with the digitalization of closed annual rings in the cross-section, are coded in the file DIPL_complete_tree_rings_top.m! This name is also exemplary for all other borders.

Loading of the matrixes with the coordinates of truncated annual rings, which have already been digitalized, is the first step of this program. Before the computation the following parameters have to be set in the input-file:

- *cip* = 1 or 0; *cip* = center in picture; a value of 1 indicates the existence of closed annual rings in this picture.

- *noctr* = value; *noctr* = number of continuous annual rings; this parameter specifies how many latewood rings are in the picture.

- *nsoctr* = 5, 6, 7 or 8; *nsoctr* = nearest side of continuous annual ring; the number specifies which border is nearest to the outermost closed annual ring (5=top, 6=left, 7=bottom, and 8=right).

The value *nsoctr* controls at which border the program searches for the *last cut annual ring* in front of a complete annual ring. From the starting point of this cut annual ring, the algorithm advances 20 pixels along this annual ring and imports the coordinates of the reached annual ring point and the angle of the normal to this annual ring at this point. The search algorithm then follows the *direction towards the inside* until a new annual ring is recognized. That is the *first continuous annual ring*, which is digitalized as described in the following section.

Determination of Closed Annual Rings

In principle the procedure is the same as for the cut annual rings, and the same problems are encountered. The coordinates of the annual ring points are saved in a matrix (*mwcoctr_1* = matrix with coordinates of closed tree rings _ 1-direction). From the first detected point the search algorithms shown in Table 4.2 are executed:

After these search algorithms the *program proceeds to the next annual ring* until the predefined number of closed annual rings is reached. So every ring will be analyzed clockwisely and anticlockwisely. First all algorithms searching anticlockwisely are run (i.e. consecutively algorithms 1, 3, 5, 7, and 9), and only afterwards the algorithms searching

Number	Searching direction anticlockwise	Coordinates
1	horizontal search algorithm with vertical progress down	*mwcoctr_1*
3	vertical search algorithm with horizontal progress right	*mwcoctr_3*
5	horizontal search algorithm with vertical progress up	*mwcoctr_5*
7	vertical search algorithm with horizontal progress left	*mwcoctr_7*
9	horizontal search algorithm with vertical progress down	*mwcoctr_9*
Number	Searching direction clockwise	Coordinates
2	horizontal search algorithm with vertical progress up	*mwcoctr_2*
4	vertical search algorithm with horizontal progress right	*mwcoctr_4*
6	horizontal search algorithm with vertical progress down	*mwcoctr_6*
8	vertical search algorithm with horizontal progress left	*mwcoctr_8*
10	horizontal search algorithm with vertical progress up	*mwcoctr_10*

Table 4.2: Table for search algorithms of closed annual rings

clockwisely are started (i.e. consecutively algorithms 2, 4, 6, 8, 10). This procedure prevents inaccuracies and produces *ten matrixes with coordinates of closed annual rings* as output.

4.4.4 Determination of the Local Inclination of the Closed Annual Rings

The procedure for evaluation of the angles of closed annual rings is the same as for the cut annual rings and is done by the file *DIPL_alpha_complete_tree_rings.m*. This file produces ten matrixes with local inclination angles according to the ten search algorithms of Table 4.2 (*mwaotrp_1* = matrix with angle of tree ring points _ direction 1) and saves them in mat-files.

4.4.5 Example of the Matrixes

This section demonstrates the digitalization procedure for an exemplary single annual ring. Figure 4.5 shows the picture with the annual ring. The pixels are defined by the coordinates in y- and z-direction, which are specified at the top border and the left border. The middle of the latewood band is defined by the black pixels. For a better orientation, these black pixels are serially identified by the letters A to P.

Table 4.3 shows the vectors with coordinates for this annual ring. The entries *pp* and *np* indicate the previous point and the next point, respectively, for the determination of the angle of the tangent at each point. If there is no previous point for the determination, such as near the borders, the algorithm uses the first point or the last point of the considered annual ring, respectively. Only a search algorithm with six points ahead and aback of the point of determination is chosen in this example. In the matrixes of coordinates for the FE-calculation, multiple coordinate matrixes of the individual annual rings that start at one border are arranged in series.
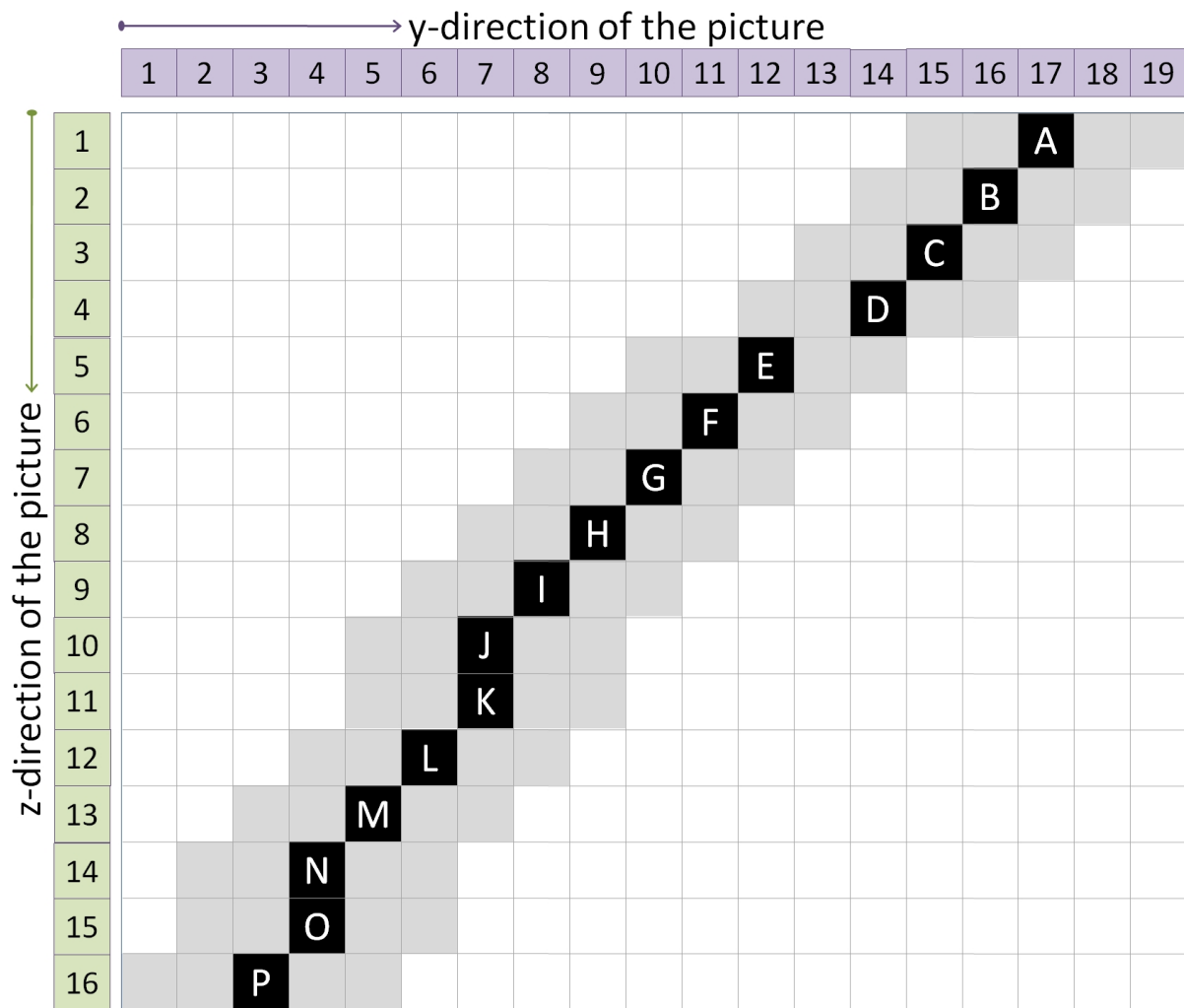
Figure 4.5: Example for the digitalization of an annual ring

Pixel	z-coor.	y-coor.	pp	np	Δz	Δy	angle β	angle α
letter	*mwcotr_t*	*mwcotr_t*						*mwaotrp_t*
A	1	17	A	G	6	-7	0.70863	2.27943
B	2	16	A	H	7	-8	0.71883	2.28963
C	3	15	A	I	8	-9	0.72664	2.29744
D	4	14	A	J	9	-10	0.73282	2.30362
E	5	12	A	K	10	-10	0.78540	2.35620
F	6	11	A	L	11	-11	0.78540	2.35620
G	7	10	A	M	12	-12	0.78540	2.35620
H	8	9	B	N	12	-12	0.78540	2.35620
I	9	8	C	O	12	-11	0.82885	2.39965
J	10	7	D	P	12	-11	0.82885	2.39965
K	11	7	E	P	11	-9	0.88507	2.45587
L	12	6	F	P	10	-8	0.89606	2.46686
M	13	5	G	P	9	-7	0.90975	2.48055
N	14	4	H	P	8	-6	0.92730	2.49810
O	15	4	I	P	7	-5	0.95055	2.52135
P	16	3	J	P	6	-4	0.98280	2.55360

Table 4.3: Example for matrixes with annual ring info

The calculation steps behind Table 4.3 are explained taking, point K as an example. First, the points six positions ahead and aback K are specified, which are the points E and P. These points define the chord of an arc with coordinate differences Δz_K and Δy_K. From these differences, the inclination angles of the tangent and the normal to the annual ring at point K, denoted by β_K and α_K, are computed. The numerical relations read as:

$$
\begin{aligned}
z_E &= 5 & ; \quad y_E & & &= 12 \\
z_P &= 16 & ; \quad y_P & & &= 3 \\
\Delta z_K &= z_P - z_E &= 16 - 5 & & &= 11 \\
\Delta y_K &= y_E - y_P &= 12 - 3 & & &= 9 \\
\beta_K &= arctan(\Delta z_K / \Delta y_K) &= arctan(11/9) & & &= 0.88507 \\
\alpha_K &= \beta_K + \pi/2 &= 0.88507 + 1.57080 & &= 2.45587
\end{aligned}
\tag{4.5}
$$

4.4.6 Merging of Matrixes with Coordinates and Angles

The described procedure results in 18 matrixes with coordinates (1 matrix for each border [4 Matrixes], 1 matrix for the second run of searching for each border [4 Matrixes], and 2 × 5 matrixes for the closed annual rings [10 Matrixes]), and 18 matrixes with angles (same partition as for the matrixes with coordinates). For a better handling the file *DIPL_alpha_matrix.m* concentrates this matrixes into a single matrix (*alpha_mat* = alpha matrix) and stores it in a mat-file (*alpha_mat.mat*). Each row of this matrix is assigned to a specific z-coordinate and each column to a specific y-coordinate of pixel in the digitalized picture. The *components* of this matrix are the *angles* of the annual rings at the points

with coordinates specified by the position of the component in the matrix.

The program runs through all matrixes with coordinates and retrieves the information of angles and associated coordinate pairs for all detected annual ring points in all matrixes. The values are then used to fill the matrix with angles, where duplicate values are simply signed over the original entries.

At the end, a matrix that has the *same dimensions as the number of pixels in the picture* is obtained. For pixels not belonging to an annual ring, a zero is entered at the position specified by the z- and y-coordinate of this pixel.

4.4.7   Transformation of the Stiffness Matrix

With the matrix of angles and the coordinates of the integration points, a *vector* including the *angles at the integration points* is produced. For example, the first coordinate pair is taken from the matrix with the integration point coordinates, and used to find the entry in the matrix with angles, for which the corresponding z- and y-coordinate approach most closely the given integration point coordinates. But not all values in *alpha_mat* represent an angle. Points that have not been detected by the digitalization algorithm of the annual rings have the value zero. If there is an integration point of a finite element at such a point, an *algorithm* will search *in squares around this point* with a rising search area until the procedure finds a non-zero entry indicating the inclination angle at the closest annual ring point. This yields a suitable approximation.

The *angles* specify the *rotation of the global coordinate frame* against the local frames aligned with the *normals and tangents to the annual rings*. They are used for the transformation of the locally defined stiffnesses to the global frame used in the FE-model. Since the local longitudinal direction is parallel to the global x-direction, only a *rotation about the x-direction or longitudinal direction* is necessary.

3D Transformation

For correct transformation of the stiffness values, Euler's rotation theorem is applied to the stiffness matrixes. Euler described a rotation by using *three angles*, named χ-*convention*. In a cartesian coordinate system these three rotations are defined by:

1. rotation around z-axis by angle ϕ,

2. rotation around new x-axis called ζ-axis by angle θ, and

3. rotation around new z-axis called z'-axis by angle ψ as

shown in Figure 4.6. Therein, θ defines the *rotation of tangential and radial axis around the longitudinal axis*. The rotation matrix can be composed of the according matrixes for the individual rotations and is defined as:

$$nn = \begin{pmatrix} cos\,\psi & sin\,\psi & 0 \\ -sin\,\psi & cos\,\psi & 0 \\ 0 & 0 & 1 \end{pmatrix} * \begin{pmatrix} 1 & 0 & 0 \\ 0 & cos\,\theta & sin\,\theta \\ 0 & -sin\,\theta & cos\,\theta \end{pmatrix} * \begin{pmatrix} cos\,\phi & sin\,\phi & 0 \\ -sin\,\phi & cos\,\phi & 0 \\ 0 & 0 & 1 \end{pmatrix}, \qquad (4.6)$$
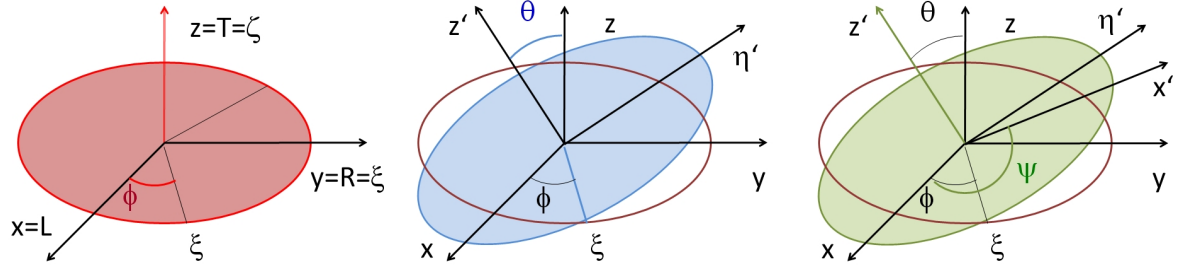
χ- convention:

1.Rotation by angle φ around **z-axis**
2.Rotation by angle θ around ζ**-axis** (new x-axis)
3.Rotation by angle ψ around **z'-axis**

Figure 4.6: 3D rotation with the χ-convention

so that the components of the global rotation matrix read as

$$
\begin{aligned}
nn_{11} &= \cos\psi * \cos\phi - \cos\theta * \sin\phi * \sin\psi\,, \\
nn_{21} &= -\sin\psi * \cos\phi - \cos\theta * \sin\phi * \cos\psi\,, \\
nn_{31} &= \sin\theta * \sin\phi\,,
\end{aligned}
\tag{4.7}
$$

$$
\begin{aligned}
nn_{12} &= \cos\psi * \sin\phi + \cos\theta * \cos\phi * \sin\psi\,, \\
nn_{22} &= -\sin\psi * \sin\phi + \cos\theta * \cos\phi * \cos\psi\,, \\
nn_{32} &= -\sin\theta * \cos\phi\,,
\end{aligned}
\tag{4.8}
$$

$$
\begin{aligned}
nn_{13} &= \sin\psi * \sin\theta\,, \\
nn_{23} &= \cos\psi * \sin\theta\,, \\
nn_{33} &= \cos\theta\,.
\end{aligned}
\tag{4.9}
$$

Applied to the stiffness tensor $\mathbb{C}_{SW}^{UC}$, the components of this tensor in the rotated base frame, $C_{rot,ijkl}$, read with $i,\,j,\,k,\,l,\,m,\,n,\,p,\,q \in [1,2,3]$ as

$$
C_{rot,ijkl} = C_{SW,mnpq}^{UC} * nn_{im} * nn_{jn} * nn_{kp} * nn_{lq}
\tag{4.10}
$$

In this thesis only angle θ is non-zero as described above.

Chapter 5

FEM-Program

The main objective of this thesis is to develop a computer program that includes the effects of *different stiffnesses* and *changing orientations* of the *principal material directions* across the grown annual rings of wood in a FEM-model. The previous two Chapters 3 and 4 are combined in this chapter. The algorithms and programs described there provide the matrix with the homogenized and transformed stiffness values for all integration points of the finite elements, which serve as basic input for the following developments. The FEM-program COMSOL is used because of the option to define the model in an m-file which can be manipulated in MATLAB. So the determination of the local density-dependent stiffnesses and the transformation of the stiffness matrixes are performed with MATLAB and then included into a FEM-file generated by COMSOL.

5.1 Steps with COMSOL and MATLAB

5.1.1 Creating an m-File with the Model Definition by COMSOL

At the beginning of the programming sessions, a basic FE-model is generated with the pre-processor of COMSOL, which will afterward be changed in MATLAB and adapted to the *specific features of the investigated wood samples*.

Boundary Conditions

For reducing the calculation time only a thin cuboid was created, which shows the same behavior as a cuboid with a realistic thickness in case of unconstrained lateral deformation. After this all boundary conditions are defined. Fixation points and areas are defined in terms of the length in x-direction, l_1, the width in y-direction, l_2, and the height in z-direction, l_3, of the cuboid (see Figure 5.1) and read as:

- base area $(x_1,x_2,0)$ fixed in z-direction,

- corner $(0,0,0)$ fixed in x-direction,

- corner $(0,l_2,0)$ fixed in x-, and y-direction,

- corner $(l_1,l_2,0)$ fixed in y-direction,

Moreover, a uniform displacement in z-direction is applied to the upper surfaces (x_1,x_2,l_3) of the sample (Figure 5.1). The dimensions l_1,l_2,l_3 of the cuboid are only placeholders for the time being and are later changed by MATLAB for each sample.
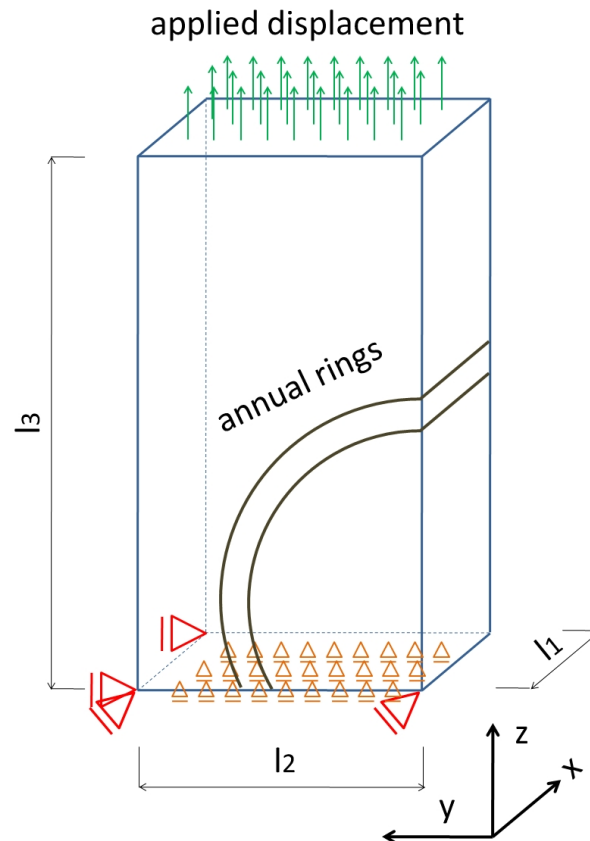
Figure 5.1: Boundary conditions of the samples

Finite Element Mesh

Beside the boundary conditions, the elastic material properties and the *unstructured FE-mesh* (Figure 5.2) are defined for the cuboid. As the dimensions, also the material and mesh parameters will be changed in the MATLAB programming code later on. The dimension of the finite elements are changed by MATLAB to place approximately *two elements* in the *width of the latewood band* of an annual ring. Figure 5.2 shows the FE-mesh used in the examples of Section 5.4. These finite elements have the *shape of tetrahedra* with *linear interpolation functions* and *four integration points*.
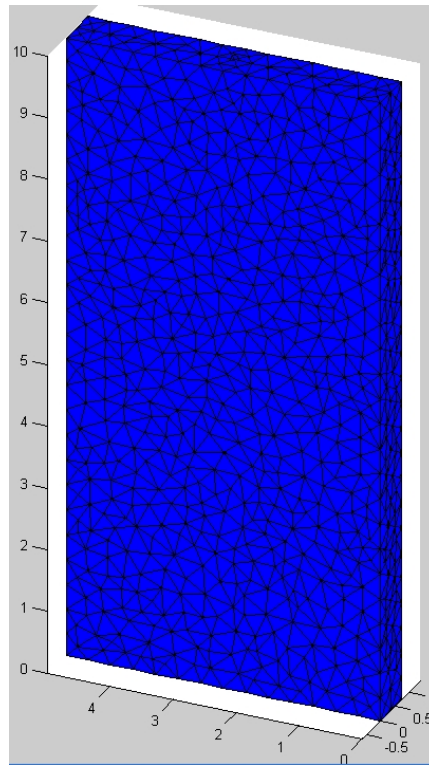
Figure 5.2: Exemplary FE-mesh

Postprocessing

These first steps enable COMSOL to compute the described little example. In the last step, the *postprocessing options* and desired displays are specified, which also appear in the m-file. COMSOL generates this m-file with the normal storage act, adding the extension *.m* to the specified filename. To enable later modification of the model in the preprocessor, the produced file should also be saved as *fl-file*, which is the internal simulation file format of COMSOL.

5.1.2 Modify the m-File in MATLAB

M-files generated by COMSOL can be executed in MATLAB and changed as described in the following steps.

5.2 Superior File

The superior file is named as equc_woodplane_v6_2.m!

The central file of the computer program takes control of of the *determination of the finite elements mesh*, *two FE-calculations*, and the *postprocessing* in COMSOL. The executions of the files for the digitalization of the annual rings, the determination of the

inclination angles, the use of the micromechanical model, and the allocation of the stiffness values to the coordinates of the integration points, are coded in MATLAB.

Before the start of the computations, this superior file deletes all *mat-* and *dat-*files from former program executions. So, no wrong information can falsify the performance. For determination of the coordinates and angles of all annual rings as described in Chapter 4, the superior file calls the function *DIPL_cut_tree_rings.m*. After that, the first out of two FEM-calculations starts. The purpose of this *first run* with constant stiffness across the whole sample is to relieve the *coordinates of the integration points of the finite elements*. This information is stored in *three dat-files* for the x-, y- and z-coordinates, respectively (*x_info_3d.dat*, *y_info_3d.dat*, and *z_info_3d.dat*). The *origin* of the *global coordinate frame in COMSOL* is at the *down right corner* with the positive y-direction pointing leftwards and the positive z-direction pointing upwards. The *origin* of the *global coordinate frame in the digitalization* of the picture is at the *top left corner* with the positive y-direction pointing rightwards and the positive z-direction pointing downwards. To combine these two definitions of coordinate frames, the results of the digitalization process have to be mirrored by the vertical central axis in z-direction and the horizontal central axis in y-direction of the simulated cuboid.

5.3 Combination of FE-Model, Annual Ring Digitalization, and Micromechanical Model

The *combination* of the information about *coordinates* and *angles* from the annual ring digitalization with the *micromechanical model* follows in the file *DIPL_image_input.m*! The first step is the calculation of a density matrix. In an input-file, the *densities of earlywood* and *latewood* and the *corresponding gray scales* are specified. These values enable computation of a conversion factor between gray scale values and densities. Between these defined density values, the densities at other gray scales are *linearly interpolated*. The density matrix is generated by calculation of the densities for the gray scales of all pixels in the picture. This is done fast because of using simple multiplication of a matrix by the conversion factor determined before.

The second step is determination of the coordinates of the integration points of the finite elements. For this purpose, the three files *x_info_3d.dat*, *y_info_3d.dat*, and *z_info_3d.dat*, generated during the first run of the FE-program, are imported into the computation. The x-coordinate is not required in the following because of the almost homogeneous material behavior in this direction. The *y- and z-coordinates* are brought together in a matrix with *two columns* (first column = y-direction, second column = z-direction) which is called *IPC* (integration point coordinates). The entries of IPC are defined in *unit meters out of COMSOL*. The *unit of a picture is pixels* and has initially no direct relation to the unit meters of the integration point coordinates. Therefore the values of the *IPC* matrix are scaled to the units of the picture.

With this information about the coordinates, a *vector with densities* from the density matrix for all coordinate pairs of the matrix *IPC* is produced. For all these densities, the micromechanical model is evaluated in order to estimate the corresponding stiffness matrixes. For an easier handling *all stiffness values* are *saved outside* in individual files,

for example in the file *C2233.mat* for the stiffness component *C2233*. During the second FEM-calculation, COMSOL reads the stiffness values at each integration point from these files. For example, the importing file for the stiffness component *C2233* is called *stiffness_3d_C2233.m*. That way the two effects of *varying stiffness* and *rotating material directions* are embedded into the FEM-program.

5.3.1 Compilation of Developed Program Codes

To get a survey of the computer program, all files are listed in the following table and are shortly described:

- *equc_woodplane_v6_2.m*

    - superior file
    - call of m-files *DIPL_cut_tree_rings.m*, *DIPL_eingabe.m*, *koord_info_3d(x,y,z).m*, and *DIPL_image_input.m*
    - first FEM-calculation for compilation of integration point coordinates of the finite elements
    - second FEM-calculation with consideration of locally varying stiffness matrixes
    - control of postprocessing and solution plotting

- *DIPL_image_eingabe.m* contains inputs about

    - name of the picture of the wood cross-section
    - dimension of the calculated sample
    - dimension of the finite elements
    - factors to switch on and off the digitalization algorithms for each border

- *DIPL_cut_tree_rings.m*

    - digitalization of the cut annual rings
    - call of m-files *DIPL_alpha_cut_tree_rings.m*, *DIPL_complete_tree_rings_top.m* (left, bottom, and right), and *DIPL_alpha_matrix.m*

- *DIPL_alpha_cut_tree_rings.m* (computation of the annual ring angles)

- *DIPL_complete_tree_rings_top.m* (digitalization of complete annual rings at top border)

- *DIPL_complete_tree_rings_left.m* (digitalization of complete annual rings at left border)

- *DIPL_complete_tree_rings_bottom.m* (digitalization of complete annual rings at bottom border)

- *DIPL_complete_tree_rings_right.m* (digitalization of complete annual rings at right border)

- *DIPL_alpha_complete_tree_rings.m* (computation of the annual ring angles)

- *DIPL_alpha_matrix.m* (compilation of the annual ring angles)

- *DIPL_image_input.m*

  - input of the gray scale picture
  - computation of the density matrix
  - call of m-file *DIPL_macro_stiffness.m* for homogenization steps
  - call of m-files *DIPL_expand.m* and *DIPL_rotate.m* for transformation of the stiffness matrixes
  - storage of values of the stiffness matrixes in mat-files (for example *C2233.m*)

- *DIPL_micro_stiffness.m* (sub file of micromechanics model)

- *hom_SCS.m* (homogenization step 1 authored by K. Hofstetter)

- *hom_MT_inclin.m* (homogenization step 2 authored by K. Hofstetter)

- *DIPL_macro_stiffness.m* (main file of micromechanics model)

- *hom_unit_cell.m* (homogenization step 3 authored by K. Hofstetter)

- *stiffness_3d_C1111.m* (example; alltogether 36 files used by *equc_woodplane_v6_2.m* to transfer the stiffness values into the FEM-calculation).

The source code of the main files is quoted in Appendix B.

5.4 Calculated Samples

5.4.1 Investigation of Special Configurations of Annual Rings

In order to illustrate the effects of the annual rings on the fields of stress, strain, and displacement, *six artificially generated pictures* with a special alignment and direction of the annual rings were used as input for the FE-program (see Figures 5.4 (a) to 5.8 (a)). The dimension of the samples are a height of 0.1 m, a width of 0.05 m and a length of 0.005 m. The first two samples have horizontal annual rings. The other four samples show vertical annual rings with different radii and variable start directions at the borders. The density of latewood was chosen as 1.1 g/cm^3 and the density of earlywood as 0.5 g/cm^3. The chemical composition is chosen according to [10] with the weight fractions of cellulose, hemicellulose, lignin and extractives amounting to 0.417%, 0.282%, 0.274%, and 0.034%, respectively. The degree of crystallinity of cellulose is set to 0.66 and the moisture content to 12%. Some latewood bands of the annual rings are marked with yellow and black lines, which help to orientate in the pictures of stress, strain, and displacement. In the result

plots, there are no transition areas between dark and light rings to better highlight the effect of different stiffnesses. The results of the simulations will be presented in the following by means of series of pictures for each sample, including a sketch of the *annual ring pattern* (Picture a), of the *strain in z-direction ez* (Picture b), of the *stress in z-direction sz* (Picture c), of the *displacement in y-direction* (Picture d), and of the *displacement in z-direction* (Picture e).

Sample with Flat Curved Horizontal Annual Rings

As a starting basis Figure 5.3 has annual rings with a *large radius* in *horizontal arrangement*. Loading is applied in radial direction by means of a *vertical displacement at the top border* of the sample. Because of the series arrangement of the annual rings and, thus, of *stiff and weaker zones*, the *stress* in radial direction (=z-direction) has to be *approximately constant*. The *strain* in this direction, on the contrary, *varies* according to the local stiffness, so that Picture (b) of Figure 5.3 resembles the annual ring pattern. Also Picture (e), displaying the deformation in vertical direction, shows a *pattern of the annual rings* because of the *abrupt change of the strains* from light rings to dark rings. In conclusion this sample demonstrates the effect of variable stiffnesses, while the varying orientation of the principal material direction is of only minor importance in this constellation.
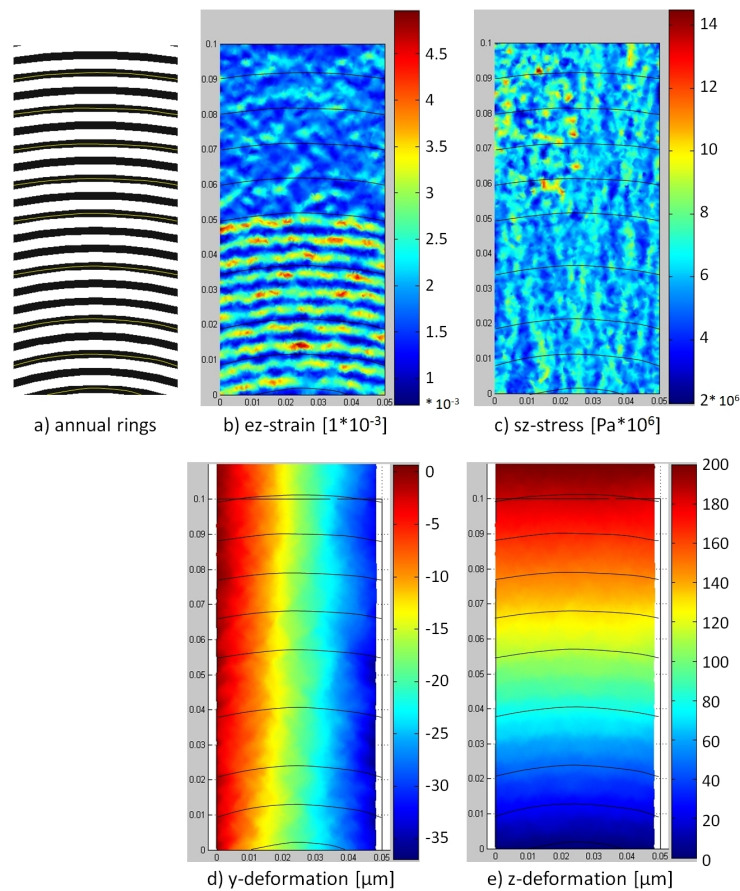
Figure 5.3: Sample with flat curved horizontal annual rings

Sample with Curved Horizontal Annual Rings next to the Center

Figure 5.4 has annual rings with a *large radius in the upper half* of the picture in *horizontal arrangement*, while the *lower part shows semicircular rings* with the center in the middle of the bottom border. Again, the sample is subjected to *vertical displacements at the top border*. The stress in radial direction varies from the top border downwards. In the upper two-thirds, the distribution of vertical stress [Picture (c) in Figure 5.4] is similar to the one in the previous sample [Picture (c) in Figure 5.3] because of the similar arrangement of the annual rings. Again, a rather homogeneous stress distribution is observed. In the lower one third of Picture (c) in Figure 5.4, however, the stress distribution resembles the *annual ring pattern* in consequence of the *varying orientations of the principal material direction*s. While the applied displacement results in almost uniformly distributed stresses in the upper two-thirds, it yields *high stresses inside the dark rings* and *low stresses inside the light rings* in the lower third of the picture. Picture (d), displaying the deformation in horizontal direction, shows a less pronounced pattern of the annual rings because of the *redirection of the stresses* from nearly horizontal rings to vertical rings. In conclusion, this sample shows the combined effect of both *variable stiffnesses* and *variable orientation* of the principal materials directions.

a) annual rings   b) ez-strain [$1*10^{-3}$]   c) sz-stress [$Pa*10^6$]

d) y-deformation [μm]   e) z-deformation [μm]
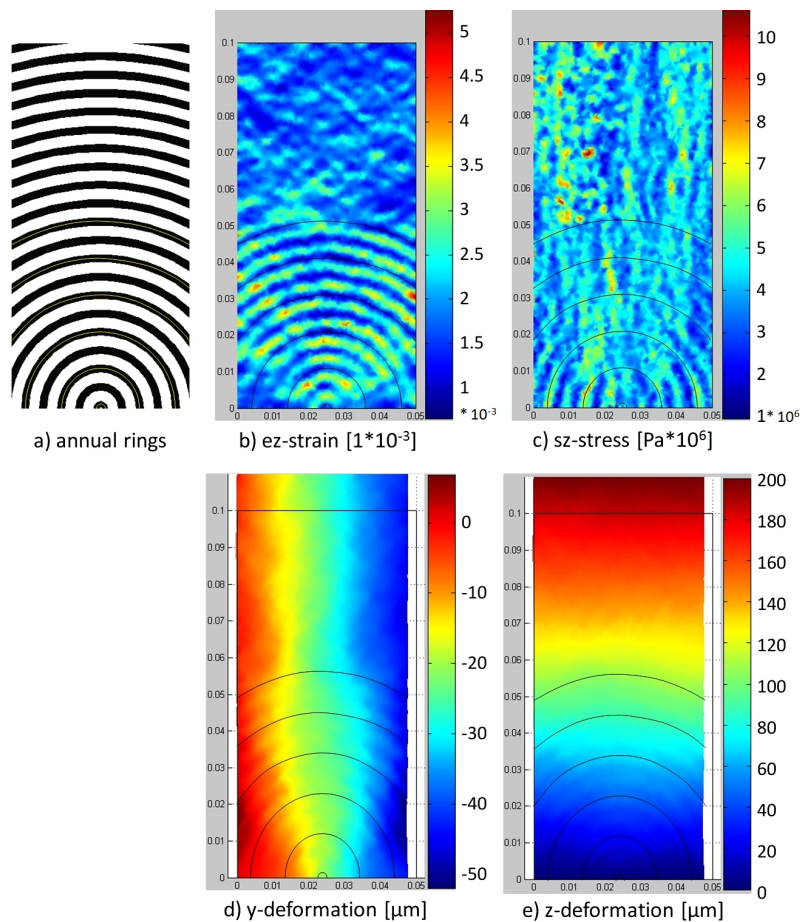
Figure 5.4: Sample with curved horizontal annual rings next to the center

Sample with Flat Curved Vertical Annual Rings

As a second reference, Figure 5.5 shows a sample with annual rings with a *large radius* in *vertical arrangement*. Still the sample is subjected to a *vertical displacement at the top border*, which now results in a *loading in tangential direction*. Unlike Picture (b) of Figure 5.3, now the *strain in tangential direction* has to be *approximately constant* [Picture (b) of Figure 5.5], while the variable stiffness values in earlywood and latewood result in an *annual ring-like pattern* in the distribution of *vertical (=tangential) stress* [Picture (c) of Figure 5.5]. Picture (e) showing the deformation in vertical direction exhibits a slight pattern of the annual rings at the corner down right because of the varying stresses in light and dark rings. In conclusion, because of the low curvature of the annual rings the strain, stress, and deformation fields in this sample are only affected by the *variable stiffnesses*, while the material directions have only a minor influence.

a) annual rings   b) ez-strain [1*10⁻³]   c) sz-stress [Pa*10⁶]

d) y-deformation [µm]   e) z-deformation [µm]
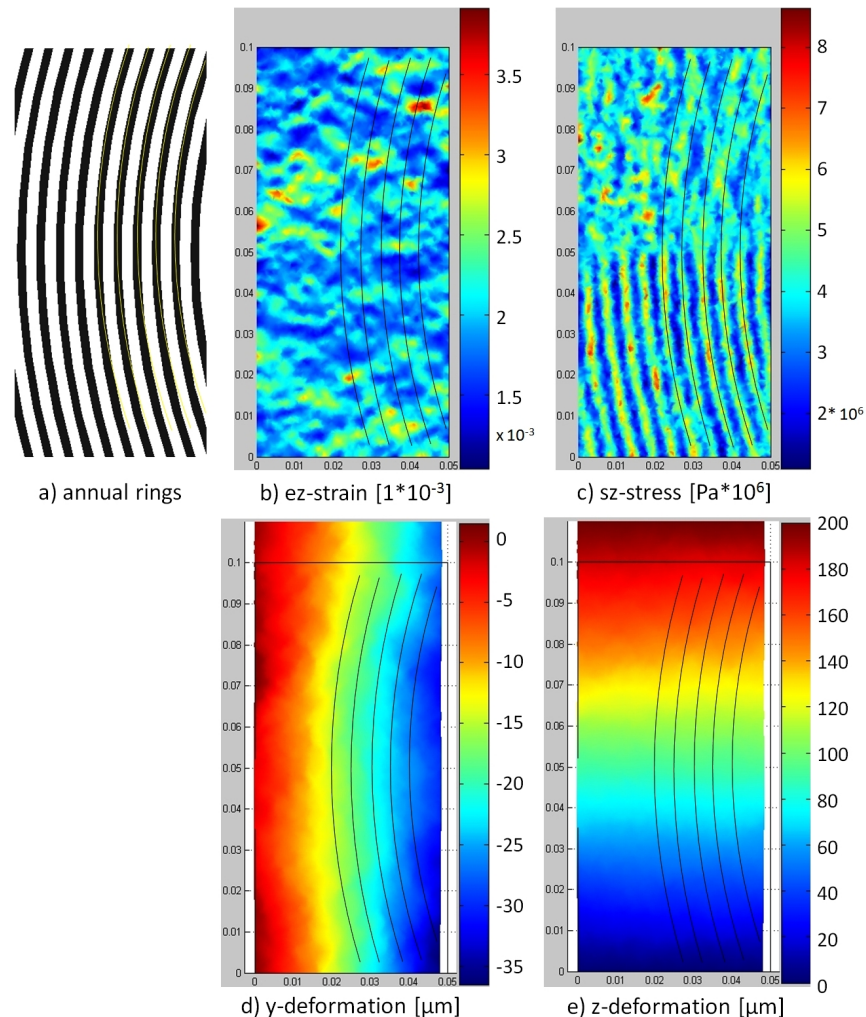
Figure 5.5: Sample with flat curved vertical annual rings

Sample with Curved Vertical Annual Rings

The sample in Figure 5.6 has annual rings with a *smaller radius* than the sample in Figure 5.5 in a *vertical arrangement.* Loading is applied in mixed tangential radial direction again by means of a *vertical displacement at the top border.* Now both Pictures (b) and (c) of Figure 5.6 with the strain and the stress in the vertical direction display an image of the annual ring pattern because of the *coupled effects* of varying stiffnesses and of rotation of radial and tangential directions, though in different regions of the sample.

a) annual rings   b) ez-strain [1*10⁻³]   c) sz-stress [Pa*10⁶]

d) y-deformation [μm]   e) z-deformation [μm]
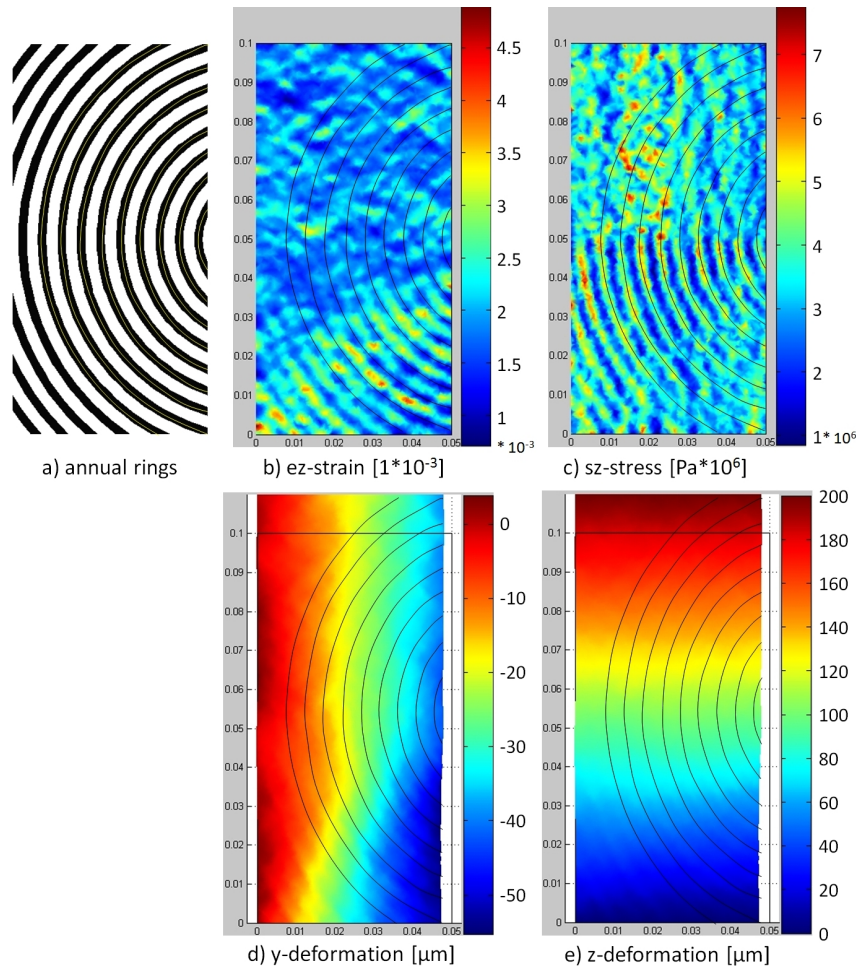
Figure 5.6: Sample with curved vertical annual rings

Sample with Curved Vertical Annual Rings next to the Center

As a third reference, the sample in Figure 5.7 exhibits annual rings with a *small radius* and *semicircular rings* at the right border in *vertical arrangement.* The sample is loaded by *vertical displacements* at the top border, resulting in radial and tangential straining depending on the location in the sample. Picture (c) of Figure 5.7 displaying the *stresses in vertical direction* shows a *clear image of the annual ring pattern*, which is also recognizable in Picture (b) with the vertical strain though much less pronounced. This pattern formation is a consequence of the *varying orientation* of local radial and tangential directions,

the *varying stiffness values* at the differently colored rings, and the transmission of the induced stresses predominantly in the darker and stiffer rings. The pattern of Picture (e) describing the deformation in vertical direction is very interesting. For the explanation the displacement value illustrated by the yellow color is chosen. It clearly shows that the *vertical deformation* is *higher at the right side* of the picture than at the left side. Concerning Picture (a) of Figure 5.7, this effect arises from the *series connection of the darker rings at the left side*, producing a stiffer material than at the *right side* of the picture where the rings show a *parallel connection*. In other words, at the right side the lighter annual rings with lower stiffness undergo a larger deformation. At the left side the darker and stiffer rings take up the bigger part of the loading and deform less than the lighter rings at the right side. So the sample is *slightly bent* by the vertical loading. A similar deformation is also observed in consequence of drying the wood sample. This effect is also obvious in Picture (d) of Figure 5.7 displaying the horizontal deformation of the sample.

a) annual rings   b) ez-strain [$1*10^{-3}$]   c) sz-stress [$Pa*10^{6}$]

d) y-deformation [µm]   e) z-deformation [µm]
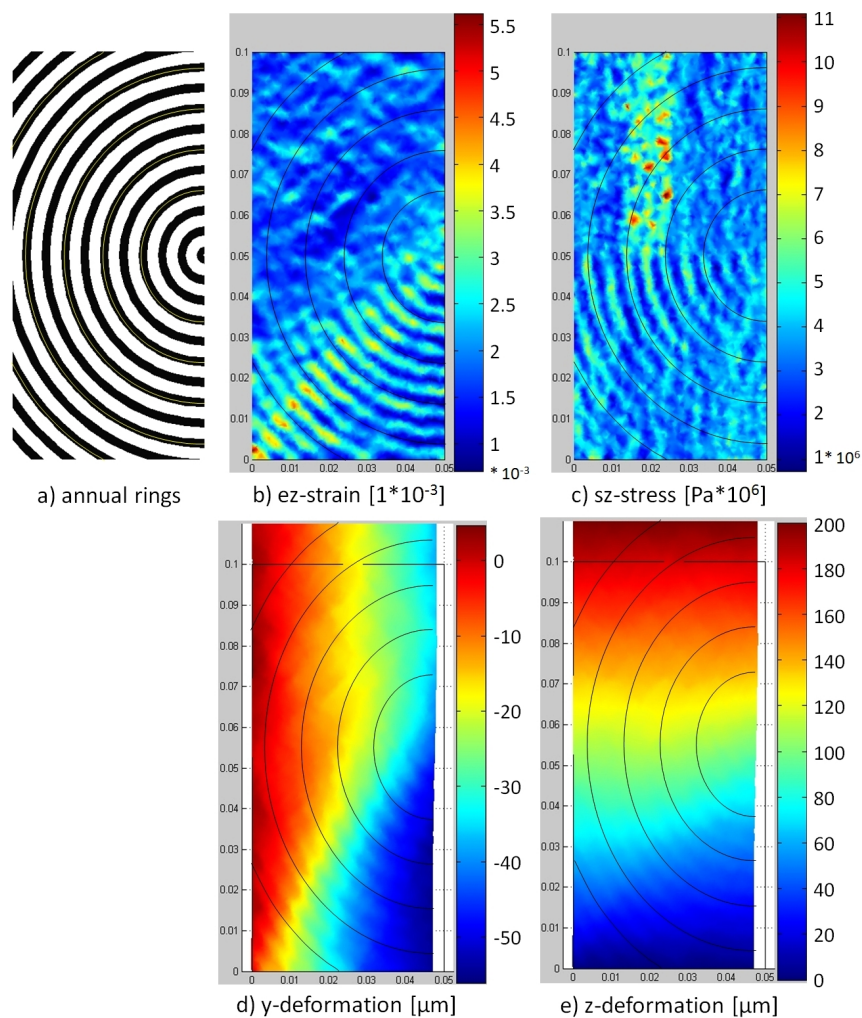
Figure 5.7: Sample with curved vertical annual rings next to the center

Sample with Curved Vertical Annual Rings with Orthogonal Start

The sample in Picture (a) of Figure 5.8 is constructed by *vertically curved* annual rings with a *vertical start* at the bottom border. In general, the effects are similar as in Figure 5.5. But the sample also shows an additional effect. At the bottom left corner of Picture (c), the *first dark ring ending at the bottom border* exhibits *higher stress* than the other ones. This is because of the *stress transfer* from the next dark ring which ends at the left border above this more strongly loaded ring. Picture (e) of Figure 5.8 displays the same effect of bending as described in relation to Figure 5.7.

a) annual rings   b) ez-strain [1*10⁻³]   c) sz-stress [Pa*10⁶]

d) y-deformation [µm]   e) z-deformation [µm]
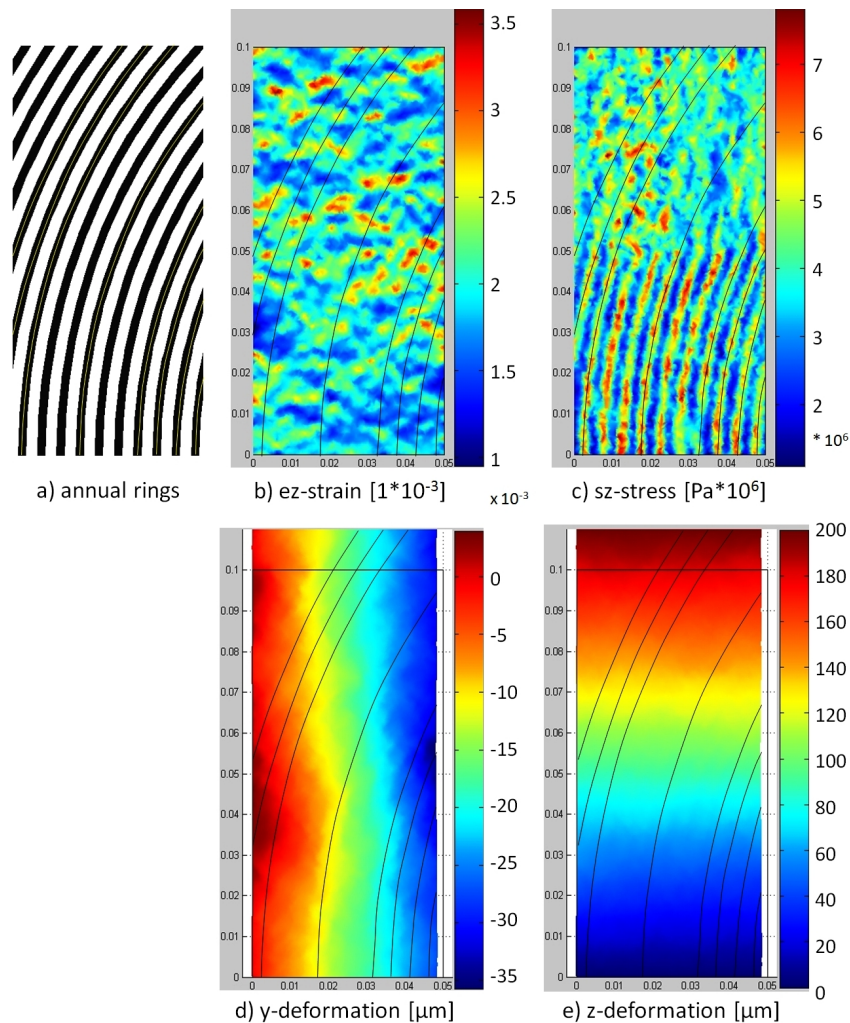
Figure 5.8: Sample with curved vertical annual rings with orthogonal start

Chapter **6**

Experimental Validation

In order to check the suitability of the developed numerical simulation procedure, mechanical tests were performed on samples with selected annual ring patterns in the transverse plane as already mentioned in Section 6.5. The observed deformation fields were compared with corresponding simulation results in a qualitative manner (cf. Figures 6.14 to 6.16 in Section 6.5. The samples were provided by Christoph Buksnowitz from the Institute of Wood Science and Technology - Department of Material Sciences and Process Engineering at the University of Natural Resources and Applied Life Sciences in Vienna [in short BOKU]. The mechanical tests were carried out at the Laboratory for Macroscopic Material Testing of the Institute for Mechanics of Material and Structures (Adolf Blamauer Gasse 1-3 in 1030 Vienna - Austria). The small stiffness of wood in the transverse direction results in the need to measure very little displacements, which was among the major challenges of the validation. Moreover, a full-field displacement measurement technique is required to enable comparison of displacement fields in the sample with computed results. This motivated the use of an optical and laminar measurement system called ESPI (Electronic Speckle Pattern Interferometry) which is installed in front of the tension testing machine (see Section 6.1.2). In anticipation of the conclusions, the *displacement pictures* obtained with this measurement system resolve the *influence of the pattern of the annual rings* and will agree with the computed displacement fields.

6.1   Used Equipment

For the tension tests, the equipment of the Laboratory for Macroscopic Material Testing was used.

6.1.1   Uniaxial Testing Machine

The tests were performed at a uniaxial electro-mechanic universal testing machine (UNIAX in short)(Figure 6.1) [18]. The machine, type LFM 150, built by Walter & Bai consists of

Figure 6.1: Uniaxial electro-mechanic universal testing machine (UNIAX) [18]

the following components:

- built-in load cell (maximum load 150 kN),

- encoder,

- spindle drive,

- hydraulic clamping jaws,

- digital controller EDC 120,

- connectors for pick-up sensors,

- PC assistance.

Employments of this machine include:

- compression, tensile and bending tests,

- quasi-static displacement controlled tests,

- material tests,

- biomechanical applications.

It is possible to control the machine by either *time*, *displacement*, or *load*. The validation tests were run under *displacement control*. Via the PC control loading steps can be defined, which are chosen for the UNIAX-loading program as follows:

- application of first displacement in order to put the machine under load;

- first hold phase under load for about 15 seconds to turn on the ESPI-system;

- loop with about 20 steps:

  - 20 μm elongation of the sample in circa 10 seconds (automatically),

  - 15 seconds intermission to activate the ESPI-system (automatically),

  - activation of the ESPI-system and measurement of displacement field (by hand).

This procedure is necessary because there is no direct connection between the ESPI-system and the UNIAX-machine, and the ESPI-system allows only displacements of at most 30 μm between two consecutive measurements.

6.1.2   3D Electronic Speckle Pattern Interferometry (ESPI)

ESPI is an *optical method for measurement* of plane deformations and displacements with an accuracy of 10 nm [19]. The used system was "gauge head Q 300", Dantec-Ettemayer, with the following features [18]:

- contact-free measurement system for deformation fields,

- system "gauge head Q300" applicable at two different distances from the sample realized by "long" and "short" arms,

- for different sizes of the measurement area ranging between 5×5 mm^2 and 100×100 mm^2,

- ISTRA software for recording and evaluation of the deformation states.

Previous employments of this system include:

- deformation measurements of wooden samples under biaxial loading,

- biomechanical applications with specimens of corticalis and cuticula.

Figure 6.2: Electronic speckle pattern interferometry (ESPI) [18]

The camera and simultaneous source of light is *fixed on a frame* of aluminum. This framework is *multiply strutted* and braced in order to stiffen the device. That is necessary because of the high measuring accuracy of the ESPI-System in the range of micrometers. So little vibrations and displacements can falsify the measurement results.

6.2   Assembly of the Equipment

The combination of the UNIAX-machine and the ESPI-system turned out to be quite critical and, thus, it was rather challenging to find a suitable arrangement of the equipment (Figure 6.3). At first the ESPI-System was mounted in combination with the frame on the base plate of the UNIAX-machine. But the vibrations, induced by the axle gear of the UNIAX-machine, considerably affected the measurement results. Furthermore, demounting the equipment for other tests was too complex.

So the frame with the ESPI-system was mounted on a heavy, movable, and fixable desk. This enables to remove the ESPI-system from the UNIAX-machine without any screwing and also prevents the influence of machine vibrations on the measurement. The disadvantage of this constellation is that a new calibration is required after installation of the ESPI-system in front of the UNIAX-machine. But after a short familiarization phase this is easy to do.

a) ESPI-system fixed on a moveable
heavy desk in front of the tension
testing machine
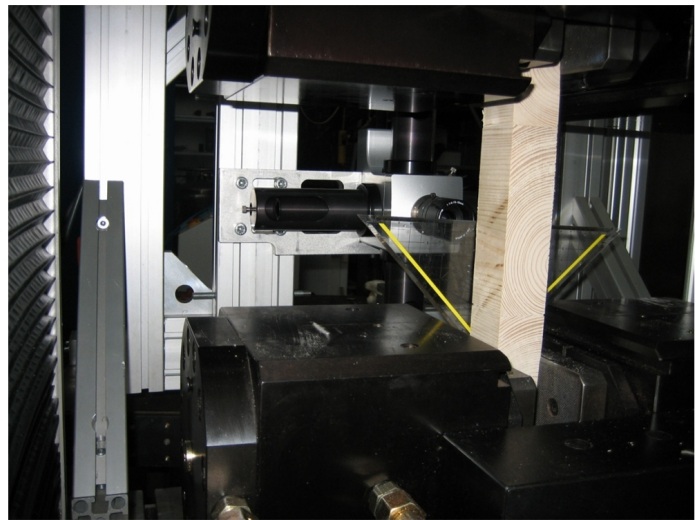
b) view from behind the testing machine, while
ESPI-system measures a sample

Figure 6.3: Combination of ESPI-system and UNIAX-testing machine

6.3 Preliminary Tests

For checking the suitability of the chosen test setup with the combination of the UNIAX-machine and the ESPI-system as well as for a *better handling of the equipment* at the real tests, a series of preliminary test on samples similar to the real test samples was made. One sample (Figure 6.4) is composed of *three wood blocks*. The middle block is the tested element, while the outer blocks are for the clamping by the jaws. Using similar samples with a radial/tangential orientation in the testing direction for all these three blocks (Figure 6.4) results in non-uniform, undefined load introduction into the testing block in the middle. Thus, alignment of the *longitudinal direction* with the *testing direction* in the *outer blocks* is much better suited (Figure 6.5) and was chosen as sample design for the validation tests.

Figure 6.4: Testing samples resulting in non-uniform load application
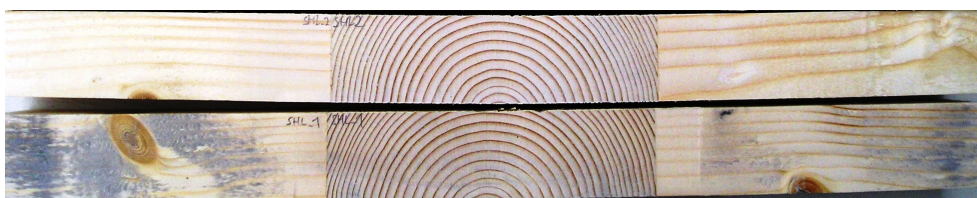
Figure 6.5: Testing samples with well-defined uniform load application

6.4 Validation Tests

The 21 samples provided by Christoph Buksnowitz from the BOKU (Figure 6.6) had been investigated in microstructural respects in the framework of the project "Large Diameter Roundwood: Quality Assessment for Optimized Processes and Products". The aim of this project was to explore the potential of large-diameter trees and to push their enhanced use in the forest product industry. The individual characteristics of the provenance of each sample are listed in Table 6.1:

Sample	Region of tree location	Sea level	Gradient of the hillside	Cutting height
		[m]	[%]	[cm]
1	1	550	35	110
4	1	550	30	110
5	1	520	65	110
29	2	850	5	110
33	2	850	5	110
36	2	850	0	110
32	2	880	0	110
17	2	440	45	110
21	2	440	15	110
21	2	440	15	110
37	2	800	5	110
45	2	800	5	110
44	2	800	15	110
61	2	940	30	110
49	1	1260	80	110
53	1	1260	80	110
6	1	520	65	810
9	1	480	45	110
28	1	850	85	110
20	2	440	40	110
66	2	940	15	810

Table 6.1: Sample provenances

6.4.1 Design of the Samples

As specified in Section 6.3, the samples were joined with *two clamping jaw blocks* by *glue joint*s. Therefor the original wood samples were cut to obtain a *cuboidal shape* and a length of 65 to 100 mm. The were not machined to obtain uniform cross-sectional dimensions at this process step (Figure 6.7). Afterwards the clamping jaw blocks were cut such that the overall *length* of the finished samples with the glued-in specimen was the *same for*

Figure 6.6: Samples from BOKU

Figure 6.7: Blank shape of the glued samples from BOKU

all samples. This is necessary for the glue application process. The cross-section of the clamping blocks was oversized (Figure 6.7) to allow an easy cutting of the samples after the gluing process. This *cutting* to *nearly parallel sides* of the whole samples including the clamping blocks was performed with a circular saw. For a correct adjustment of the sides the samples were afterwards planed with a planing machine. Finally, the *central measurement region* of samples was *sanded* in order to get a *fine surface*. This step also resulted in a slightly smaller cross-section of the measurement block compared to the cross-section of the clamping blocks.

The first test of a sample showed that the compression of the clamping jaw blocks results in considerable lateral strains and stresses inside the glued joint. To prevent this undesired effect, the samples were provided with *cuts* at the side of the clamping jaw blocks (see Figure 6.8). These *release cuts* permit the clamping jaws to *compress the clamping jaw*
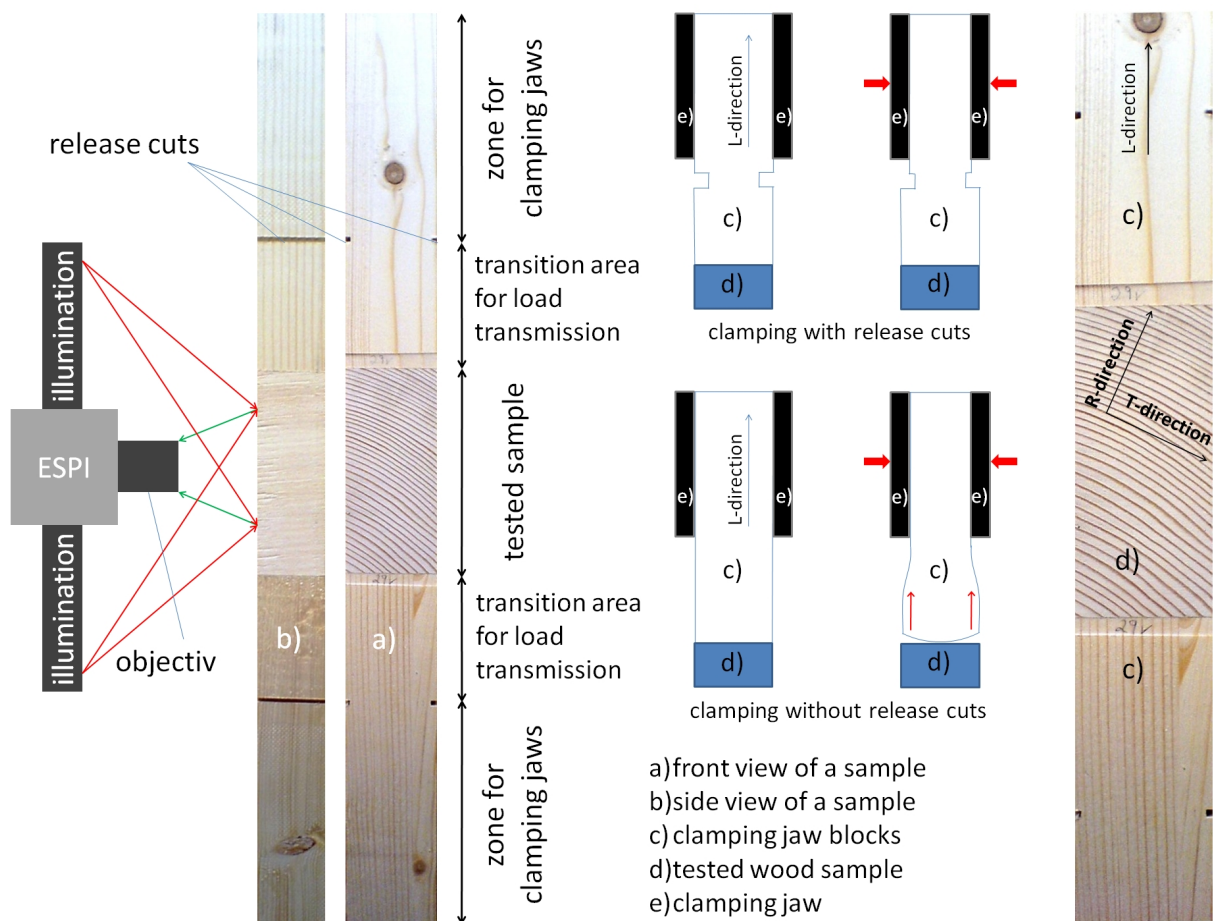
Figure 6.8: Finished samples for tension testing

blocks of the samples at the surfaces *without loading the outer grains* in the measurement region. Out of the 21 samples three samples will be investigated in more detail in the following, heading for the validation of the simulation model. The final dimension of these samples are summarized in Table 6.2, where the following denotations are used (see also Figure 6.9):

- height of test sample [mm] ...hsw (z-direction),

- width of test sample [mm] ...wsw (y-direction),

- length of test sample [mm] ...lsw (x-direction),

- height of clamping jaw blocks [mm] ...hcb (z-direction),

- width of clamping jaw blocks [mm] ...wcb (y-direction),

- length of clamping jaw blocks [mm] ...lcb (x-direction).
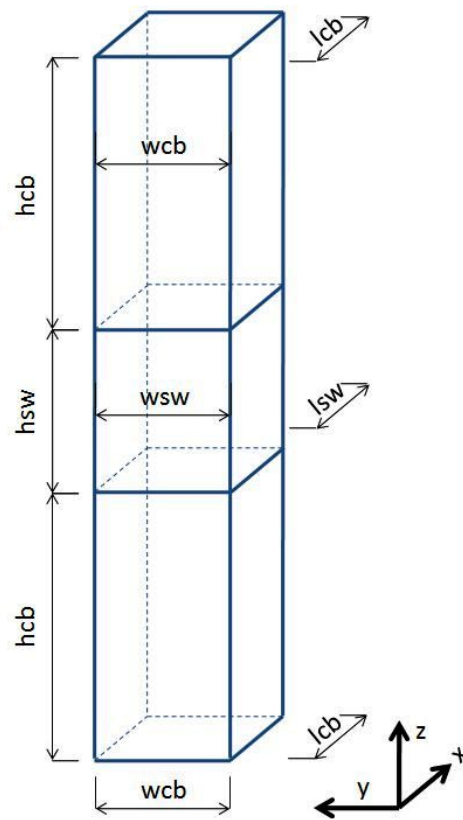
Figure 6.9: Dimensions of finished samples

Sample number	hsw	wsw	lsw	hcb	wcb	lcb
5	73.5	44.0	32.6	188.5	44.2	33.0
21-1	70.0	43.9	32.0	191.2	44.2	33.0
49	99.6	44.1	32.0	175.7	44.2	33.0

Table 6.2: Sample dimensions [mm]

6.4.2 Results of ESPI Measurements

Figures 6.10, 6.11, and 6.12 show the results of the measurements with the ESPI-system during the uniaxial tension tests for the three considered samples. They were collected at *loading step nine* for *Sample Number 5* corresponding to a *displacement* at the top border of 180 μm and at *loading step ten* for *Sample Number 21-1 and 49* corresponding to a *displacement* at the top border of 200 μm. Pictures (a) and (b) in these figures show the cross-section of the samples with the overlayed ESPI pattern in Picture (a). The red borders define the used measurement area of the ESPI-system in all pictures of these figures. Picture (c) displays the cross-section in a photo taken by a digital camera. This picture shows the pattern of the annual rings inside the measurement area. Pictures (d1) and (d2) show the displacement in z-direction (positive in upwards direction) and y-direction (positive towards the right) by colored grading of the displacement values. Picture (e) exhibits the displacement arrows, which are the combination of the displacements in y- and z-direction, in a qualitative manner. The coloration in Picture (e) shows the deformation in x-direction. The unit of the colored deformation plot is micrometer (μm). Figure 6.13 shows the pattern of the annual rings which can also be identified in the displacement plots from the ESPI-system.
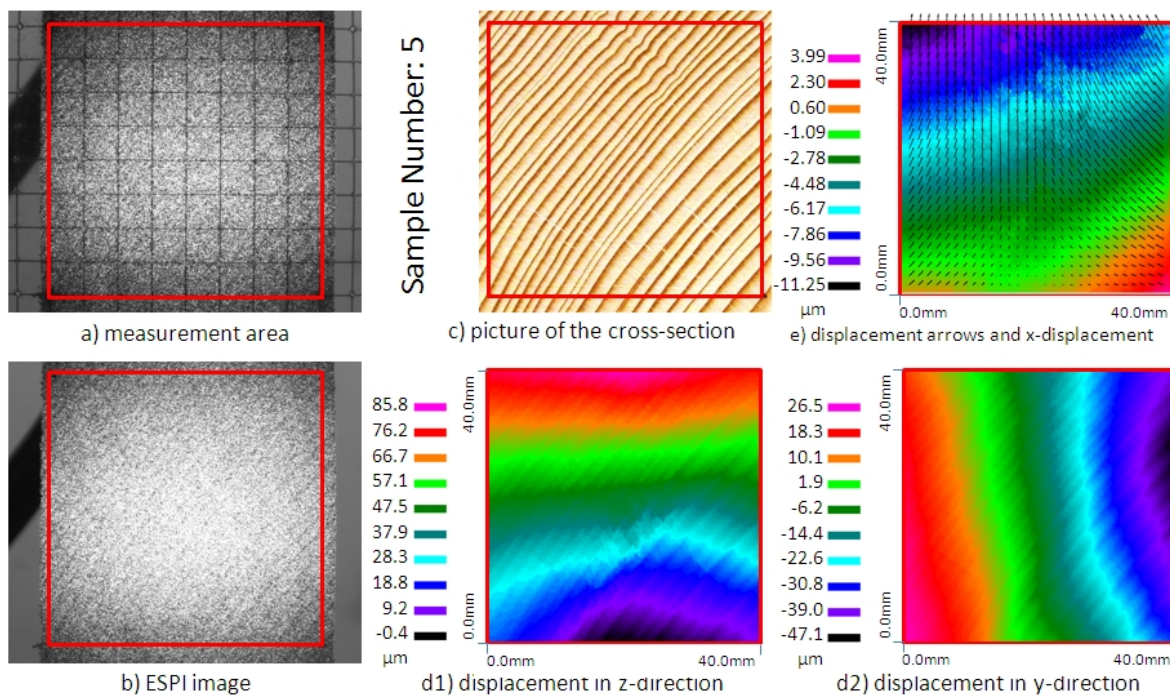
Figure 6.10: Pictures of ESPI-system for Sample Number 5
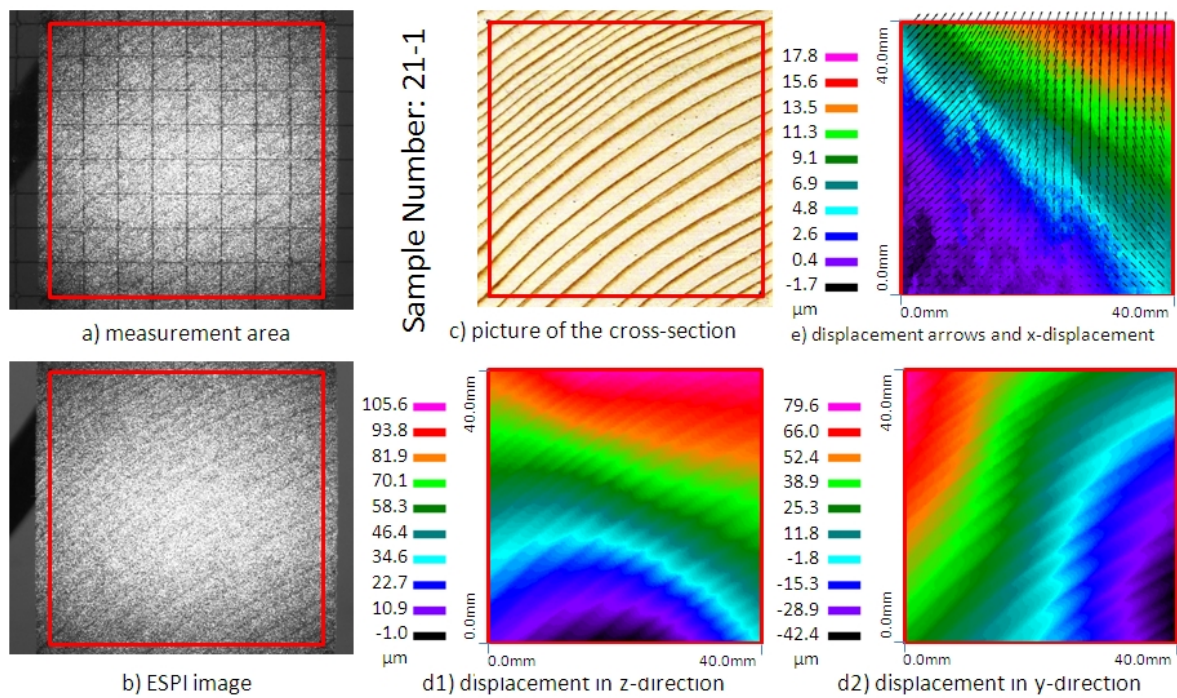
Figure 6.11: Pictures of ESPI-system for Sample Number 21-1
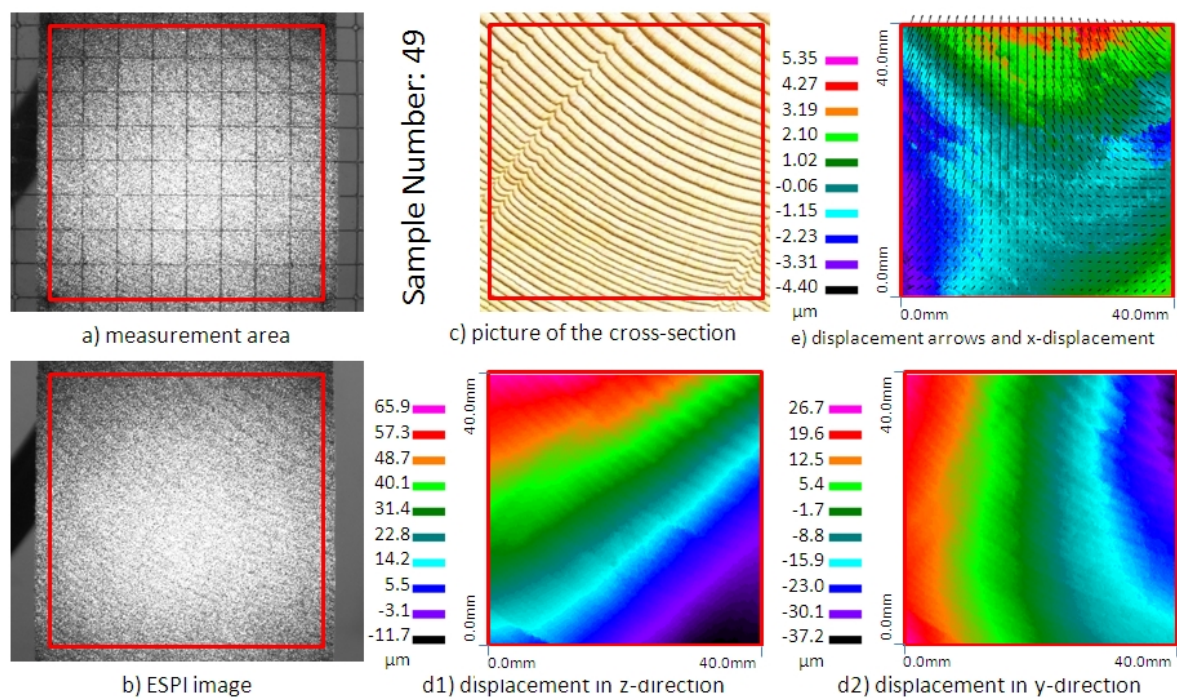
Figure 6.12: Pictures of ESPI-system for Sample Number 49
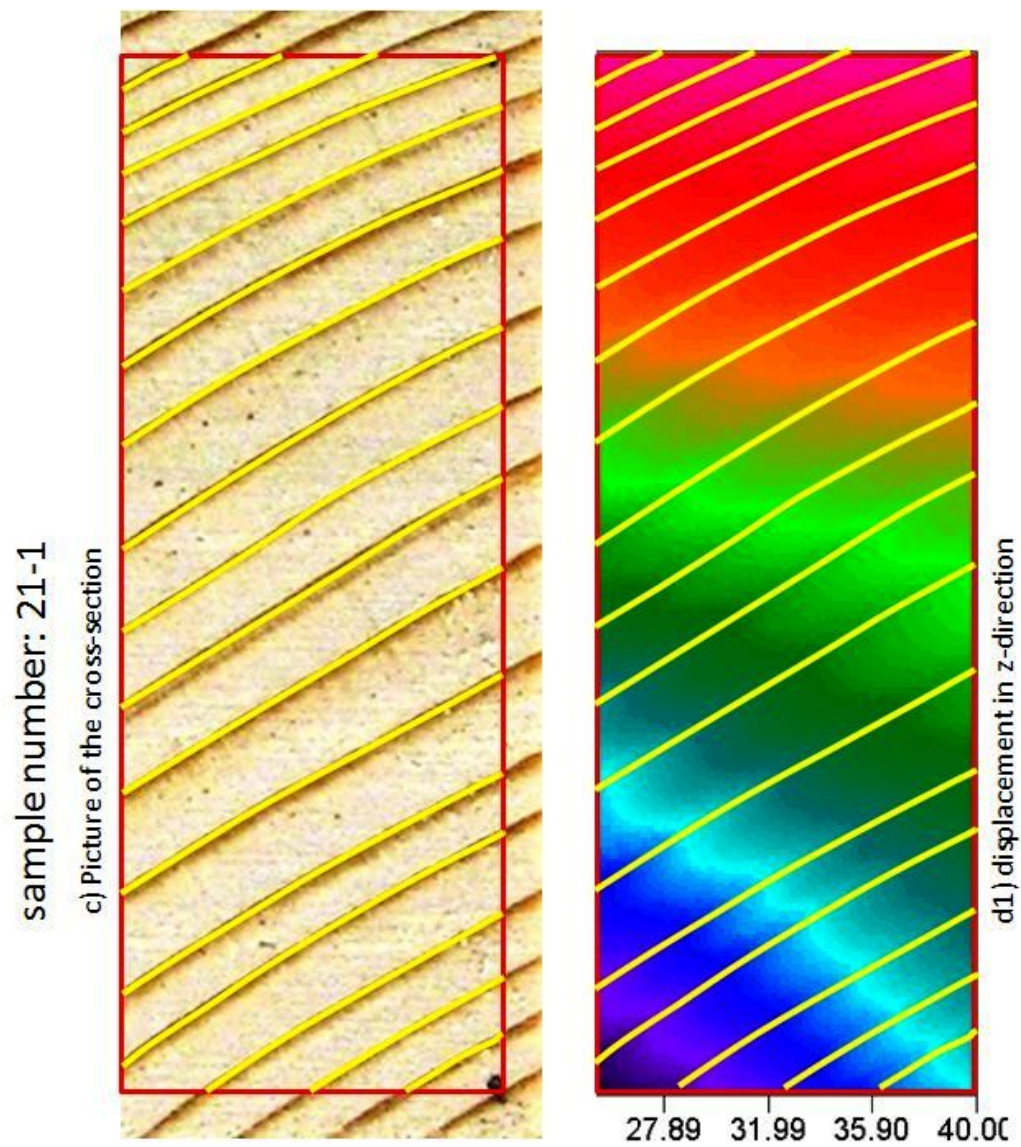
Figure 6.13: Pattern of the annual rings in a picture of the cross-section and in the displacement plot from the ESPI-system

6.5   Comparison of Displacement Plots from ESPI and FE-Calculation

Besides the samples with artificially generated annual ring patterns, also real samples were analyzed by means of the FEM-program (see Figures 6.14 to 6.16). These samples were also investigated in uniaxial tension tests. The comparison of the computed displacement yields from the FE-calculation with measurement by an ESPI-system served for model validation as described in the figures. The simulations were performed for an earlywood density of 0.35 g/cm^3 and a latewood density of 0.87 g/cm^3 [10]. The weight fractions of the basic chemical constituents for the micromechanical model were determined at a chemical laboratory of the BOKU and are summarized in Table 6.3. The deviation of the

Sample	Cellulose	Hemicellulose	Lignin (insoluble)	Lignin (soluble)	Extractives
5	48.9	24.5	18.0	0.2	6.7
21-1	53.0	21.8	16.9	0.2	4.8
49	51.3	21.9	16.0	0.2	5.8

Table 6.3: Weight fractions of the main components from the wood samples [%]

sum of the weight fractions for each sample from 100 % comes from the limited accuracy of the chemical analytic processes, which ranges from one to five percent. The degree of crystallinity was again set to 0.66 and the moisture content to 12 %. In this section simulation results are presented in a similar way as for the academic samples in Section 5.4.1. The red quadrat shows the measurement area of the ESPI-system in the tension tests. The effect of displaying a pattern of the annual rings in the plot of the stress or strain distribution in case of predominantly tangential loading is not so distinctive as in the section before for the academic samples. This is because of the loading in mixed radial and tangential direction. A weak image of the annual rings is observed in the bottom left corner at Picture (c) of Figure 6.15, where the stress in the latewood bands is higher than in the earlywood.

Also the Figures 6.14, 6.15, and 6.16 compare the deformation plots obtained with the ESPI-system and the numerical simulations. Pictures (d) and (e) show the deformation in z-direction, and the Pictures (f) and (g) in y-direction. The plots of the FE-results concern the whole sample, while the pictures showing the ESPI-output only pertain to the measurement area int the tests (red quadrat). The points of origin of the deformation are on the bottom left corner for the numerical simulation and at the middle of the bottom border of the measurement area (red quadrat) for the ESPI-system. So the difference of the displacement in z-direction to the displacement of the lower border of the red quadrat in the picture of the FE-calculation has to be compared with the results of the ESPI-measurement.

a) annual rings
Sample Number 5

b) ez-strain [1*10^{-3}]

c) sz-stress [Pa*10^6]

d) z-deformation – numerical
simulation [μm]

e) z-deformation –
ESPI-system [μm]

f) y-deformation - numerical
simulation [μm]

g) y-deformation –
ESPI-system [μm]
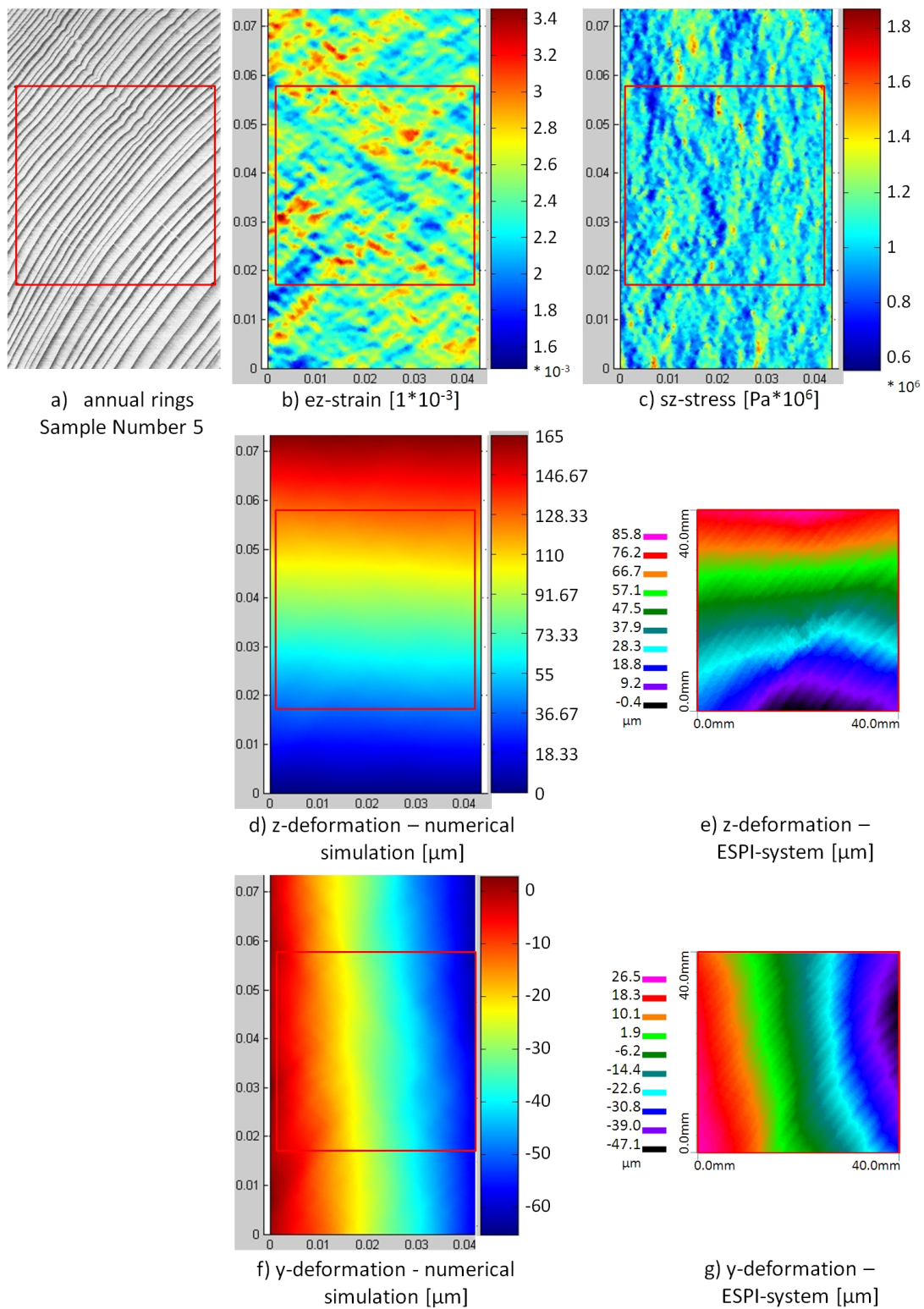
Figure 6.14: Comparison of the results of the numerical simulation and the tension test at Sample 5

a) annual rings
Sample Number 21-1

b) ez-strain [1*10⁻³]

c) sz-stress [Pa*10⁶]

d) z-deformation – numerical
simulation [μm]

e) z-deformation –
ESPI-system [μm]

f) y-deformation - numerical
simulation [μm]

g) y-deformation –
ESPI-system [μm]
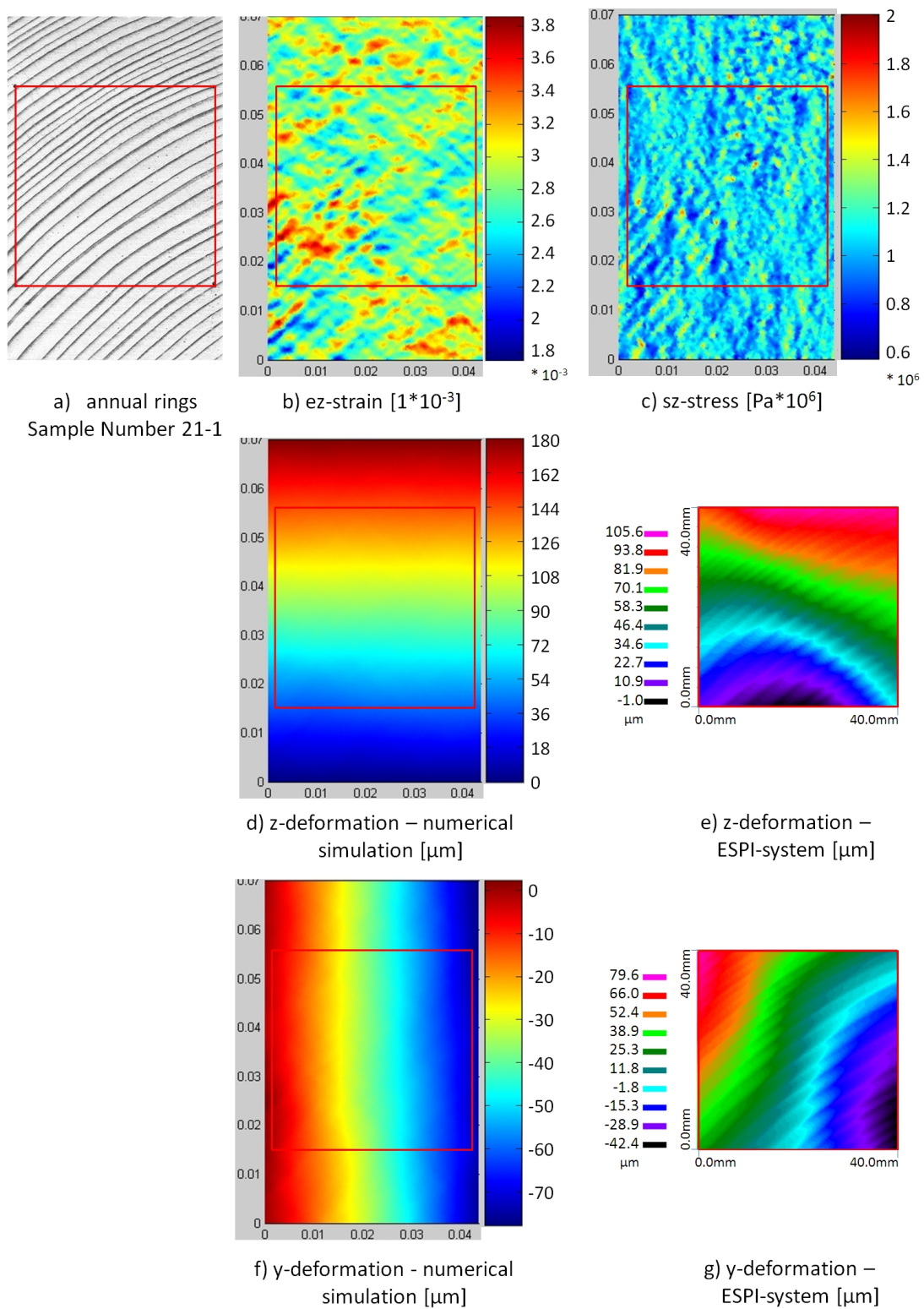
Figure 6.15: Comparison of the results of the numerical simulation and the tension test at Sample 21-1

a) annual rings
Sample Number 49

b) ez-strain [1*10⁻³]

c) sz-stress [Pa*10⁶]

d) z-deformation –
FE-program [µm]

e) z-deformation –
ESPI-system [µm]

f) y-deformation –
FE-program [µm]

g) y-deformation –
ESPI-system [µm]
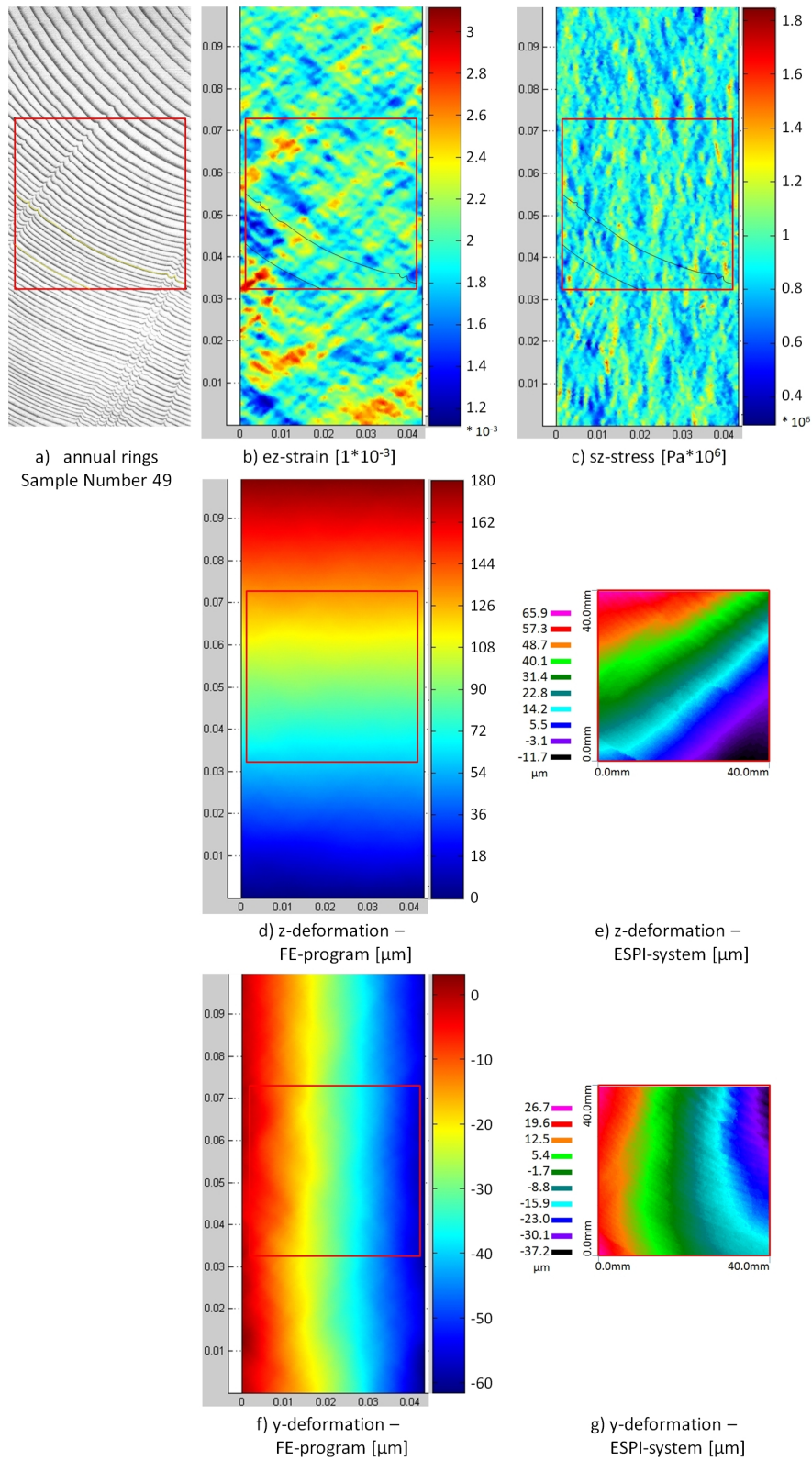
Figure 6.16: Comparison of the results of the numerical simulation and the tension test at Sample 49

Chapter 7

Comparison of Theory and Validation

7.1 Summary

This thesis presents the potential of combining finite element simulations with a micromechanical model to investigate the effects of varying stiffness and changing orientation of the local material directions across the annual rings on the mechanical behavior of wood. Being caused by the four growth phases of wood in our latitudes, the origin of the differences between latewood and earlywood is found in the microstructure of wood. At a length scale of some nanometers the ingredients of wood, namely cellulose, hemicellulose, lignin, extractives and water build the material of cell walls. These honeycomb-like cells have a different structure in latewood and earlywood. The differences result from the varying thickness of the cell walls, which is larger in latewood, and from the different widths of the lumens inside the cells, which are smaller in latewood than in earlywood. Since density is closely correlated with stiffness, these characteristics bring about stiffer latewood bands in an annual ring, while the earlywood bands manage the transport of water and nutrients as a main function. The density distribution in a cross-section can be detected by a gray scale picture, where the latewood bands are darker than earlywood bands in case of spruce.

The determination of stiffness properties from the local density is performed by means of a micromechanical model. This model allows to estimate the stiffness of wood from microstructural characteristics such as density through three homogenization steps, which are established by the self-consistent scheme, the Mori-Tanaka scheme, and the unit cell method. The resulting stiffness values, which depend on the local density of wood, serve as a first input to the FE-model. Moreover the varying direction of the principal material directions in the transverse plane of wood has to be considered. This is important because of the orthotropic material behavior of wood, showing double stiffness in the radial direction orthogonal to the annual rings compared to the tangential direction. For the transformation of the stiffness matrixes from local coordinate frames aligned with the principal material directions to a single global frame, the local inclination angles of the annual rings have to be determined. This is done by means of a digitalization algorithm, which starts off from

a picture of the annual ring pattern in the cross-section.

The resulting local stiffness values served as input for an FE-model at the integration point level. The model was generated in COMSOL and afterwards modified in MATLAB. The model was applied to the numerical simulation of six academic examples with typical regular annual ring patterns and of three real samples, which were also investigated in uniaxial tension tests in the transverse direction. While the first examples delivered fundamental insight into the effect of the annual rings on the stress, strain, and deformation fields in the cross-sectional plane, the latter samples served the purpose of model validation by comparing the computed results with corresponding measured data.

7.2   Conclusions from the Theoretical Experiment

The six samples with specially configured annual rings were used to study the effects of varying density and varying orientation of the local material directions on the local straining of the sample at loading perpendicular to the grain. At constant loading perpendicular to the annual rings, the weaker earlywood bands and the stiffer latewood bands are arranged in series, resulting in constant stress and alternating strain in the loading direction. Despite the very stiff latewood bands this constellation of annual rings results in a high deformation because of the earlywood bands with low stiffness. Otherwise, loading in tangential direction results in a parallel connection of the earlywood and latewood bands and, thus, in constant strains, but varying stresses. The stiffer latewood bands show higher loading at this arrangement of the annual rings. In comparison to the serial connection, deformations in loading direction are smaller. In samples with curved and/or inclined annual rings, a mixed loading parallel and normal to the annual rings is generally observed. The described effects are then superimposed and may vary in different regions of the sample.

7.3   Conclusions from the Experiments with ESPI

For the purpose of model validation, tension tests in the transverse direction were performed on three selected samples of a strong wood project from BOKU. An ESPI-system was used for full-field displacement measurement in oder to study the influence of the annual rings in practice. The deformation plots generated by the ESPI-system resemble the annual ring pattern of the cross-section, where the stiffer latewood bands show less deformation than the weaker earlywood bands of an annual ring. Also the bending effects at tensile loading, which are induced in samples with curved annual rings, can be seen in the deformation pictures from the ESPI-system. This effect results from the different arrangement of the annual rings - rather in parallel and rather an series, respectively - towards the two lateral edges of the sample. The larger elongation at the side with the series connection brings about the bending-like deformation.

The results of the measurement with the ESPI-system and corresponding results of the numerical simulations show an overall good agreement. Slight deviations between the results for the displacements in the loading direction in quantitative respects can be the result of the elongation of the clamping jaw blocks in the tension tests, which are only considered in an approximate manner in the simulations. Furthermore, the values of the

predefined densities for latewood and earlywood can differ in a small range in the real samples.

On the whole, the performed numerical simulations and mechanical tests delivered interesting insight into the effect of annual rings on the local mechanical behavior of wood. Varying material properties in earlywood and latewood and varying orientations of the principal material directions in the the cross-section are particularly relevant at wood drying and moisture-induced dimensional changes of wood. Extended by hygro-mechanical aspects, the developed FE-simulations program is expected to be a valuable prognosis tool for product and process optimization in timber engineering and timber industry.

Bibliography

[1] L. Hoffmeyer, L. Damkilde, and T. N. Pedersen. Structural timber and glulam in compression perpendicular to grain. *Holz als Roh- und Werkstoff*, 58:73–80, 2000.

[2] A. N. Nairn. A numerical study of the transverse modulus of wood as a function of grain orientation and properties. *Holzforschung*, 61:406–413, 2007.

[3] C.-J. Lin, M.-J. Tsai, C.-J. Lee, S.-Y. Wang, and L.-D. Lin. Effects of ring characteristics on the compressive strength and dynamic modulus of elasticity of seven softwood species. *Holzforschung*, 61:414–418, 2007.

[4] A. Shipsha and L. A. Berglund. Shear coupling effects on stress and strain distributions in wood subjected to transverse compression. *Composites Science and Technology*, 67:1362–1369, 2006.

[5] http://de.wikipedia.org/wiki/Holz, March 2008. 28.03.2008.

[6] http://de.wikipedia.org/wiki/Glucose, March 2008. 28.03.2008.

[7] www.greenspirit.org.uk/Resources/cellulose.gif, March 2008. 28.03.2008.

[8] http://chemistry.umeche.maine.edu/CHY431/Wood1.html, March 2008. 31.03.2008.

[9] http://de.wikipedia.org/wiki/Cellulose, March 2008. 28.03.2008.

[10] K. Hofstetter, C. Hellmich, and J. Eberhardsteiner. Development and experimental validation of a contnuum micromechanics model for the elasticity of wood. *European Jounal of Mechanics A/Solids*, 24:1030–1053, 2005.

[11] http://de.wikipedia.org/wiki/Zellwand, March 2008. 28.03.2008.

[12] D. Fengel and G. Wegener. *WOOD Chemistry, Ultrastructure, Reactions*. Verlag Kessel, Munich, 2003.

[13] http://de.wikipedia.org/wiki/Fr%C3%BChholz#Periodische_Entwicklungsphasen, March 2008. 28.03.2008.

[14] A. Zaoui. Continuum micromechanics: Survey. *Journal of engineering mechanics*, 128(8):808–816, 2002.

[15] H. Böhm. *A short introduction to continuum micromechanics*. Springer Verlag, Wien, New York, 2004.

[16] P. Suquet. *Elements of homogenization for inelastic solid mechanics.* Springer Verlag, Wien, New York, 1987.

[17] K. Hofstetter, C. Hellmich, and J. Eberhardsteiner. Micromechanical modeling of solid-type and plate-type deformation patterns within softwood materials. A review and an improved approach. *Holzforschung*, 61:343–351, 2006.

[18] http://www.imws.tuwien.ac.at/labors/labor-rella-halle/ausstattung.html, March 2008. 28.03.2008.

[19] H. Mang and G. Hofstetter. *Festigkeitslehre.* Verlag Springer, Wie, New York, 2004.

Appendix A

Determination of the Wood Constituents at a Chemical Laboratory

To identify the content of the various ingredients of wood, a chemical analysis has to be done. As described in Section 2.2, dry wood consists basically of the following constituents:

- extractives,

- cellulose,

- hemicellulose, and

- lignin.

For dissolving these ingredients, the wood samples needs a *high surface area*. Otherwise the dissolving fluids cannot penetrate into the core of the wood pieces.

A.1 Preparatory Work

From the investigated samples, *little splints* with a maximal length of 35 mm (optimal length 15 to 20 mm) and a cross-sectional area of about 1 mm^2 are chipped. The chipping is necessary for the subsequent *milling procedure*. A *high-frequency ultra fine centrifugal-mill* grind these little pieces of wood to particles with a characteristic dimension of 0.25 μm. Inside the mill a high-frequency motor rotates a steel-plate with 15000 *revolutions per minute*. First, the wood splints are broken when they hit the rotating steel-plate. The steel-plate has *crack wedges* at the border of the round base plate, where the broken wood splints break a second time. Finally, a *grater* pulverizes the fractured splinters to a dimension of maximally 0.25 μm.

To exclude the influence of water, the fine powder is dried by a *vacuum furnace* at a temperature of 40 °C and 20 mbar subpressure. After cooling the powder in an *exsiccator* to room temperature under prevention of access of moisture, *testing cells* are filled with an amount of 1.5 g of each sample for determination of the extractives.

A.2   Dissolving of the Extractives

The testing cells filled with a small amount of wood powder have locking caps at both ends, each with a small hole. Through these holes the powder samples are loaded with *pressure* and consecutively with the *four extracting fluids*. Additionally an *oven* heats up the cells to speed up the solution process. The extraction is done by an *ASE-machine* (ASE . . . accelerated solvent extractor, from concern Dionex). Every cell is rinsed thoroughly with each of the four fluids at a temperature of 100 °C and a pressure of 110 bar. These fluids are:

- cyclohexan and ethanol in a ratio of 2:1,

- ethanol,

- ethanol and water in a ratio of 1:1,

- deionized water.

The durations of the flushing procedures are specified in Table A.1.

Fluid	Rinsing periods	Extract bottle
cyclohexan:ethanol 2:1	5 × 5 min	bottle 1
ethanol	1 × 5 min	bottle 1
ethanol:water 1:1	5 × 5 min	bottle 2
deionized water	5 × 5 min	bottle 3

Table A.1: Flushing procedures

The extracts of the four extraction steps and the solution fluids run into three bottles as indicated in Table A.1. The equipment for these flushing processes is shown in Figure A.1. The contents of these bottles are *decanted into flasks*, which are tared and heated above the boiling point. So the *solution fluids boil away* and the extractives are left inside the flasks. The flasks with the extractives are then dried at 105 °C, kept in an dehydrator (exsiccator) for one hour and weighed after cooling down. The *content of the extractives* is calculated as relation between the weight of the extractives and the weight of the wood sample, which was filled into the testing cell. Beside the fraction of extractives, also the wood samples without these extractives are obtained, which are used to estimate the fractions of lignin, hemicellulose, and cellulose. The procedure of the determination of the extractives is illustrated in Figure A.2.
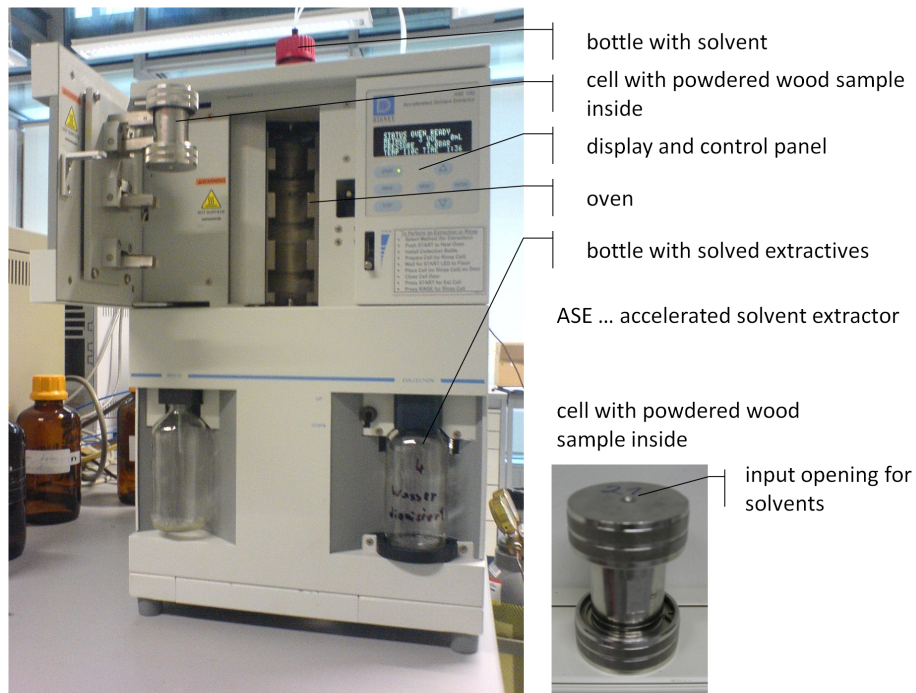
Figure A.1: Accelerated solvent extractor (ASE)
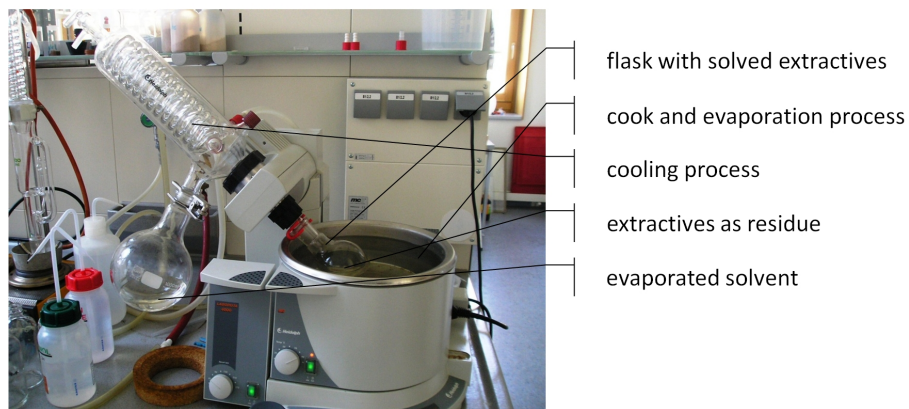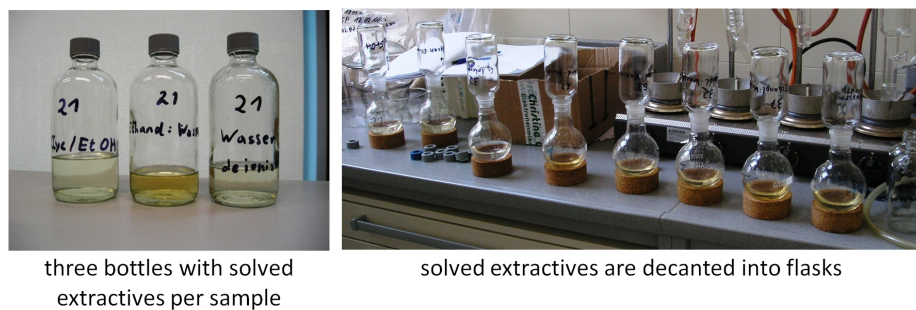
Figure A.2: Determination of the extractives

A.3   Determination of Lignin

To measure the *fraction of lignin*, the other components are solved by an acid. One possibility is *sulfuric acid* that *transforms cellulose and hemicellulose to saccharides* (sugar) and washes them out of the sample. So only the fraction of *insolvable lignin* is left. The content of *solvable lignin* is measured by ultraviolet rays.

For the solution of cellulose and hemicellulose two beakers are filled with an amount of 0.5 g of an extracted sample at a time, which is admixed with 7.5 ml cold sulfuric acid. This mixture has to be orderly crushed to push the sulfuric acid to each wood particle, while the beaker stands in ice water to hold it at a constant temperature. *Green coloration* after combination of extracted wood powder and sulfuric acid is *typical of spruce*. Afterwards the beakers are put into a *water bath* with a temperature of 20 ℃ for two hours. Then the beakers' content is washed into a *glass plunger* and filled up to a content of 285 g with deionized water. The glass plunger and, thus, its content are cooked in water at about 100 ℃ for *four hours*, resulting in partial evaporation of the water. After the cooking the plunger is cooled to room temperature and filled up with deionized water to a content of 285 g again. In a next step, the content of the plunger percolates through a *filter paper* and the *filter glass* into a second plunger. At first, only part of the water with suspended particles is washed through the filter. An amount of 10 ml of the filtrated water is taken to analyze the content of *acid-soluble lignin*. In the second step the flask and the filtrate inside the filter glass is washed with boiling deionized water in order to wash out both, the *acid-soluble lignin* and the *sulfuric acid*. The filter glasses with the samples are dried in a drying chamber and weighed after cooling down in an exsiccator. The fraction of *acid-soluble lignin* is determined by the absorption of the sample at 205 nm *ultraviolet-rays* in a ultraviolet-cuvette. A 3% sulfuric acid is used as a blank. The equipment for the flushing procedure is shown in Figure A.3.

A.4   Determination of Cellulose and Hemicellulose

The *principle* of determination of cellulose and hemicellulose contents contains approximately the *same steps as for the lignin determination*. Both, cellulose and hemicellulose are *hydrolyzed by acids*. The hydrolysis splits the organic chemical bonds into their *monomers* (components). Only the target and quantities are different to the steps described in Section A.3.

A.4.1   Determination of Cellulose

At first an amount of 10 mg of the extracted wood powder is filled into a test tube and mixed with sulfuric acid. This step solves the *polysaccharide cellulose* into its *monomers* that are *glucose units*. Sulfuric acid breaks the chain links, and the emerging sugar-monomers are soluble in water. Lignin is left in non-soluble form. For the determination of lignin the deposition is weighed.

The test tube with wood powder inside is immersed into a water bath at 20 ℃ for two hours. After that the tube is heated by a drying oven at a temperature of 125 ℃ for another two hours. These steps dissolve the cellulose. To protect the equipment of the

wood assays with sulfuric acid for disconnecting the cellulose chains

soluble lignin (assay from e))

a)

b)

c)

d)

e)

insoluble lignin

a)filter glass for the soluble lignin
b)glass with the wood sample cooked in
    285 ml deionized water
c)glass for an assay of soluble lignin
d)deionized water for flushing

e) flushed soluble lignin and
    cellulose
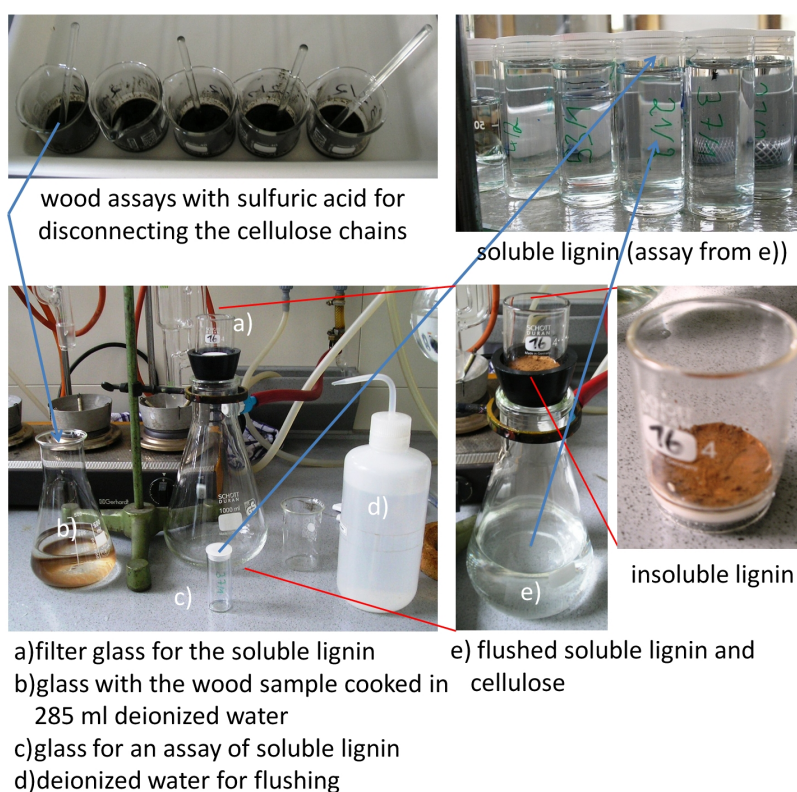
Figure A.3: Determination of lignin

gas chromatography in the last step against the aggressive sulfuric acid, the sample is neutralized by *barium hydroxide*. Barium sulfate is formed in this process which is hardly soluble and precipitates. The neutralized solution is evaporated and, finally, the glucose content is determined by *gas chromatography*.

A.4.2 Determination of Hemicellulose

The *basic units* of hemicellulose are *hexose* ($C_6H_{12}O_6$) and *pentose* ($C_5H_{10}O_5$), depending on the wood species. For determination of the hemicellulose fraction, a *methanolysis* is done. Extracted wood powder is mixed with *methanolic salt acid* in a closed test tube and heated up to 103 ℃ for five hours. Only hemicellulose is dissipated by the salt acid but not the cellulose. The glucose (sugar) content is determined as described in section A.4.1.

Appendix B

Program Code

B.1 equc_woodplane_v6_2.m

```
% COMSOL Multiphysics Model M-file
% Generated by COMSOL 3.3a (COMSOL 3.3.0.511, $Date: 2007/02/02
19:05:58 $)

% =========================================================================
% Explanations to this program
% -------------------------------------------------------------------------
% This program consists of two calculation steps at which the first
% step detects the integration points of the finite elements and second
% step arrange the FEM-calculation, in the global scheme of things.

% The command delete (for example: x_info_3d.dat) all values from
% a previous calculation to prevent wrong FEM-calculations.

% At the begin the file "DIPL_eingabe.m" brings the input values to the
% calculation steps.
%        - picture ... name of the gray picture
%        - sd      ... vector with the side length of the cuboid
%                      x-Richtung = longitudinal direction
%                      y-Richtung = horizontal direction at cross sect.
%                      z-Richtung = vertical direction at cross-section

% Point "equ.c" determines the integration point coordinates and saves
% them with the file "koord_info_3d(x,y,z),m". These informations are
% storaged in three .mat-files with the names x_info_3d.mat,
% y_info_3d.mat and z_info_3d.mat.

% "DIPL_image_input.m" calculates a vector with the name
% "density_vector" and deliver this to the file
% "DIPL_macro_stiffness.m", which estimates the matrixes of stiffness
% named "ChomIII_komp". With the coordinates from x_info_3d.mat,
% y_info_3d.mat and z_info_3d.mat "DIPL_image_input.m"
% arrange a matrix with all stiffness values for all integration points
% and divide it into vectors, for example called "C1111.mat", with equal
% directed stiffness values.
% =========================================================================
% Now the second calculation step is following!
% At the point "equ.c" the values from "C1111.mat", "C1122.mat" and so
% on are inserted done by the files "stiffness_3d_C1111.m",
% "stiffness_3d_C1122.m" and so on.
```

```
% =======================================================================
% First calculation step to determine the INTEGRATION POINT COORDINATES
% =======================================================================

profile on

'Beginn der Berechnung'

'Lschen eventuell vorhandener Koordinateninfos'
delete x_info_3d.dat; delete y_info_3d.dat; delete z_info_3d.dat

delete density_vector.mat; delete alpha_vector.mat; delete alpha_mat.mat

delete mwcotrp_t.mat; delete mwaotrp_t_rad.mat; delete mwcotrp_l.mat; delete mwaotrp_l_rad.mat
...
delete mwcotr_t.mat; delete mwcotr_t2.mat; delete mwcotr_l.mat; delete mwcotr_l2.mat
...
delete C3333.mat; delete C3322.mat
...
delete C2333.mat; delete C2331.mat
...
delete C2211.mat; delete C1233.mat
...
delete C1122.mat; delete C1111.mat
...

delete mwcotrp_t2.mat; delete mwaotrp_t2_rad.mat; delete mwcotrp_l2.mat; delete mwaotrp_l2_rad.mat
...
clear all

flclear fem

% =======================================================================
DIPL_cut_tree_rings
% =======================================================================
% Program for digitalization of the annual rings calculates the angles
% of the annual rings. The values are storaged in output-files (.mat) to
% access at each state of calculation.
% =======================================================================

% COMSOL version
clear vrsn
vrsn.name = 'COMSOL 3.3';
vrsn.ext = 'a';
vrsn.major = 0;
vrsn.build = 511;
vrsn.rcs = '$Name:  $';
vrsn.date = '$Date: 2007/02/02 19:05:58 $';
fem.version = vrsn;

'Einlesen der Geometrie 1-er Schritt'

% =======================================================================
% DIPL_eingabe.m put the geometrical informations into the program.
% =======================================================================
[picture,sd,hauto,pf,hmaxfact]=DIPL_eingabe();
picture
sd
% =======================================================================

% Geometry
g1=block3(sd(1),sd(2),sd(3),'base','corner','pos',{'0','0','0'},
'axis',{'0','0','1'},'rot','0');

% Analyzed geometry
clear s
s.objs={g1};
s.name={'BLK1'};
s.tags={'g1'};
```

```
fem.draw=struct('s',s);
fem.geom=geomcsg(fem);

'FEM-MESH 1-er Schritt'

% ====================================================================
% hauto defines the cuteness of the finite elements mesh.
% ====================================================================
hauto
% ====================================================================

hmaxfact

% Initialize mesh
fem.mesh=meshinit(fem, ...
                  'hmaxfact',hmaxfact, ...
                  'hcurve',0.2, ...
                  'hgrad',1.3, ...
                  'hcutoff',0.001, ...
                  'hnarrow',1);
% ====================================================================

% (Default values are not included)

% Application mode 1
clear appl
appl.mode.class = 'FlSolid3';
appl.gporder = 2;
appl.cporder = 1;
appl.assignsuffix = '_sld';

clear prop
prop.elemdefault='Lag1';
appl.prop = prop;

clear pnt
pnt.Hy = {0,0,0,1,1,0,1,1};
pnt.Hx = {0,1,1,1,1,0,0,0};
pnt.Hz = {0,1,0,1,0,1,1,0};
pnt.ind = [2,3,4,5,6,1,7,8];
appl.pnt = pnt;

clear bnd
bnd.Hz = {0,1,1};
bnd.Rz = {0,0,0.0002};
bnd.ind = [1,1,2,3,1,1];
appl.bnd = bnd;

clear equ
equ.nu = 'mat1_nu';
equ.E = 'mat1_E';
equ.rho = 'mat1_rho';
equ.ind = [1];
appl.equ = equ;
fem.appl{1} = appl;
fem.frame = {'ref'};
fem.border = 1;

clear units;
units.basesystem = 'SI';
fem.units = units;

'EQU.C 1-er Schritt'

% Subdomain settings
clear equ
equ.c = {{{ % start first matrix
         'koord_info_3d(x,y,z)',0,0;0,1,0;0,0,1}, ...
```

```
                {0,1,0;1,0,0;0,0,0}, ...
                {0,0,1;0,0,0;1,0,0}; ...
                {0,1,0;1,0,0;0,0,0}, ...
                {1,0,0;0,1,0;0,0,1}, ...
                {0,0,0;0,0,1;0,1,0}; ...
                {0,0,1;0,0,0;1,0,0}, ...
                {0,0,0;0,0,1;0,1,0}, ...
                {1,0,0;0,1,0;0,0,1}}};


fem.lib = lib;

% Multiphysics
fem=multiphysics(fem, ...
   'sdl',[]);

% Extend mesh
fem.xmesh=meshextend(fem);

% Solve problem
fem.sol=femstatic(fem, ...
                  'solcomp',{'w','v','u'}, ...
                  'outcomp',{'w','v','u'}, ...
                  'linsolver','spooles');

% Save current fem structure for restart purposes
fem0=fem;

% =======================================================================
% File DIPL_image_input.m determines the stiffness components for the
% FEM-calculation.
% =======================================================================

'DIPL_image_input fr die Jahrringdigitalisierung'

DIPL_image_input;

% =======================================================================
% Second calculation step = main FEM-calculation
% =======================================================================

'2-ter Rechenschritt'

'EQU.C 2-ter Schritt'

% Subdomain settings
clear equ
equ.c = {{{ % start first matrix
            'stiffness_3d_C1111(x,y,z)', ...      %C1111
             0, ...                               %C1112 = 0-Matrix
             0; ...                               %C1113 = 0-Matrix
             0, ...                               %C1211 = 0-Matrix
            'stiffness_3d_C1212(x,y,z)', ...      %C1212
            'stiffness_3d_C1231(x,y,z)'; ...      %C1213
             0, ...                               %C1311 = 0-Matrix
            'stiffness_3d_C3112(x,y,z)', ...      %C1312
            'stiffness_3d_C3131(x,y,z)'}, ...     %C1313
             % end first matrix
             % begin second matrix
            {0, ...                               %C1121 = 0-Matrix
            'stiffness_3d_C1122(x,y,z)', ...      %C1122
            'stiffness_3d_C1123(x,y,z)'; ...      %C1123
            'stiffness_3d_C1212(x,y,z)', ...      %C1221
             0, ...                               %C1222 = 0-Matrix
             0; ...                               %C1223 = 0-Matrix
            'stiffness_3d_C3112(x,y,z)', ...      %C1321
             0, ...                               %C1322 = 0-Matrix
             0}, ...                              %C1323 = 0-Matrix
             % end second matrix
```

```
                % begin third matrix
               {0, ...                             %C1131 = 0-Matrix
               'stiffness_3d_C1123(x,y,z)', ...    %C1132
               'stiffness_3d_C1133(x,y,z)'; ...    %C1133
               'stiffness_3d_C1231(x,y,z)', ...    %C1231
                0, ...                             %C1232 = 0-Matrix
                0; ...                             %C1233 = 0-Matrix
               'stiffness_3d_C3131(x,y,z)', ...    %C1331
                0, ...                             %C1332 = 0-Matrix
                0}; ...                            %C1333 = 0-Matrix
                % end third matrix
                % begin fourth matrix
               {0, ...                             %C2111 = 0-Matrix
               'stiffness_3d_C1212(x,y,z)', ...    %C2112
               'stiffness_3d_C1231(x,y,z)'; ...    %C2113
               'stiffness_3d_C2211(x,y,z)', ...    %C2211
                0, ...                             %C2212 = 0-Matrix
                0; ...                             %C2213 = 0-Matrix
               'stiffness_3d_C2311(x,y,z)', ...    %C2311
                0, ...                             %C2312 = 0-Matrix
                0}, ...                            %C2313 = 0-Matrix
                % end fourth matrix
                % begin fifth matrix
               {'stiffness_3d_C1212(x,y,z)', ...   %C2121
                0, ...                             %C2122 = 0-Matrix
                0; ...                             %C2123 = 0-Matrix
                0, ...                             %C2221 = 0-Matrix
               'stiffness_3d_C2222(x,y,z)', ...    %C2222
               'stiffness_3d_C2223(x,y,z)'; ...    %C2223
                0, ...                             %C2321 = 0-Matrix
               'stiffness_3d_C2322(x,y,z)', ...    %C2322
               'stiffness_3d_C2323(x,y,z)'}, ...   %C2323
                % end fifth matrix
                % begin sixth matrix
               {'stiffness_3d_C1231(x,y,z)', ...   %C2131
                0, ...                             %C2132 = 0-Matrix
                0; ...                             %C2133 = 0-Matrix
                0, ...                             %C2231 = 0-Matrix
               'stiffness_3d_C2223(x,y,z)', ...    %C2232
               'stiffness_3d_C2233(x,y,z)'; ...    %C2233
                0, ...                             %C2331 = 0-Matrix
               'stiffness_3d_C2323(x,y,z)', ...    %C2332
               'stiffness_3d_C2333(x,y,z)'}; ...   %C2333
                % end sixth matrix
                % begin seventh matrix
               {0, ...                             %C3111 = 0-Matrix
               'stiffness_3d_C3112(x,y,z)', ...    %C3112
               'stiffness_3d_C3131(x,y,z)'; ...    %C3113
               'stiffness_3d_C2311(x,y,z)', ...    %C3211
                0, ...                             %C3212 = 0-Matrix
                0; ...                             %C3213 = 0-Matrix
               'stiffness_3d_C3311(x,y,z)', ...    %C3311
                0, ...                             %C3312 = 0-Matrix
                0}, ...                            %C3313 = 0-Matrix
                % end seventh matrix
                % begin eighth matrix
               {'stiffness_3d_C3112(x,y,z)', ...   %C3121
                0, ...                             %C3122 = 0-Matrix
                0; ...                             %C3123 = 0-Matrix
                0, ...                             %C3221 = 0-Matrix
               'stiffness_3d_C2322(x,y,z)', ...    %C3222
               'stiffness_3d_C2323(x,y,z)'; ...    %C3223
                0, ...                             %C3321 = 0-Matrix
               'stiffness_3d_C3322(x,y,z)', ...    %C3322
               'stiffness_3d_C3323(x,y,z)'}, ...   %C3323
                % end eighth matrix
                % begin ninth matrix
               {'stiffness_3d_C3131(x,y,z)', ...   %C3131
                0, ...                             %C3132 = 0-Matrix
```

```
               0; ...                           %C3133 = 0-Matrix
               0, ...                           %C3231 = 0-Matrix
            'stiffness_3d_C2323(x,y,z)', ...    %C3232
            'stiffness_3d_C2333(x,y,z)'; ...    %C3233
               0, ...                           %C3331 = 0-Matrix
            'stiffness_3d_C3323(x,y,z)', ...    %C3332
            'stiffness_3d_C3333(x,y,z)'}}};     %C3333
            % end ninth matrix

equ.ind = [1];
equ.dim = {'u','v','w'};
equ.var = {'Fxg_sld',0,'Fyg_sld',0,'Fzg_sld',0,'disp_sld','sqrt(real(u)^2+real(v)^2+real(w)^2)','sx_sld',
  '(stiffness_3d_C1111(x,y,z))*ex_sld+(stiffness_3d_C1122(x,y,z))*ey_sld+(stiffness_3d_C1133(x,y,z))
  *ez_sld','sy_sld','(stiffness_3d_C2211(x,y,z))*ex_sld+(stiffness_3d_C2222(x,y,z))*ey_sld+(stiffness_3d_C2233(x,y,z))
  *ez_sld','sz_sld','(stiffness_3d_C3311(x,y,z))*ex_sld+(stiffness_3d_C3322(x,y,z))*ey_sld+(stiffness_3d_C3333(x,y,z))
  *ez_sld','sxy_sld','(stiffness_3d_C1212(x,y,z))*exy_sld','syz_sld','(stiffness_3d_C2323(x,y,z))
  *eyz_sld','sxz_sld','(stiffness_3d_C3131(x,y,z))*exz_sld','ex_sld','ux','ey_sld','vy','ez_sld','wz','exy_sld',
  '0.5*(uy+vx)','eyz_sld','0.5*(vz+wy)','exz_sld','0.5*(uz+wx)','K_sld','E_sld/(3*(1-2*nu_sld))','G_sld',
  '0.5*E_sld/(1+nu_sld','mises_sld','sqrt(sx_sld^2+sy_sld^2+sz_sld^2-sx_sld*sy_sld-sy_sld*sz_sld-sx_sld*sz_sld+
  3*sxy_sld^2+3*syz_sld^2+3*sxz_sld^2','Ws_sld','0.5*(sx_sld*ex_sld+sy_sld*ey_sld+sz_sld*ez_sld+2*sxy_sld*exy_sld+
  2*syz_sld*eyz_sld+2*sxz_sld*exz_sld)','evol_sld','ex_sld+ey_sld+ez_sld','tresca_sld','max(max(abs(s1_sld-s2_sld,
  abs(s2_sld-s3_sld,abs(s1_sld-s3_sld','E_sld','mat1_E','rho_sld','mat1_rho','alphadM_sld',1,'betadK_sld',0.001,
  'eta_sld',0,'mixedform_sld',0,'mu_sld',800000,'C10_sld',200000,'C01_sld',200000,'kappa_sld',10000000000,
  'ETkin_sld',20000000000,'ETiso_sld',20000000000,'Sys_sld',200000000,'Syfunc_sld','mises_sld','Syfunc_kin_sld',
  'misesKin_sld','Shard_sld','20000000000[Pa]*epe_sld/(1-20000000000[Pa]/200000000000[Pa]','alpha_sld',1.2e-005,
  'nu_sld','mat1_nu','Ex_sld',200000000000,'nuxy_sld',0.33,'Gxy_sld',75200000000,'alphax_sld',1.2e-005,'sxi_sld',0,
  'sxyi_sld',0,'exi_sld',0,'exy_sld',0,'Ey_sld',200000000000,'nuyz_sld',0.33,'Gyz_sld',75200000000,'alphay_sld',1.2e-005,
  'syi_sld',0,'syzi_sld',0,'eyi_sld',0,'eyzi_sld',0,'Ez_sld',200000000000,'nuxz_sld',0.33,'Gxz_sld',75200000000,
  'alphaz_sld',1.2e-005,'szi_sld',0,'sxzi_sld',0,'ezi_sld',0,'exzi_sld',0,'Fx_sld',0,'FxAmp_sld',1,'FxPh_sld',0,'Fy_sld',
  0,'FyAmp_sld',1,'FyPh_sld',0,'Fz_sld',0,'FzAmp_sld',1,'FzPh_sld',0,'Temp_sld',0,'Tempref_sld',0,'velx_sld',0,'accx_sld',
  0,'vely_sld',0,'accy_sld',0,'velz_sld',0,'accz_sld',0,'Rx_sld',0,'Ry_sld',0,'Rz_sld',0,'dx_sld','dx_guess_sld','Lx_sld',
  'dx_sld','dy_sld','dy_guess_sld','Ly_sld','dy_sld','dz_sld','dz_guess_sld','Lz_sld','dz_sld','dr_sld','dr_guess_sld',
  'Lr_sld','dr_sld','R0_sld','R0_guess_sld','X0_sld','X0_guess_sld','Y0_sld','Y0_guess_sld','Z0_sld','Z0_guess_sld',
  'x0_sld',0,'y0_sld',0,'z0_sld',0,'n_sld',1};
fem.equ = equ;

% Library materials
clear lib
lib.mat{1}.name='Structural steel';
lib.mat{1}.varname='mat1';
lib.mat{1}.variables.nu='0.33';
lib.mat{1}.variables.E='200e9[Pa]';
lib.mat{1}.variables.mur='1';
lib.mat{1}.variables.sigma='4.032e6[S/m]';
lib.mat{1}.variables.epsilonr='1';
lib.mat{1}.variables.alpha='12.3e-6[1/K]';
lib.mat{1}.variables.C='475[J/(kg*K)]';
lib.mat{1}.variables.rho='7850[kg/m^3]';
lib.mat{1}.variables.k='44.5[W/(m*K)]';

fem.lib = lib;

% Multiphysics
fem=multiphysics(fem, ...
  'sdl',[]);

% Extend mesh
fem.xmesh=meshextend(fem);

% Solve problem
fem.sol=femstatic(fem, ...
                 'solcomp',{'w','v','u'}, ...
                 'outcomp',{'w','v','u'}, ...
                 'linsolver','spooles');

% Save current fem structure for restart purposes
fem0=fem;

% =========================================================================
```

```
% Output as coloured plots.
% =====================================================================

'Plotten des Ergebnisses'

% Plot solution
figure;
postplot(fem, ...
         'slicedata',{'w','cont','internal','unit','um'},'slicexspacing',3,'sliceyspacing',0,'slicezspacing',0,
'slicemap','jet(1024)','deformsub',{'u','v','w'},'deformscale',100,'title','Slice: z-displacement [um]
Deformation:Displacement[m]','grid','on','campos',[10*sd(2),sd(2)/2,sd(3)/2],'camtarget',[0,sd(2)/2,
sd(3)/2],'camup',[0,0,1],'camva',12.11573742228453);

figure;
meshplot(fem)
profile viewer
```

B.2 DIPL_cut_tree_rings.m

```
delete density_vector.mat; delete alpha_vector.mat; delete alpha_mat.mat

delete mwcotrp_t.mat, delete mwaotrp_t_rad.mat ...

delete mwcotr_t.mat, delete mwcotr_t2.mat ...

warning off all

[picture,sd,hauto,pf]=DIPL_eingabe(); % Seitenlngen in x-, y- und
z-Richtung
picture;

image=imread(picture,'jpg');
image_modified=double(image);
image_picture=imshow(picture);

row_IMM=size(image_modified,1);
col_IMM=size(image_modified,2);

% Matlab defines a point in a matrix with two values (z,y). Z stands for
% the row while y prescribe the column.

% graphically:

% % %                                   Y-Koord. = col   \
% % %                  ------------------------   --------------\
% % %                  |                      |              /
% % %                  |                      |             /
% % %                  |                      |
% % %                  |      pixel picture   |
% % %                  |                      |
% % %                  |                      |
% % %                  |_____|
% % %                  |
% % %      Z-Koord.    |
% % %          =       |
% % %        row   \ | /
% % %               \|/

top=pf(11); left=pf(12); bottom=pf(13); right=pf(14)
top_2=pf(15); left_2=pf(16); bottom_2=pf(17); right_2=pf(18);

% =====================================================================
% picture finishing
% =====================================================================
% For a better handling all points respectively each pixel that is
% lighter than 190 is transformed to 245 and all darker pixels into 10.
```

```
image_grayscale=image_modified;

gsb=190; %gsb ... gray scale break

for y=1:col_IMM;
    for z=1:row_IMM;
        if image_modified(z,y)<gsb;
            image_modified(z,y)=10;
        else;
            image_modified(z,y)=245;
        end;
    end;
end;


% =====================================================================
% searching at the imageborder
% =====================================================================
topbor=image_modified(1,:);          % top border
lefbor=image_modified(:,1);          % left border
botbor=image_modified(row_IMM,:);    % bottom border
rigbor=image_modified(:,col_IMM);    % rigbot border
% =====================================================================
% Calculation of the annual ring starts.
% =====================================================================

if top==1

for i=1:col_IMM;
    topbor_ind(1,i)=0;
    if topbor(1,i)<100;
        topbor_ind(1,i)=1;
    end
end

for j=1:col_IMM;
    noo=0; % noo ... number of ones
    if topbor_ind(1,j)==1;
        for a=0:100;
            if j+a>col_IMM;
                noo=a+1;
                break;
            end;
            if topbor_ind(1,j+a)==0;
                noo=a+1;
                break;
            end;
        end;
        for b=0:(noo-1);
            c=round(noo/2)-1;
            if b==c;
                topbor_ind(1,j+b)=1;
            else;
                topbor_ind(1,j+b)=0;
            end;
        end;
    end;
end;
topbor_ind;
end;


% =====================================================================
% Identification of number and coordinates of the annual ring starts.
% =====================================================================

% mwcotr_t ... matrix with coordinates of tree rings_top border
% mwcotr_l ... matrix with coordinates of tree rings_left border
% mwcotr_b ... matrix with coordinates of tree rings_bottom border
% mwcotr_r ... matrix with coordinates of tree rings_right border
```

```
% notr_t ... number of tree ring_top border
% notr_l ... number of tree ring_left border
% notr_b ... number of tree ring_bottom border
% notr_r ... number of tree ring_right border

if top==1
notr_t=0; % notr ... number of tree rings for top border
mwcotr_t=zeros(2,2);
for y=1:col_IMM;
    if topbor_ind(1,y)==1;
        notr_t=notr_t+1;
        mwcotr_t(1,(notr_t*2-1))=1;
        mwcotr_t(1,(notr_t*2))=y;
    end
end
end


% =====================================================================
% All annual rings are scanned pixel by pixel and the coordinates of the
% middle of the tree ring is storaged in a matrix.
% =====================================================================

sa=20; %sa ... searching area
% ---------------------------------------------------------------------
% mwcotr_t ... matrix with coordinates of tree rings_top border
% ---------------------------------------------------------------------

if top==1
    'top ist eingeschalten'
for i=1:notr_t;
    z_coor=mwcotr_t(1,(i*2-1)); % z-coordinate of the initial point
    y_coor=mwcotr_t(1,(i*2));   % y-coordinate of the initial point
    y=y_coor;

    for z=1:(row_IMM-1);
        y_min=y-sa;
        y_max=y+sa;
        grayscale=image_modified(z,y);
        for m1=(y):-1:y_min;
            if m1<1;
                m1=1;
                break;
            elseif image_modified(z+1,m1)<(grayscale-100);
                m1=m1+1;
                break;
            elseif image_modified(z+1,m1)>(grayscale+100);
                m1=m1+1;
                break;
            else;
                m1=m1;
            end;
        end;

        for m2=(y):1:y_max;
            if m2>col_IMM;
                m2=col_IMM;
                break;
            elseif image_modified(z+1,m2)<(grayscale-100);
                m2=m2-1;
                break;
            elseif image_modified(z+1,m2)>(grayscale+100);
                m2=m2-1;
                break;
            else;
                m2=m2-1;
            end;
        end;

        y=round((m1+m2)/2);
```

```
        if y==1;
            yy=2;
            if image_modified(z+1,y)>gsb & ...
                image_modified(z+1,yy)>gsb;
            break;
            end;
        elseif y==2;
            yy=1;
            if image_modified(z+1,y)>gsb & ...
                image_modified(z+1,yy)>gsb;
            break;
            end;
        elseif y==3;
            yy=2;
            if image_modified(z+1,y)>gsb & ...
                image_modified(z+1,yy)>gsb;
            break
            end
        elseif y==col_IMM;
            yy=col_IMM-1;
            if image_modified(z+1,y)>gsb & ...
                image_modified(z+1,yy)>gsb;
            break;
            end;
        elseif y==(col_IMM-1);
            yy=col_IMM;
            if image_modified(z+1,y)>gsb & ...
                image_modified(z+1,yy)>gsb;
            break;
            end;
        elseif y==(col_IMM-2);
            yy=col_IMM-1;
            if image_modified(z+1,y)>gsb & ...
                image_modified(z+1,yy)>gsb;
            break;
            end;
        else;
            y=y;
            yy=y-1;
            yyy=y+1;
            yyyy=y-2;
            yyyyy=y+2;
            yyyyyy=y-3;
            yyyyyyy=y+3;
            if image_modified(z+1,y)>gsb & ...
                    image_modified(z+1,yy)>gsb & ...
                    image_modified(z+1,yyy)>gsb & ...
                    image_modified(z+1,yyyy)>gsb & ...
                    image_modified(z+1,yyyyy)>gsb & ...
                    image_modified(z+1,yyyyyy)>gsb & ...
                    image_modified(z+1,yyyyyyy)>gsb;
            break;
            end;
        end;
        mwcotr_t((z+1),(i*2-1))=z+1; % z-coordinate of the next point
        mwcotr_t((z+1),(i*2))=y; % y-coordinate of the next point
    end;

mwcotr_t;
save 'mwcotr_t.mat' mwcotr_t

% All other seven search algorithms operate in an analogous manner.
% ------------------------------------------------------------------------

'DIPL_alpha_cut_tree_rings fr die punktuelle Winkelermittlung'

DIPL_alpha_cut_tree_rings % Calculates the angles of the annual rings.
```

```
cip=pf(1); % cip ... center in picture
nsoctr=pf(2); % nsoctr ... nearest side of continuous tree ring

if cip==1
    if nsoctr==5;
        DIPL_complete_tree_rings_top
    elseif nsoctr==6;
        DIPL_complete_tree_rings_left
    elseif nsoctr==7;
        DIPL_complete_tree_rings_bottom
    elseif nsoctr==8;
        DIPL_complete_tree_rings_right
    end
    DIPL_alpha_complete_tree_rings
end

'DIPL_alpha_matrix fr die Zusammenstellung der alpha-Matrix'

DIPL_alpha_matrix % Compilation of the annual ring angles.
```

B.3 DIPL_alpha_cut_tree_rings.m

```
[picture,sd,hauto,pf]=DIPL_eingabe();

top=pf(11); left=pf(12); bottom=pf(13); right=pf(14);
top_2=pf(15); left_2=pf(16); bottom_2=pf(17); right_2=pf(18);

% =======================================================================
if top==1;
load mwcotr_t; % mwcotr_t ... matrix with coordinates of tree rings_top
notr_t=(size(mwcotr_t,2))/2; % notr_t ... number of tree rings_top
mh_t=size(mwcotr_t,1); % mh_t ... matrix high_top
end;

% =======================================================================
% Calculation of the angles of the annual rings for top border.
% =======================================================================
if top==1
for i=1:notr_t; % i bezieht sich auf die Spalte mit den z-Koordinaten.

    if mh_t<6;
        mwaotrp_t_rad=0;
        mwcotrp_t=0;
        mwaotrp_t=0;
        break;
    end;

    for a=1:mh_t; % a luft die Matrix von oben nach unten durch.
        zp=mwcotr_t(a,(i*2-1));
        if zp==0;
            break;
        end;
        yp=mwcotr_t(a,(i*2));

% =======================================================================
% Continuous number arrives first border.
% =======================================================================
        if a>6;
            z1=mwcotr_t((a-6),(i*2-1));
            y1=mwcotr_t((a-6),(i*2));
            z2=mwcotr_t((a-5),(i*2-1));
            y2=mwcotr_t((a-5),(i*2));
        end;

        for g=0:5;
            if a==g+1;
```

```
                z1=mwcotr_t((a-g),(i*2-1));
                y1=mwcotr_t((a-g),(i*2));
                z2=mwcotr_t((a-g+1),(i*2-1));
                y2=mwcotr_t((a-g+1),(i*2));
            end;
        end;
% =====================================================================
% Continuous number arrives second border.
% =====================================================================
        if a<(mh_t-5);
            z4=mwcotr_t((a+5),(i*2-1));
            y4=mwcotr_t((a+5),(i*2));
            z5=mwcotr_t((a+6),(i*2-1));
            y5=mwcotr_t((a+6),(i*2));
        end;

        for g=0:5
            if a==mh_t-g;
                z4=mwcotr_t((a+g-1),(i*2-1));
                y4=mwcotr_t((a+g-1),(i*2));
                z5=mwcotr_t((a+g),(i*2-1));
                y5=mwcotr_t((a+g),(i*2));
            end
        end
% =====================================================================
% Continuous number arrives first border.
% =====================================================================
        for g=1:5;
            if a==g;
                z4=mwcotr_t((a+g-1),(i*2-1));
                y4=mwcotr_t((a+g-1),(i*2));
                z5=mwcotr_t((a+g),(i*2-1));
                y5=mwcotr_t((a+g),(i*2));
            end;
        end;

        for h=6:-1:1;
            if z4==0 & a<(mh_t-h);
                z4=mwcotr_t((a+h),(i*2-1));
                y4=mwcotr_t((a+h),(i*2));
            elseif z4>0;
                break;
            end;
        end;

        if z5==0;
            z5=z4;
            y5=y4;
        end;

        zm1=z5-z1;
        ym1=y1-y5;

        zm2=z4-z2;
        ym2=y2-y4;
% =====================================================================
% Angle of a annual ring point is the means of two calculated angles.
% =====================================================================
        alpha1=atan(zm1/ym1)+pi/2;
        alpha2=atan(zm2/ym2)+pi/2;

        if zm1==0 & ym1==0;
            alpha1=0;
        end;

        if zm2==0 & ym2==0;
            alpha2=0;
        end;
```

```
        if alpha1==0 & alpha2~=0;
            alpha=alpha2;
        elseif alpha1~=0 & alpha2==0;
            alpha=alpha1;
        else;
            alpha=(alpha1+alpha2)/2;
        end;

% =====================================================================
% Building of a matrix with the angles of the annual rings.
% =====================================================================
        mwaotrp_t(a,i)=alpha;
%        mwaotrp_t ... matrix with angel of tree ring point_top
% =====================================================================
% Calculation of radius and curvature.
% =====================================================================
        zs=abs(zm1);
        ys=abs(ym1);

        zs1=abs(z5-zp);
        ys1=abs(yp-y5);

        if a>(mh_t-5);
            zs1=abs(z1-zp);
            ys1=abs(yp-y1);
        end

        s=(zs^2+ys^2)^(1/2);
        s1=(zs1^2+ys1^2)^(1/2);

        beta=acos((s/2)/s1);
        phi=abs(2*beta);

        if phi==0;
            phi=0.000001;
        end

        r=(s/2)/sin(phi);
        kappa=1/r;

        mwrotrp_t(a,i)=r;
%         mwrotrp_t ... matrix with radius of tree ring point_top
        mwcotrp_t(a,i)=kappa;
%         mwcotrp_t ... matrix with curvature of tree ring point_top
    end;
end;

mwaotrp_t_rad=mwaotrp_t;
if mh_t<6
    mwaotrp_t_rad=zeros(5,4);
end
save 'mwaotrp_t_rad.mat' mwaotrp_t_rad;
mwaotrp_t_deg=mwaotrp_t_rad*180/pi;
save 'mwcotrp_t.mat' mwcotrp_t;
mwcotrp_t;

end

% mwaotrp_t_rad ... matrix with angel of tree ring points_top_radian
% mwaotrp_t_deg ... matrix with angel of tree ring points_top_degree

% =====================================================================
% Plot of the angles.
% =====================================================================
l=8;
s=2;
ps=pf(5);
% =====================================================================
% Picture for all annual rings which start at top border.
```

```
% ======================================================================
figure;

if top==1
for i=1:notr_t; % i bezieht sich auf die Spalte mit den z-Koordinaten.

    if mh_t<6
        break
    end

    for a=1:ps:mh_t; % a luft die Matrix von oben nach unten durch.
        zp=mwcotr_t(a,(i*2-1));
        if zp==0;
            break;
        end;
        yp=mwcotr_t(a,(i*2));
        alphap=mwaotrp_t_rad(a,i);

        z1=zp-(l*sin(alphap));
        y1=yp+(l*cos(alphap));

        z2=zp+(s*sin(alphap));
        y2=yp-(s*cos(alphap));

        z3=zp-(s*cos(alphap));
        y3=yp-(s*sin(alphap));

        z4=zp+(s*cos(alphap));
        y4=yp+(s*sin(alphap));

        hold on

        plot([y1,y2],[-z1,-z2],'r');
        plot([y3,y4],[-z3,-z4],'r');
    end
end
end
hold off
% ======================================================================
% Picture of the coordinates of all annual rings which start at top
% border.
% ======================================================================
figure;
if top==1
for i=1:notr_t; % i bezieht sich auf die Spalte mit den z-Koordinaten.

    if mh_t<6
        break
    end

    for a=1:ps:mh_t; % a luft die Matrix von oben nach unten durch.
        zp=mwcotr_t(a,(i*2-1));
        if zp==0;
            break;
        end;
        yp=mwcotr_t(a,(i*2));
        hold on

        plot(yp,-zp,'rv','MarkerSize',5);
    end
end
end
hold off

% ======================================================================
% All calculation steps for the other borders operate in an analogous
% manner.
% ======================================================================
```

B.4   DIPL_alpha_matrix.m

```
[picture,sd,hauto,pf]=DIPL_eingabe();

cip=pf(1) % cip ... center in picture
top=pf(11); left=pf(12); bottom=pf(13); right=pf(14);
top_2=pf(15); left_2=pf(16); bottom_2=pf(17); right_2=pf(18);
% =====================================================================

if cip==1

% Continuous annual rings inside the picture.
% The calculation steps deals with the same algoritms as without
% continuous annual rings.

% []]]]]]]]]]]]]]]]]]]]]]]]]]]]]]]]]]]]]]]]]]]]]]]]]]]]
else
% []]]]]]]]]]]]]]]]]]]]]]]]]]]]]]]]]]]]]]]]]]]]]]]]]]]]

% No continuous annual rings inside the picture.
% =====================================================================
if top==1;
load mwcotr_t; % mwcotr_t ... matrix with coordinates of tree rings_top
notr_t=(size(mwcotr_t,2))/2; % notr_t ... number of tree rings_top
mh_t=size(mwcotr_t,1); % mh_t ... matrix high_top
load mwaotrp_t_rad;
% mwaotrp_t_rad ... matrix with alpha of tree ring point_t
end;
% =====================================================================

% ()()()()()()()()()()()()()()()()()()()()()()()()()()()()()()()()
% () Inputs for alpha from: top border
% ()()()()()()()()()()()()()()()()()()()()()()()()()()()()()()()()

if top==1
for i=1:notr_t;
    for h=1:mh_t;
        z=mwcotr_t(h,(i*2-1));
        y=mwcotr_t(h,(i*2));
        if z==0
            z=1;
        end
        if y==0
            y=1;
        end
        alpha=mwaotrp_t_rad(h,i);
        if alpha==0;
            alpha=0.001;
        end;
        alpha_mat(z,y)=alpha;
    end
end
end;
'Speichern der alpha-Matrix'
save 'alpha_mat.mat' alpha_mat
```

B.5   koord_info_3d(x,y,z).m

```
function [C11] = koord_info_3d(x,y,z)
[C11]=ones(size(x))

outfile=fopen('x_info_3d.dat','a');
fprintf(outfile,'%6.3f;\n',x);
fclose(outfile);

outfile=fopen('y_info_3d.dat','a');
```

```
fprintf(outfile,'%6.3f;\n',y);
fclose(outfile);

outfile=fopen('z_info_3d.dat','a');
fprintf(outfile,'%6.3f;\n',z);
fclose(outfile);
```

B.6 DIPL_image_input.m

```
[picture,sd,hauto,pf]=DIPL_eingabe(); % Seitenlngen in x-, y- und
z-Richtung
picture;
image=imread(picture,'jpg');
image_info=imfinfo(picture)
size_image=size(image)
image_modified=image;
size_image_modified=size(image_modified);

% ====================================================================
% This program part calculates the density for all pixels by
% transforming the gray value.
graypoint_LW=pf(6)
density_LW=pf(7) % [kg/m]
% LW...late wood
graypoint_EW=pf(8)
density_EW=pf(9) %[kg/m]
% EW...early wood - Frhholz

'Berechnung der Dichtematrix'

grayscale_mat_LW=graypoint_LW*ones(size_image_modified);
density_mat_LW=density_LW*ones(size_image_modified);
GSTM=double(image_modified);
% GSTM ... Graustufenmatrix = gray scale matrix
grayscale_diff_mat=GSTM-grayscale_mat_LW;
density_scale=(density_LW-density_EW)/(graypoint_EW-graypoint_LW);
density_scale_mat=density_scale*grayscale_diff_mat;
density_mat=(density_mat_LW-density_scale_mat);

% sl=sd(1) %Gibt die Seitenlnge in x-Richtung wieder
sb=sd(2); %Gibt die Seitenlnge in y-Richtung wieder
sh=sd(3); %Gibt die Seitenlnge in z-Richtung wieder

load 'x_info_3d.dat';
load 'y_info_3d.dat';
load 'z_info_3d.dat';
x_coord=x_info_3d;
y_coord=y_info_3d;
z_coord=z_info_3d;

nop=size(y_coord,1); % nop...number of points
IPC=zeros(nop,2);
% IPC ... integration point coordinates
IPC(:,1)=y_coord;
IPC(:,2)=z_coord;

% ====================================================================
size_density_mat=size(density_mat);
size_IPC=size(IPC);
row_n_c=size_IPC(1);
col_n_c=size_IPC(2);
z_pixel=size_density_mat(1);
y_pixel=size_density_mat(2);
scale_multiplier=(y_pixel/sb);
for i=1:col_n_c;
    for j=1:row_n_c;
        if IPC(j,i)<0.5/scale_multiplier;
```

```
            IPC(j,i)=0.5/scale_multiplier;
        end;
    end;
end;
IPC=round(IPC*scale_multiplier);

% =====================================================================
size_IPC=size(IPC);
row_IPC=size_IPC(1)
col_IPC=size_IPC(2);
% =====================================================================
% Vector with density for all integration points.
density_vector=zeros(row_IPC,1);
for i=1:row_IPC;
    IPC_row=IPC(i,2);
    IPC_col=IPC(i,1);
    density_vector(i,1)=density_mat(IPC_row,IPC_col);
end;
% =====================================================================
% Vector with selected densities for a faster calculation.
density_LW;
density_EW;
density_accuracy=pf(10);
graypoint_LW;
graypoint_EW;

delta_d=(density_LW-density_EW)/(graypoint_EW-graypoint_LW)
density_LW=density_LW+(graypoint_LW*delta_d)
density_EW=density_EW-((255-graypoint_EW)*delta_d)

delta_density=(density_LW-density_EW)/density_accuracy

for d=1:(density_accuracy+1)
    density_vector_short(d,1)=density_EW+(d-1)*delta_density;
end
% =====================================================================

% Input of the micro mechanics model.
'Berechnung von ChomIII_komp'
cd homo_wood_cell.d
ChomIII_komp_short=DIPL_macro_stiffness(density_vector_short);
cd ..
ChomIII_komp_short
'ChomIII_komp berechnet'
% =====================================================================

'alpha-Vektor wird berechnet'
load alpha_mat;
z_alpha_mat=size(alpha_mat,1);
y_alpha_mat=size(alpha_mat,2);
alpha_vector=zeros(row_IPC,1);

for i=1:row_IPC;
    IPC_row=IPC(i,2);
    IPC_col=IPC(i,1);
    alpha_vector(i,1)=alpha_mat(IPC_row,IPC_col);
    if alpha_vector(i,1)==0

        z=IPC_row;
        y=IPC_col;
        max_r=10;
        for r=1:max_r;

            z_min=z-r;
            if z_min<1;
                z_min=1;
            end;

            z_max=z+r;
```

```
            if z_max>z_alpha_mat;
                z_max=z_alpha_mat;
            end;

            y_min=y-r;
            if y_min<1;
                y_min=1;
            end;

            y_max=y+r;
            if y_max>y_alpha_mat;
                y_max=y_alpha_mat;
            end;
%           --------------
            for zz=z_min:z_max;
                yy=y_min;
                alpha_vector(i,1)=alpha_mat(zz,yy);
                if alpha_vector(i,1)~=0;
                    break;
                end;
            end;
%           --------------
            if alpha_vector(i,1)~=0;
                    break;
            end;
%           --------------
            for zz=z_min:z_max;
                if alpha_vector(i,1)~=0;
                    break;
                end;
                yy=y_max;
                alpha_vector(i,1)=alpha_mat(zz,yy);
                if alpha_vector(i,1)~=0;
                    break;
                end;
            end;
%           --------------
            if alpha_vector(i,1)~=0;
                    break;
            end;
%           --------------
            for yy=y_min:y_max;
                if alpha_vector(i,1)~=0;
                    break;
                end;
                zz=z_min;
                alpha_vector(i,1)=alpha_mat(zz,yy);
                if alpha_vector(i,1)~=0;
                    break;
                end;
            end;
%           --------------
            if alpha_vector(i,1)~=0;
                    break;
            end;
%           --------------
            for yy=y_min:y_max;
                zz=z_max;
                alpha_vector(i,1)=alpha_mat(zz,yy);
                if alpha_vector(i,1)~=0;
                    break;
                end;
            end;
%           --------------
            if alpha_vector(i,1)~=0;
                    break;
            end;
%           --------------
        end;
```

```
    end;
end;

save 'alpha_vector.mat' alpha_vector
save 'density_vector.mat' density_vector
% ====================================================================
% Rotation of the stiffness matrix values with the information from
% alpha_vector.
% ====================================================================

row_density=size(density_vector,1)
row_alpha=size(alpha_vector,1)

phi=0;
psi=0;
ChomIII_rotated=zeros((row_density*6),6);

for f=1:row_density
    density=density_vector(f,1);
    alpha=alpha_vector(f,1);

    for d=1:(density_accuracy+1)
        density_short=density_vector_short(d,1);
        density_short_half=density_short+delta_density/2;
        density_short_next=density_short+delta_density;

        if density>=density_short & density<density_short_half
            place=d;
            break
        elseif density>=density_short_half & density<density_short_next
            place=d+1;
            break
        end
    end

    for z=1:6
        dz=((d-1)*6)+z;
        for y=1:6
            ChomIII_place(z,y)=ChomIII_komp_short(dz,y);
        end
    end

    % Expansion of each matrix.
    Ce=DIPL_expand(ChomIII_place);
    % Alpha for each matrix is searched.
    theta=alpha_vector(f);
    % Rotation and compression of the matrix.
    Cc=DIPL_rotate(phi,theta,psi,Ce);

        dzz=1+(f-1)*6;
    ChomIII_rotated(dzz,1)=Cc(1,1); ChomIII_rotated(dzz+1,1)=Cc(2,1); ChomIII_rotated(dzz+2,1)=Cc(3,1);
    ChomIII_rotated(dzz+3,1)=Cc(4,1); ChomIII_rotated(dzz+4,1)=Cc(5,1); ChomIII_rotated(dzz+5,1)=Cc(6,1);
    ChomIII_rotated(dzz,2)=Cc(1,2); ChomIII_rotated(dzz+1,2)=Cc(2,2); ChomIII_rotated(dzz+2,2)=Cc(3,2);
    ChomIII_rotated(dzz+3,2)=Cc(4,2); ChomIII_rotated(dzz+4,2)=Cc(5,2); ChomIII_rotated(dzz+5,2)=Cc(6,2);
    ChomIII_rotated(dzz,3)=Cc(1,3); ChomIII_rotated(dzz+1,3)=Cc(2,3); ChomIII_rotated(dzz+2,3)=Cc(3,3);
    ChomIII_rotated(dzz+3,3)=Cc(4,3); ChomIII_rotated(dzz+4,3)=Cc(5,3); ChomIII_rotated(dzz+5,3)=Cc(6,3);
    ChomIII_rotated(dzz,4)=Cc(1,4); ChomIII_rotated(dzz+1,4)=Cc(2,4); ChomIII_rotated(dzz+2,4)=Cc(3,4);
    ChomIII_rotated(dzz+3,4)=Cc(4,4); ChomIII_rotated(dzz+4,4)=Cc(5,4); ChomIII_rotated(dzz+5,4)=Cc(6,4);
    ChomIII_rotated(dzz,5)=Cc(1,5); ChomIII_rotated(dzz+1,5)=Cc(2,5); ChomIII_rotated(dzz+2,5)=Cc(3,5);
    ChomIII_rotated(dzz+3,5)=Cc(4,5); ChomIII_rotated(dzz+4,5)=Cc(5,5); ChomIII_rotated(dzz+5,5)=Cc(6,5);
    ChomIII_rotated(dzz,6)=Cc(1,6); ChomIII_rotated(dzz+1,6)=Cc(2,6); ChomIII_rotated(dzz+2,6)=Cc(3,6);
    ChomIII_rotated(dzz+3,6)=Cc(4,6); ChomIII_rotated(dzz+4,6)=Cc(5,6); ChomIII_rotated(dzz+5,6)=Cc(6,6);

    if f==round(row_density*0.25)
        '25% von ChomIII_rotated geschafft'
    elseif f==round(row_density*0.5)
        '50% von ChomIII_rotated geschafft'
    elseif f==round(row_density*0.75)
        '75% von ChomIII_rotated geschafft'
```

```
        elseif f==round(row_density*0.999999)
            '100% von ChomIII_rotated geschafft'
        end
end

'ChomIII_rotated'

% ========================================================================
% Fragmentation of ChomIII_rotated into stiffness components (C1111,
% C1112,usw.). The components are storaded as .mat-files.
% ========================================================================

'Abspeichern der einzelnen Matrizen fr C1111, C1122 usw.'

row_ChomIII=size(ChomIII_rotated,1)
col_ChomIII=size(ChomIII_rotated,2)
row_IPC=row_ChomIII/6

C1111=zeros(1,row_IPC);
C1122=zeros(1,row_IPC);
...

for g=1:row_IPC;

    p=g*6-5;
    C1111(1,g)=ChomIII_rotated(p,1); C1122(1,g)=ChomIII_rotated(p,2); C1133(1,g)=ChomIII_rotated(p,3);
    C1123(1,g)=ChomIII_rotated(p,4); %C1131(1,g)=ChomIII_rotated(p,5); %C1112(1,g)=ChomIII_rotated(p,6);

    p=g*6-4;
    C2211(1,g)=ChomIII_rotated(p,1); C2222(1,g)=ChomIII_rotated(p,2); C2233(1,g)=ChomIII_rotated(p,3);
    C2223(1,g)=ChomIII_rotated(p,4); %C2231(1,g)=ChomIII_rotated(p,5); %C2212(1,g)=ChomIII_rotated(p,6);

    p=g*6-3;
    C3311(1,g)=ChomIII_rotated(p,1); C3322(1,g)=ChomIII_rotated(p,2); C3333(1,g)=ChomIII_rotated(p,3);
    C3323(1,g)=ChomIII_rotated(p,4); %C3331(1,g)=ChomIII_rotated(p,5); %C3312(1,g)=ChomIII_rotated(p,6);

    p=g*6-2;
    C2311(1,g)=ChomIII_rotated(p,1); C2322(1,g)=ChomIII_rotated(p,2); C2333(1,g)=ChomIII_rotated(p,3);
    C2323(1,g)=ChomIII_rotated(p,4); %C2331(1,g)=ChomIII_rotated(p,5); %C2312(1,g)=ChomIII_rotated(p,6);

    p=g*6-1;
%     C3111(1,g)=ChomIII_rotated(p,1); %C3122(1,g)=ChomIII_rotated(p,2); %C3133(1,g)=ChomIII_rotated(p,3);
%C3123(1,g)=ChomIII_rotated(p,4);
    C3131(1,g)=ChomIII_rotated(p,5); C3112(1,g)=ChomIII_rotated(p,6);

    p=g*6-0;
%     C1211(1,g)=ChomIII_rotated(p,1); %C1222(1,g)=ChomIII_rotated(p,2); %C1233(1,g)=ChomIII_rotated(p,3);
%C1223(1,g)=ChomIII_rotated(p,4);
    C1231(1,g)=ChomIII_rotated(p,5); C1212(1,g)=ChomIII_rotated(p,6);

    if g==round(row_IPC*0.25)
        '25% von Speichervorgang fr C1111, C1122 usw. geschafft'
    elseif g==round(row_IPC*0.5)
        '50% von Speichervorgang fr C1111, C1122 usw. geschafft'
    elseif g==round(row_IPC*0.75)
        '75% von Speichervorgang fr C1111, C1122 usw. geschafft'
    elseif g==round(row_IPC*0.999999)
        '100% von Speichervorgang fr C1111, C1122 usw. geschafft'
    end

end;

save 'C1111.mat' C1111; save 'C1122.mat' C1122; save 'C1133.mat' C1133; save 'C1123.mat' C1123;
% save 'C1131.mat' C1131; % save 'C1112.mat' C1112; save 'C2211.mat' C2211; save 'C2222.mat' C2222;
 save 'C2233.mat' C2233; save 'C2223.mat' C2223; %save 'C2231.mat' C2231; % save 'C2212.mat' C2212...
```

B.7 DIPL_macro_stiffness.m

```
function [ChomIII_komp]=DIPL_macro_stiffness(density_vector_short)

% This is the third step of homogenization. The original file was made
% by Hofstetter Karin, Univ.Ass. Dipl.-Ing. Dr.techn.
% =====================================================================
% input
%   - ChomII
%   - rhoSW: density of softwood
%   - rhow: density of cellwall
% =====================================================================
% step 3: softwood - unit cell method
%---------------------------------------------------------------------

ChomII=...
    [8.3988    4.3792    5.4833    0.0000    0.0000    0.0000;...
    ;4.3792    8.3988    5.4833   -0.0000    0.0000   -0.0000;...
    ;5.5156    5.5156   35.6188   -0.0000    0.0000    0.0000;...
    ;0.0000    0.0000   -0.0000    8.0906   -0.0000   -0.0000;...
    ;0.0000   -0.0000   -0.0000   -0.0000    8.0906    0.0000;...
    ;0.0000   -0.0000    0.0000   -0.0000    0.0000    4.0196]

rhow=1.4182;

% Both, ChomII and rhow are calculated with DIPL_micro_stiffness.m

% =====================================================================
lam=1; % aspect ratio of unit cell lT/lR;

%        phi _____
%        |--/         \   |
%        | /           \  |
%        |/             \ |
%         \             / lR
%          \           /  |
%           _____/   |
%          -----lT-----

phi=20*pi/180;  % inclination angle of radial cell walls
red=1; % reduced lengths (free lengths) for computation
% of out-of-plane deformations of cell wall
% segments
% red=1 -> reduced, free length of segments
% red=0 -> not reduced, axis lengths of segments

%   \ \ \                     / / /
%    \ \ \                   / / /
%     \ \ \                 / / /
%      \ \ \---------------/ / /
%       | |----------------- | |
%      / / /---------------\ \ \
%     / / /                 \ \ \
%    / / /                   \ \ \
%   / / /   ____ _red=1_____   \ \ \
%         _____red=0_____
% =====================================================================
size_dv=size(density_vector_short,1);

for i=1:size_dv;
    rhoSW(i)=density_vector_short(i,1);
    fwall(i)=rhoSW(i)/rhow;
    fpor3(i)=1-fwall(i);

    ChomIII_K=hom_unit_cell(ChomII,fpor3(i),lam,phi,red);
%     ChomIII_K ... definition according to Karin Hofstetter
%     ChomIII_S ... definition according to Stefan Gloimller (COMSOL)

    ChomIII_S=zeros(6,6);
```

```
    ChomIII_S(1,1)=ChomIII_K(3,3); ChomIII_S(1,2)=ChomIII_K(1,3); ChomIII_S(1,3)=ChomIII_K(2,3);
    ChomIII_S(2,1)=ChomIII_K(1,3); ChomIII_S(2,2)=ChomIII_K(1,1); ChomIII_S(2,3)=ChomIII_K(1,2);
    ChomIII_S(3,1)=ChomIII_K(2,3); ChomIII_S(3,2)=ChomIII_K(1,2); ChomIII_S(3,3)=ChomIII_K(2,2);
    ChomIII_S(4,4)=ChomIII_K(6,6); ChomIII_S(5,5)=ChomIII_K(4,4); ChomIII_S(6,6)=ChomIII_K(5,5);

    for y=1+6*(i-1):6+6*(i-1);
        for x=1:6;
            ChomIII_komp(y,x)=ChomIII_S(y-(i-1)*6,x);
        end;
    end;
end;
```

B.8   DIPL_micro_stiffness.m

```
% This file calculates step one and two of the homogenization.
% ------------------------------------------------------------------------
% input
%   o weight fractions of cellulose, hemicellulose, lignin (input[1:3])
%   o water content u (input[4])
%   o apparent density rhoExp (input[5]) at macroscopic scale
%   o weight fraction of extractives (input[6])
%   o volume fraction of vessels (input[7])
%   o microfibril angle (input[8])
%   o aspect ratio of unit cell lam=lT/lR (input[9])
%   o inclination angle of radial walls in unit cell phi (input[10])
%   o use of reduced / non-reduced lengths (input[11])
%   (all weight fractions are related to weight of dry cell wall)
%------------------------------------------------------------------------
% output
%   o computed stiffness tensors at different observation scales
%     ChomI: polymer network
%     ChomII: cell wall material (matrix+cellulose fibers)
%     ChomIII: cell wall + lumen pores = softwood
%------------------------------------------------------------------------
% required functions
%     o comp_volfrac.m
%     o hom_SCS.m
%     o hom_MT_inclin.m
%        * fun_Psph_1111.m
%        * fun_Psph_1122.m
%        * fun_Psph_1133.m
%        * fun_Psph_2323.m
%        * fun_Psph_3333.m
%        * rot2.m
%        * expand.m
%        * compress.m
%     o hom_unit_cell.m
% ====================================================================
% 1 ... number
% 2 ... cellulose (total, ac+cc)
% 3 ... hemicellulose
% 4 ... lignin
% 5 ... extractives
% 6 ... vessels
%
% 2-5: weight fractions related to dry cell wall
% 6: volume fraction

% 1   2     3     4     5     6
chem=...
 [2 0.417 0.282 0.274 0.034 0] % Spruce, norway(?) Uhlmann
cheminp=chem(2:6)
% ====================================================================
    uinp=0.12 % moistness of the samples
    rhoinp=0.450
input=[cheminp(1:3) uinp rhoinp cheminp(4:5) theta lam phi red];
% ====================================================================
```

```
I=[1 0 0 0 0 0; 0 1 0 0 0 0; 0 0 1 0 0 0;...
   0 0 0 1 0 0; 0 0 0 0 1 0; 0 0 0 0 0 1];
K=[1/3 1/3 1/3 0 0 0; 1/3 1/3 1/3 0 0 0; 1/3 1/3 1/3 0 0 0;...
   0 0 0 0 0 0; 0 0 0 0 0 0; 0 0 0 0 0 0];
J=I-K;

wC=input(1);
wHC=input(2);
wL=input(3);
wH2O=input(4);
rhoWW=input(5);
wExt=input(6);
fgef=input(7);
theta=input(8);
lam=input(9);
phi=input(10);
red=input(11);
%-----------------------------------------------------------------------
% define elastic constants of single phases (subsequent values in
% [N/mm^2])
%-----------------------------------------------------------------------
% types: 1 - morphology 1...sphere, 2...circ. cyl.
%        2 - material   1...isotropic, 2...trans. isotropic

% crystalline cellulose
%-----------------------------------------------------------------------
cCC(1,1)=34.855;
cCC(2,2)=cCC(1,1);
cCC(3,3)=167.8;  % axis direction
%cCC(3,3)=134;  % axis direction
cCC(1,2)=0.0;
cCC(2,1)=cCC(1,2);
cCC(1,3)=0.0;
cCC(3,1)=cCC(1,3);
cCC(3,2)=cCC(3,1);
cCC(2,3)=cCC(3,2);
cCC(4,4)=2*5.805;
cCC(5,5)=cCC(4,4);
cCC(6,6)=2*0.5*(cCC(1,1)-cCC(1,2));

typeCC = [2 2];  % trans. isotropic, cylinder;

% cellulose amorphous
%-----------------------------------------------------------------------
EAC=5;
nuAC=0.35;
kAC=EAC/(3*(1-2*nuAC));
muAC=EAC/(2*(1+nuAC));
cAC=2*muAC*J+3*kAC*K;

typeAC = [1 2];  % isotropic, cylinder;

% hemicellulose
%-----------------------------------------------------------------------
EHC=8;
nuHC=0.35;
kHC=EHC/(3*(1-2*nuHC));
muHC=EHC/(2*(1+nuHC));
cHC=2*muHC*J+3*kHC*K;

typeHC = [1 1];  % isotropic, sphere;

% lignin
%-----------------------------------------------------------------------
EL=6;
nuL=0.3;
kL=EL/(3*(1-2*nuL));
muL=EL/(2*(1+nuL));
cL=2*muL*J+3*kL*K;
```

```matlab
typeL = [1 1];  % isotropic, sphere;

% water
%-------------------------------------------------------------------------
kH2O=2.3;
cH2O=3*kH2O*K;

typeH2O = [1 1];  % isotropic, sphere;

% pores
%-------------------------------------------------------------------------
cpor=zeros(size(cH2O));

%-------------------------------------------------------------------------
% define volume fractions of single phases
%-------------------------------------------------------------------------
% densities of the components; Dichten der einzelnen Komponenten

rhoCC = 1.59; % crystalline cellulose
rhoAC = 1.50; % amorphous cellulose
rhoHC = 1.50; % hemicelluoses
rhoL = 1.37; % lignin
rhoH2O = -1.17*wH2O^3+2.35*wH2O^2-1.22*wH2O+1.3; % compaction of the
% water at adsorption;
rhoExt = 0.90; % extractives
rhocomp = [rhoCC rhoAC rhoHC rhoL rhoH2O rhoExt];

% degree of crystallinity of cellulose;

dCCv = 0.66; % volume fraction
dCCw = dCCv/(dCCv+(1-dCCv)*rhoAC/rhoCC); % weight fraction
wCC = wC*dCCw; % weight fraction of crystalline cellulose
wAC = wC*(1-dCCw); % weight fraction of amorphous cellulose
wHC = wHC+(1-(wC+wHC+wL+wExt)); % any deviations from 1 are added to HC
% phase

% computation of volume fractions
[vfracs,rhow] = comp_volfrac(wCC,wAC,wHC,wL,wH2O,wExt,rhocomp);

if (abs(sum(vfracs)-1)>10^(-5))
  disp('Error in computation of basic volume fractions')
  return
end

fwall=rhoWW/rhow; fCC=vfracs(1); fAC=vfracs(2); fHC=vfracs(3); fL=vfracs(4); fH2O=vfracs(5); fExt=vfracs(6);
%-------------------------------------------------------------------------
% computation of homogenized stiffness matrices
%-------------------------------------------------------------------------
% step 1: polymer network - self-consistent scheme
%-------------------------------------------------------------------------
% phases: HC, L, H2O+Ext

fph1I=fHC/(1-fCC-fAC); cph1I=cHC; tph1I=typeHC(2);
fph2I=fL/(1-fCC-fAC); cph2I=cL; tph2I=typeL(2);
fph3I=(fH2O+fExt)/(1-fCC-fAC); % extractives added to water fraction
cph3I=cH2O; tph3I=typeH2O(2);

if (abs(fph1I+fph2I+fph3I-1)>10^(-5))
  disp('Error in computation of volume fractions of matrix in 1st step')
  return
end

fsI = [fph1I fph2I fph3I]; csI = [cph1I cph2I cph3I]; tsI = [tph1I tph2I tph3I];

ChomI=hom_SCS(csI,fsI,tsI); % function

% step 2: cell wall material - Mori-Tanaka
%-------------------------------------------------------------------------
```

```
tph2II = typeCC(2);
% phase 1 = matrix phase!!
tsII = [1 2 tph2II];
csII = [ChomI cAC cCC];
fsII = [(1-fCC-fAC) fAC fCC];

ChomII=hom_MT_inclin(csII,fsII,tsII,theta)
rhow
```

B.9   stiffness_3d_C1111(x,y,z).m

```
function [c1111] = stiffness_3d_C1111(x,y,z)
load 'C1111'
clear ind ges_vec ges_ind
ind=(find(abs(x(1)-x)<10^-2 & abs(y(1)-y)<10^-2 & abs(z(1)-z)<10^-2));
ges_vec=x(ind:ind+(size(x,2)-1));
ges_ind=[ind:ind+size(x,2)-1];
c1111=C1111(ges_ind)
```

B.10   DIPL_rotate.m

```
function [Cc] = DIPL_rotate(phi,theta,psi,Ce)
% Components nij for z-x'-z''-rotation

nn(1,1) = cos(psi)*cos(phi)-cos(theta)*sin(phi)*sin(psi);
nn(2,1) = -sin(psi)*cos(phi)-cos(theta)*sin(phi)*cos(psi);
nn(3,1) = sin(theta)*sin(phi);
nn(1,2) = cos(psi)*sin(phi)+cos(theta)*cos(phi)*sin(psi);
nn(2,2) = -sin(psi)*sin(phi)+cos(theta)*cos(phi)*cos(psi);
nn(3,2) = -sin(theta)*cos(phi);
nn(1,3) = sin(psi)*sin(theta);
nn(2,3) = cos(psi)*sin(theta);
nn(3,3) = cos(theta);

Crot=zeros(6,6);
index1=[1,2,3,2,3,1];
index2=[1,2,3,3,1,2];

for a=1:6;
    for b=a:6;
        i=index1(a);
        j=index2(a);
        k=index1(b);
        l=index2(b);
        for m=1:3;
            for n=1:3;
                for p=1:3;
                    for q=1:3;
                        Crot(a,b)=Crot(a,b)+Ce(m,n,p,q)* ...
                            nn(i,m)*nn(j,n)*nn(k,p)*nn(l,q);
                    end;
                end;end;end;
        Crot(b,a)=Crot(a,b);
    end;
end;
W = sqrt(2) ;
A = [ 1 1 1 W W W; ...
      1 1 1 W W W; ...
      1 1 1 W W W; ...
      W W W 2 2 2; ...
      W W W 2 2 2; ...
      W W W 2 2 2 ] ;
Cc=Crot.*A;
```

List of Figures

List of Tables